EFFECT OF STRUCTURE DESIGN ON THE COMPRESSIVE STRENGTH AND ENERGY ABSORPTION OF DIFFERENT RESIN-3D PRINTED IRREGULAR VORONOI STRUCTURES BY SLA TECHNIQUE

A Thesis
Submitted to the Council of the Erbil Technical Engineering College at Erbil Polytechnic University in Partial Fulfillment of the Requirements for the Degree of Master of Science in Mechanical and Energy Engineering

By

Zainab Zakariya Ali

Refrigeration and Air-conditioning Engineering, B.Sc.

Supervised by

Zhwan Dilshad Ibrahim, Ph.D.

Erbil-Kurdistan
February 2023

DECLARATION

I declare that the Master Thesis entitled: "**Effect of Structure Design on the Compressive Strength and Energy Absorption of Different Resin-3D Printed Irregular Voronoi Structures by SLA Technique"** is my own original work, and hereby I certify that unless stated, all work contained within this thesis is my own independent research and has not been submitted for the award of any other degree at any institution, except where due acknowledgment is made in the text.

Signature:

Student Name: Zainab Zakariya Ali

Date: 1. 4. 2023

LINGUISTIC REVIEW

I confirm that I have reviewed the thesis titled **"Effect of Structure Design on the Compressive Strength and Energy Absorption of Different Resin-3D Printed Irregular Voronoi Structures by SLA Technique"** from the English linguistic point of view, and I can confirm that it is free of grammatical and spelling errors.

Signature:	
Name of Reviewer:	Dr. Seyed Saber Alavi
Date:	22/12/2022
Email:	Saber_a@payap.ac.th
Address:	TESOL Department, International College, Payap University

SUPERVISOR CERTIFICATE

This thesis has been written under my supervision and has been submitted for the award of the degree of Master of Science in Mechanical and Energy Engineering with my approval as supervisor.

Signature:

Dr. Zhwan Dilshad Ibrahim

Name:

2/4/2023

Date:

I confirm that all requirements have been fulfilled.

Signature:

Name: Asst. Prof. Dr. Ahmed Mohammed Adham

Head of the Department of Technical Mechanical and Energy Engineering

Date: 3/4/2023

Erbil Polytechnic University
Mechanical and Energy Engineering Techniques Department
Erbil Technical Engineering College

I confirm that all requirements have been fulfilled.

Postgraduate Office

Signature:

Name: Mr. Byad Abdulqader Ahmed

Date: 4-4-2023

EXAMINING COMMITTEE CERTIFICATION

We certify that we have read this thesis: "**Effect of Structure Design on the Compressive Strength and Energy Absorption of Different Resin-3D Printed Irregular Voronoi Structures by SLA Technique"** and as an examining committee examined the student (**Zainab Zakariya Ali)** in its content and what related to it. We approve that it meets the standards of a thesis for the degree of Master in Engineering Science.

Signature:
Name: Asst. Prof. Dr. Rizgar Muhammad
Member
Date: 29 - 3 - 2023

Signature:
Name: Asst. Prof. Dr. Payman Suhbat
Member
Date: 29 - 3 - 2023

Signature:
Name: Dr. Zhwan Dilshad Ibrahim
Supervisor
Date: 30/3/2023

Signature:
Name: Prof. Dr. Basim Mohammed
Chairman
Date: 3 April 2023

Signature:
Name: Prof. Dr. Ayad Zaki Saber Agha
Dean of the College of Technical Engineering
Date: 4 - 4 - 2023

ACKNOWLEDGEMENTS

In the name of Allah, the most gracious the most merciful

This research has come to an end; I have met people I am proud to know. We started it step by step, and now we are reaping the benefits of a year journey in which our goal was clear, and we worked hard every day to achieve and reach it. Thank Allah first and foremost. This work would not have been possible without the support of all those who assisted me. I am grateful to everyone with whom I have had the opportunity to collaborate on this project.

I am particularly indebted to Zhwan Dilshad Ibrahim, Ph.D., the supervisor of my thesis, and I would like to express my heartfelt gratitude to him. He provided me with extensive guidance and taught me a lot about scholarly research. As my mentor and supervisor, he has instructed me in more things that I could possibly give him credit for in this field. In addition, he provided me with a lot of research, which added a lot of value to my research. Through his example, it turned out that the teacher is a candle that lights the way for others, and he helps them become in the best place they can be. Furthermore, he is someone who makes a difference in your life. Without his invaluable supervision and tremendous patience, this thesis would not have been possible.

Additionally, I am deeply indebted to Ali Arab, Ph.D., for his helpful advice, generous support, and invaluable contribution to completing this work.

I am extremely grateful to Erbil Polytechnic University\ College of Technical Engineering/ Mechanical and Energy Engineering Department, for giving me the opportunity to gain more knowledge. I would like to express my deepest appreciation to the head of the Mechanical and Energy Engineering Department\ Ahmed Mohammed Adham, Ph.D., for his invaluable help and support. In addition, special thanks to the honorable members of the master thesis

examining committee; Prof. Dr. Basim Mohammed, Asst. Prof. Dr. Rizgar Muhammad, and Asst. Prof. Dr. Payman Suhbat.

Next, I would like to thank the head of the Aviation Engineering Department\ College of Salahaddin University-Erbil, Iyd Eqqab Maree, Ph.D., for his ongoing encouragement and kind support.

I would like to convey my special thanks to Fatima Belok, Ph.D., for her contribution to the completion of this work. Her instructions and support facilitated the use of 3D Rhinoceros software. I am also grateful to all my friends and colleagues for their kind support.

Finally, no one has been more important to me in pursuing this thesis than my family members. I would like to thank my parents, brothers, and sister whose affection and counsel accompany me in everything I do, as well as for their patience and understanding. They are the perfect examples to follow. My deepest gratitude to them.

TABLE OF CONTENTS

ACKNOWLEDGEMENTS V
LIST OF TABLES IX
LIST OF FIGURES X
LIST OF SYMBOLS XIII
LIST OF ABBREVIATIONS XIV
LIST OF UNITS XVI
ABSTRACT XVII
CHAPTER 1: INTRODUCTION 1
1.1 Natural Structures 1
1.2 Inspired Structural Designs from Nature 3
1.2.1 Columnar joints 6
1.2.2 Triangular Lattice Configurations 7
1.3 Real-life Applications of Structural Design 11
1.4 Mechanical Properties of the Natural Inspiration Designs 14
1.5 Crashworthiness Parameters 15
1.6 Failure Modes of Structures 16
1.7 Additive Manufacturing Techniques 17
1.7.1 AM Techniques 19
1.8 AM Printing Materials 25
1.9 Problem Statement 27
1.10 Research Aim and Objectives 29
1.11 Thesis Plan 30
1.12 Limitations 32
1.13 Thesis Outline 32
CHAPTER 2: LITERATURE REVIEW 33
2.1 Introduction 33
2.2 Bio-inspiration 33
2.3 Voronoi Tessellation 34
2.4 Compression Properties 35
2.5 Additive Manufacturing 38
2.5.1 SLA Technique 39

2.6 Plant-based Biopolymer 41
2.7 Failure Mode 42
2.8 Summary 43
CHAPTER 3: METHODOLOGY 45
3.1 Introduction 45
3.2 Used Material 45
3.3 Used Equipment 47
3.3.1 SLA 3D Printer 47
3.3.2 Compression Test Machine 48
3.4 Experiment Plan 49
3.4.1 Constant Factors 49
3.4.2 Variables and Levels 50
3.4.3 Design Limitations 52
3.4.4 Response Data 52
3.5 Samples Fabrication 55
3.5.1 Designing the Samples 55
3.5.2 3D Printing of the Samples 58
3.6 Compression Test 60
CHAPTER 4: RESULTS AND DISCUSSION 61
4.1 Introduction 61
4.2 Compression Resistance 61
4.3 Energy Absorption 68
4.4 Failure Modes 72
CHAPTER 5: CONCLUSION AND FUTURE RECOMMENDATIONS 74
5.1 Conclusion 74
5.2 Future Recommendations 75
REFRENCES R1
APPENDIX A1
SPECIAL GRATITUDE

LIST OF TABLES

Table 3-1 Biopolymer/Plant-based resin properties (Anycubic, 2022). 46

Table 3-2 The details of the designed models. 52

Table 3-3 The porosity of the designed models. 54

LIST OF FIGURES

Figure 1-1 Classification of cellular structures (Park, Min and Roh, 2022) 1

Figure 1-2 Periodic Cellular Core Topologies (Wadley, Fleck and Evans, 2003). 2

Figure 1-3 Examples of 3D-Printing innovation by mimicking natural materials and designs. a) bone inspired, and **b)** butterfly inspired (Nikkhah, Crupi and Baroutaji, 2020; Bandyopadhyay, Traxel and Bose, 2021). 5

Figure 1-4 Design of a drone inspired by the insect wing. **a)** and **b)** Wings of a cicada (Saito et al., 2021). 6

Figure 1-5 Columnar jointed rocks. Reprinted/adapted with permission from (Rhea, 2022). 7

Figure 1-6 Voronoi diagram parameters. 10

Figure 1-7 Two-dimension Voronoi tessellation generation steps. **a)** seed distribution, **b)** delauney triangulation, **c)** identification of the bisector lines, and **d)** Voronoi cellular structure (Jiao and Torquato, 2011; Angelucci and Mollaioli, 2018). 11

Figure 1-8 Conventional techniques for scaffold fabrication. **a)** scaffold block, **b)** cutting tools, and **c)** pores making for the scaffold (Karp et al., 2003). 13

Figure 1-9 An illustration of, **a)** bending-dominated structure, and **b)** stretch-dominated structure (Alghamdi et al., 2020). 15

Figure 1-10 Deformation pattern of the 3D: **a)** normal Voronoi structures, and **b)** elongated Voronoi structures. 16

Figure 1-11 Growth of RP process (Wong and Hernandez, 2012). 18

Figure 1-12 3D printing process. 19

Figure 1-13 Classification of Additive Manufacturing techniques commonly used in 3D printing. 21

Figure 1-14 The main principle of stereolithography (SLA) (Gross, Lockwood and Spence, 2017). 23

Figure 1-15 An illustration of the difference in surface roughness of the final 3D printed part between the SLA and FDM technique (Formlabs, 2022). 25

Figure 1-16 Categorization of biopolymers (Vedantu, 1800). 26

Figure 1-17 Research objective. 31

Figure 2-1 Variation of the elastic modulus with porosity (Zhu et al., 2021). 38

Figure 2-2 3D scaffold fabricated by FDM (Hutmacher, 2000). 40

Figure 2-3 The morphology of a fabricated SLA scaffold by SEM (Kim *et al.*, 2011). 41

Figure 3-1 Biopolymer used in samples 3D printing (Anycubic, 2022). 46

Figure 3-2 SLA 3D printer. 47

Figure 3-3 GOTECH AI-3000 controlled testing machine for micro samples. 49

Figure 3-4 The designed cylinder details. 50

Figure 3-5 An illustration of designed irregular structures. **a)** elongated Voronoi, **b)** normal Voronoi, **c)** the top view of the three models; **I)** homogenous cylinder, **II)** hollow (with core) cylinder (gradient I), and **(III)** filled core cylinder (gradient II). 51

Figure 3-6 3dm Rhinoceros file. 55

Figure 3-7 Steps of designing the models in Rhinoceros 7/Grasshopper software. 56

Figure 3-8 The Grasshopper file for the **a)** homogeneous elongated Voronoi structure (E1), and **b)** homogeneous normal Voronoi structure (N1). 57

Figure 3-9 Illustration of **a)** STL file, and **b)** slicing software file. 58

Figure 3-10 An illustrative of the printed samples. 59

Figure 4-1 Stiffness of the Voronoi structures. 62

Figure 4-2 Young's modulus of the various Voronoi structures design. 63

Figure 4-3 Compression properties of the six Voronoi structures. **a)** the ultimate strength, and **b)** the maximum deformation. 64

Figure 4-4 Stress-strain curve for the six samples under uniaxial compression load. **a)** homogeneous model for elongated (E1) and normal (N1) Voronoi structures, **b)** gradient I model for elongated (E2) and normal (N2) Voronoi structures, and **c)** gradient II model for elongated (E3) and normal (N3) Voronoi structures. 67

Figure 4-5 Variation in energy absorption (EA) as a function of displacement for the six Voronoi structures. **a)** homogeneous model for elongated (E1) and normal (N1) Voronoi structures, **b)** gradient I model for elongated (E2) and normal (N2) Voronoi structures, and **c)** gradient II model for elongated (E3) and normal (N3) Voronoi structures. 70

Figure 4-6 Specific energy absorption of the six models. 71

Figure 4-7 Failure mode of homogeneous elongated Voronoi structure. **I)** failure mode under compression machine; **a)** fracture prediction starts, **b)** collapse, and **c)** fracture propagation, and **II)** microscopic illustration of the fracture mode. 73

LIST OF SYMBOLS

$A_\circ$	The square unit area of Voronoi diagram
A	Cross-section area of the sample
$d_\circ$	Distance between two seed point
d_f	The final crushing distance
d_i	The initial crushing distance
E^*	Apparent Young's modulus of the cellular structure
F	The applied force
H	The height of the cylinder
L_i	Initial length of the sample
L_f	Final length of the sample
n	Number of cells
P_{ave}	The mean crushing force
R	The outer diameter of the cylinder
r	The inner diameter of the hollow cylinder
S^*	Apparent stiffness of the cellular structure
W_{max}	The maximum deformation
ΔL	Displacement
$\rho_{material}$	Density of the material
ρ_s	Apparent density of the structure
σ^*	Apparent compressive stress of the cellular structure
ε^*	Apparent strain of the cellular structure
α	Regularity parameter
δ	The minimum distance between any two adjacent seed points.

LIST OF ABBREVIATIONS

AM	Additive Manufacturing
BTE	Bone Tissue Engineering
CAD	Computer-Aided Design
DIC	Digital Image Correlation
EA	Energy Absorption
FDM	Fused Deposition Modelling
IEVSs	Irregular Elongated Voronoi structures
INVSs	Irregular Normal Voronoi structures
LTDM	Low Temperature Deposition Manufacturing
PA	Polyamide
PAM	Pressure Assisted Micro
PC	Polycarbonate
PCL	Polycaprolactone
PDS	Polydioxanone
PE	Polyethylene
PED	Precision Extrusion Deposition
PETG	Polyethylene terephthalate glycol
PGA	Polyglycolide
PHB	Polyhydroxybutyrate
PLA	Polylactic Acid
PMMA	Poly (methyl methacrylate
PP	Polypropylene
PPF	Poly (Propylene Fumarate)
PTFE	Polytetrafluoroethylene
PU	Polyurethane
PVC	Polyvinyl chloride
RP	Rapid prototyping

RSM	Response Surface Methodology
SEA	Specific Energy Absorption
SLA	Stereolithography
SLM	Selective Laser Melting
SLS	Selective Laser Sintering
ST	Sierpinski Triangle
STL	Standard Tessellation Language
TEA	Total Energy Absorption
Ti-6Al-4V ELI	Titanium alloys
TIPS	Thermally Induced Phase Separation
TPMS	Triply Periodic Minimal Surface
US	Ultimate Strength
UTS	Ultimate Tensile Strength
UV	Ultraviolet
VEA	Volumetric Energy Absorption
VOCs	Volatile Organic Compounds
2D	Two-dimensional
3D	Three-dimensional
3DP	Three-dimensional printing

LIST OF UNITS

cm^3	Centimeter cubic
g	Gram
GPa	Giga Pascal
J	Joule
mm	Millimeter
MPa	Mega Pascal
N	Newton
P	Load
sec	Second

ABSTRACT

Nature-like designs inspired designers to adapt them in real-life applications due to their strength and optimal mechanical properties. In the current study, irregular Voronoi structures were prepared through using of Rhinoceros 7\Grasshopper software. Both normal and elongated Voronoi designs (based on the columnar joints that exist naturally) were designed, having three separate models per each, homogeneous, gradient I, and gradient II are based on homogeneity and having a core inside the samples. Stereolithography (SLA) three-dimensional (3D) printing was used to fabricate biopolymer Plant-based materials to be prepared for mechanical testing. Generally, the experimental results showed that the proposed Voronoi designs with elongated structures have better mechanical properties. They are about 21% superior to the normal Voronoi structures in terms of resisting deformation and approximately 30 % in energy absorption. Hence, these designs are promising topologies for future applications. Moreover, the failure mode of the six structures occurred due to the collapse in three stages: the cells' strut fracture, cell collapse, and eventually, fracture growth. In regard to the designed models, the homogeneous model type showed a higher stiffness and ultimate strength while the gradient I model exhibited a higher Young's modulus. Furthermore, the homogeneous and gradient II models showed a great energy absorption property. Besides, the gradient II model possessed the poorest mechanical properties due to its weak geometry design. Hence, this model is not preferred in lightweight-to-strength applications.

CHAPTER 1

INTRODUCTION

1.1 Natural Structures

Cellular structures exist in nature such as bones of living things, honeycombs, and leaves (Gibson, Ashby and Harley, 2010). Generally, cellular structures are divided into foam (stochastic) and lattice structures (non-stochastic) based on the configuration of their unit cells, as shown in Figure 1-1.

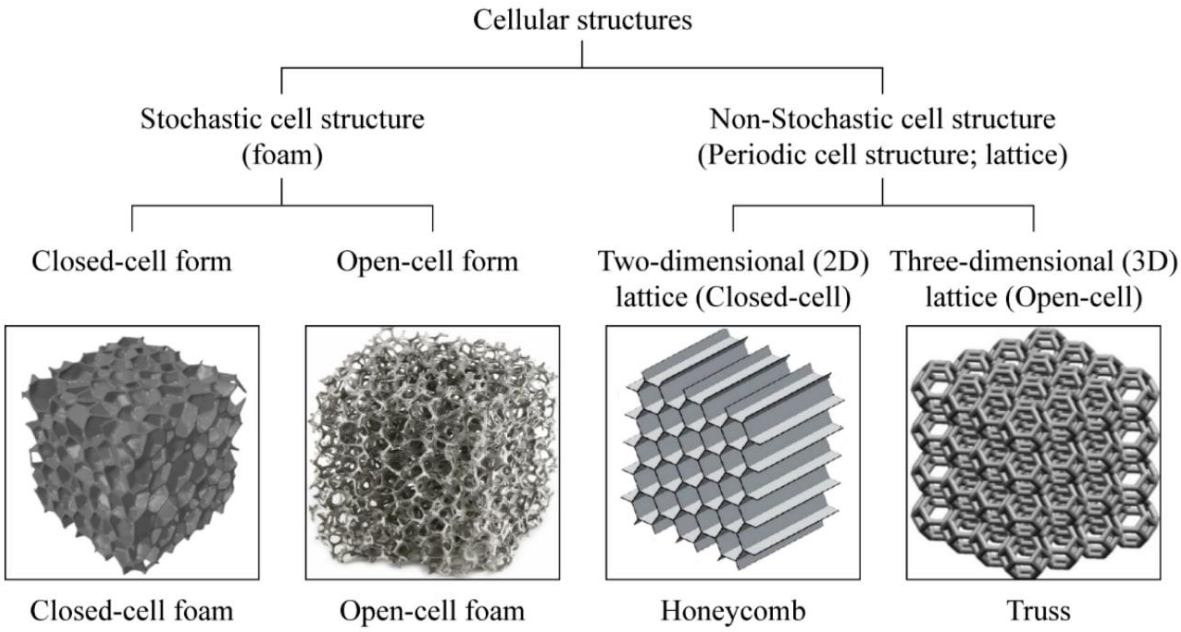

Figure 1-1 Classification of cellular structures (Park, Min and Roh, 2022)

Non-stochastic lattice structures are periodic structures made of repetitive groupings of smaller units of cells. Periodic lattice structures are subdivided into the 2D honeycomb and 3D truss (Wagner *et al.*, 2019). The most popular periodic

cellular topologies are illustrated in Figure 1-2. On the other hand, the stochastic foam structures are divided into closed-cell structures and open-cell structures. Usually, in closed-cell foam structures, the cell walls are closed making the structure impermeable and nonporous. While open-cell structures have open cell walls that are typically made with an artificially inflated agent throughout manufacturing that allows fluids to pass through (Gibson LJ, 1997; Dossi, Brennan and Moesen, 2017). Voronoi tessellation is an important example of open-cell foam structures.

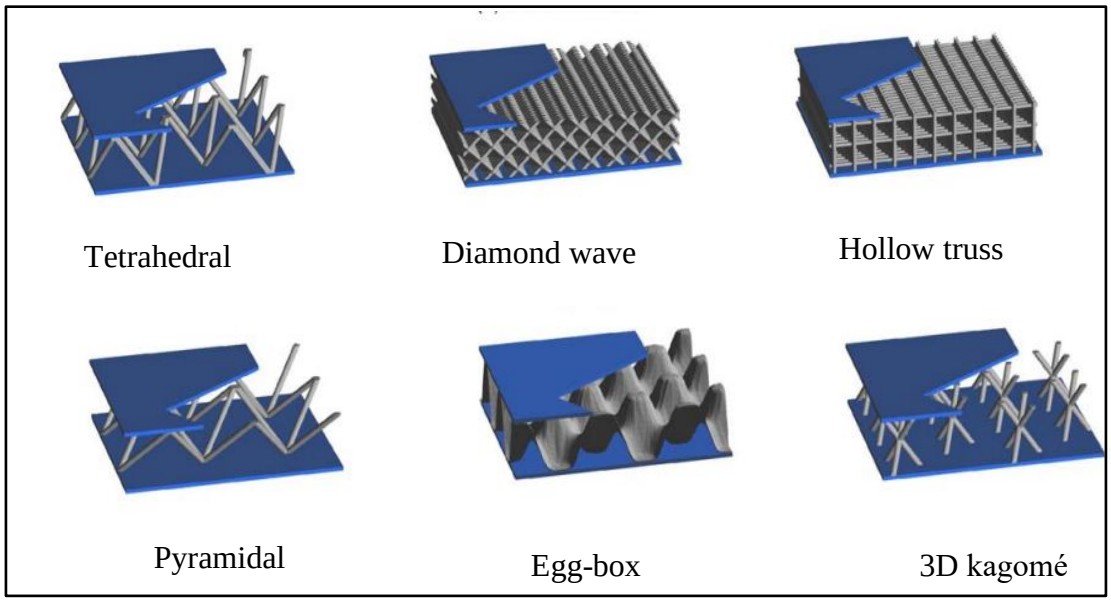

Figure 1-2 Periodic Cellular Core Topologies (Wadley, Fleck and Evans, 2003).

Due to the fact that open-cell foams are 3D structures composed of nodes and struts, it has been demonstrated that their performance is influenced by a variety of variables (Sun, Guo and Shim, 2021). Apart from the cell size (Cao *et al.*, 2018), relative density (Alomarah *et al.*, 2020), and variability in fabrication, the topology of the unit cell is a significant factor affecting the macroscopic mechanical behavior of foam structures (Bonatti and Mohr, 2017). The usefulness of foam could be increased further by combining it with a hybrid form, wherein the relative density or

the unit cell topology of the structure is altered. Hybrid foam structures are classified into two types: (a) structurally or functionally graded foam structures; in which parameters such as relative density fluctuate as a gradient across the structure (Teimouri and Asgari, 2021), and (b) mixed topology foam structures, where topology of the structure varies between discrete unit cells (Li *et al.*, 2020).

Cellular structures are ubiquitous in nature as basic components. By incorporating their fundamentals into industrial design, they can improve some mechanical properties such as energy absorption and weight-to-strength ratio (Gibson LJ, 1997). Unit cell-based periodic designs in 2D or 3D arrays (Mullen *et al.*, 2009) are common techniques for the construction of cellular structures, for instance, stochastic and complex geometries (Mullen *et al.*, 2010; Yan *et al.*, 2015). Besides, there are several factors that affect the features of cellular structures, including geometry, and material (Rehme, 2010). By virtue of their presence in nature, designers have recently resorted to taking advantage of nature and drawing inspiration from cellular structures found in nature for engineering designs where the resulting properties of these cellular structures can be tailored to meet desired engineering requirements. Nature provides many geometric shapes, such as regular geometries and irregular ones. Irregular geometries are based on Voronoi tessellation, with high specifications that exceed those that are made by humans themselves.

1.2 Inspired Structural Designs from Nature

Outstanding designs of structural materials are occurs naturally at all scales, while conventional human-centered materials design necessitates optimizing factors such as strength and ductility, among numerous other examples, recent research has demonstrated that structures found in nature frequently break down those barriers, producing materials with vastly enhanced properties over anything designed by humans, as shown in Figure 1-3 (Bandyopadhyay, Traxel and Bose, 2021). These distinct properties have piqued the interest of researchers looking to uncover the secrets behind these structures in order to replicate the features required to incorporate these naturally occurring evolutionary advantages into science and technology (Tee *et al.*, 2021). Nikkhah, Crupi and Baroutaji, (2020) proposed energy absorbing structures that have unique thin-walled structures bio-inspired by the microstructure of Morpho wings. In addition, in designing the on-water sports board, Aref Soltani *et al.*, (2020) were inspired by the carbon atom configuration, honeycomb, and spider web, their work discovered that the bio-inspired, operationally classed honeycomb structure had the greatest bending performance. Moreover, Ghazlan *et al.*, (2020) designed a demo model by finite element model based on Voronoi tessellation inspired by bone structure. The results showed a significant improvement in energy absorption by 69 %.

3D Voronoi structures are the most common example of cellular structures. They are another attractive nature-inspired design that adds greatly to the development of mechanical properties of additive manufactured materials, especially in tissue engineering applications. Additionally, they are widely preferred in fabricating scaffolds as they can provide a biological environment that improves better cell proliferation (Sun *et al.*, 2012). Recently, the concept of Voronoi tessellation has been used to generate the random properties of cell architectures. Moreover, there is the concept of the weight-to-strength ratio, which plays an

important role in engineering designs. Thus, in the realms of modern manufacturing, energy saving, and environmental protection, the lightweight design of porous structures is not only a vital issue but also a tough one. These advantages of porous architectures on the mechanical behavior can be attributed to the following (Herath *et al.*, 2021): these structures have a large number of pores, the weight of products is reduced significantly, as the consumption of materials and energy is decreased.

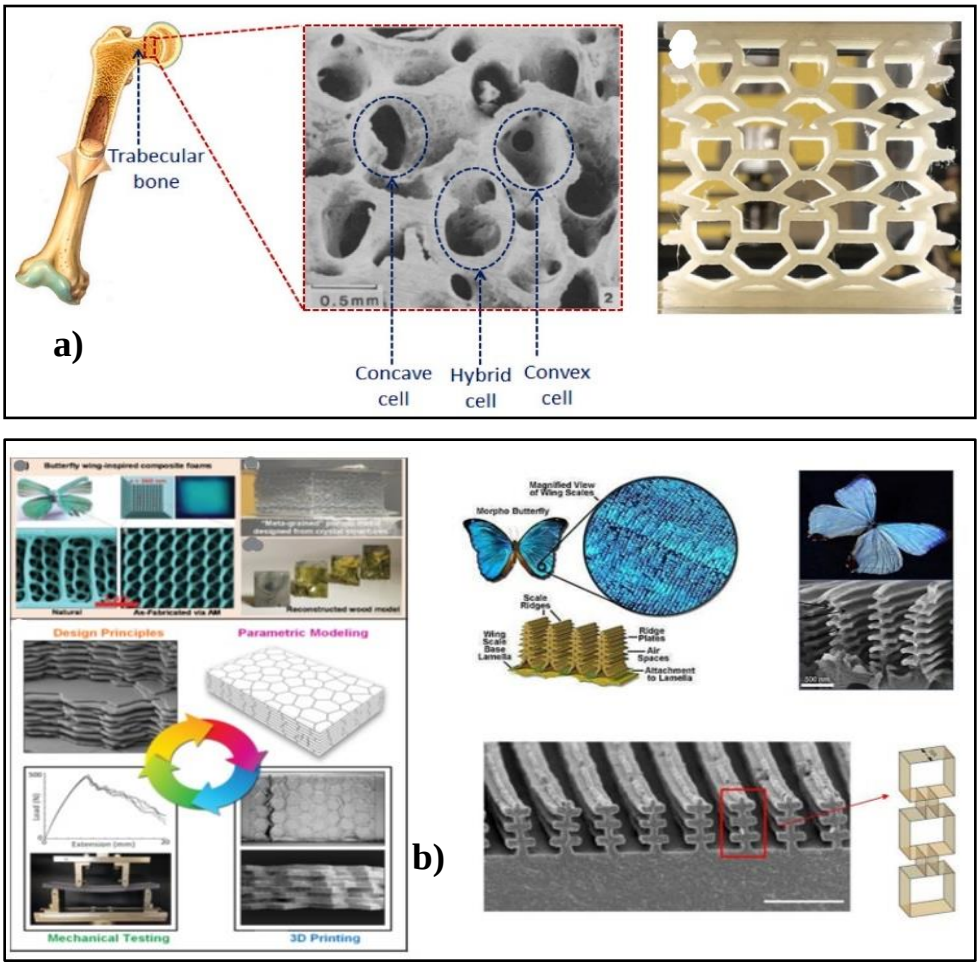

Figure 1-3 Examples of 3D-Printing innovation by mimicking natural materials and designs. a) bone inspired, and **b)** butterfly inspired (Nikkhah, Crupi and Baroutaji, 2020; Bandyopadhyay, Traxel and Bose, 2021).

In addition, the porous structure can be efficiently modified to match the functionally gradient target by adjusting the pore size, pore distribution, pore shape,

and other characteristics. Eventually, it is identical to the natural porosity cellular structure, which has good qualities that allow cells to interconnect and grow. Saito *et al.*, (2021) designed artificial wings based on Voronoi tessellation for a drone inspired by cicada insect wings, as indicated in Figure 1-4. This design provided lightweight and high-strength features for the wings which can be applied in aircraft applications in the future.

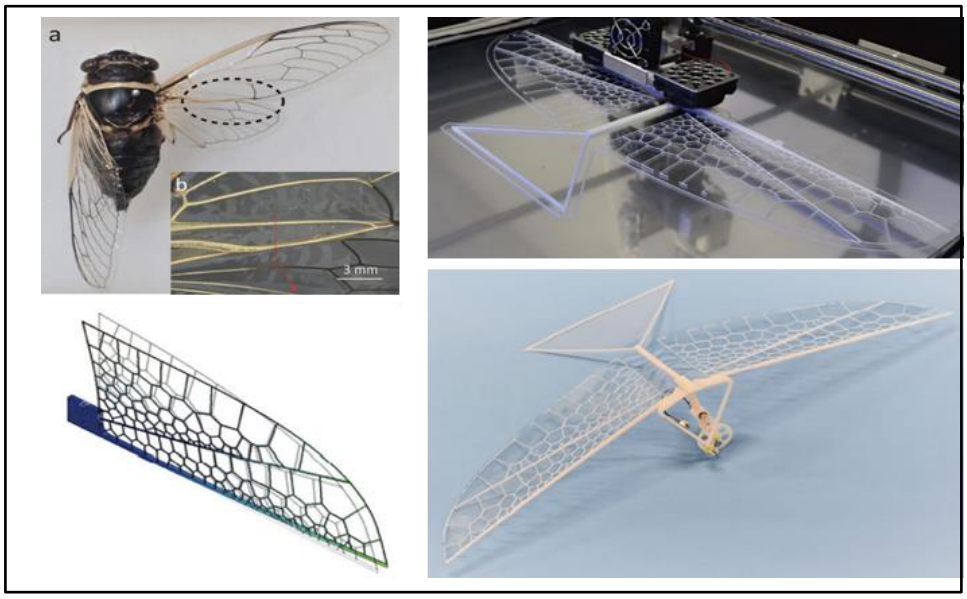

Figure 1-4 Design of a drone inspired by the insect wing. **a)** and **b)** Wings of a cicada (Saito *et al.*, 2021).

1.2.1 Columnar joints

Biomimetic concepts, which seek to derive natural inspiration for the development of new engineering technological solutions, can be used to construct innovative lightweight engineering structures. Diabase (Rhea, 2022) and basalt (Jiang *et al.*, 2014) are among the most powerful stones in nature. Whereas they are strongest in compression (Diabase; 350 MPa and basalt; 300 MPa), tension (Diabase;

35 MPa and basalt; 30 MPa), and shear stress (60 MPa for both). Several studies have indicated that this strength possessed by these rocks is due to their geometrical structure. Figure 1-5 shows that these stones are columnar jointed, in other words, they have an elongated shape. This inspired us to implement this design in the lightweight-to-strength application and evaluate how the elongated Voronoi structure improves the mechanical properties for crashworthiness applications. Designing a lightweight and meantime a less dense structure having a geometry that provides improved mechanical properties, is the main objective of this research. Recently, Voronoi tessellation is widely used in lightweight applications. However, its mechanical properties are not satisfactory yet in some applications. Therefore, we made modifications to the cell geometry of the normal Voronoi tessellation, which lead to the enhancement of its mechanical properties to a great extent.

Figure 1-5 Columnar jointed rocks. Reprinted/adapted with permission from (Rhea, 2022).

1.2.2 Triangular Lattice Configurations

Triangular lattice configurations usually refer to the Voronoi tessellation (Gibson *et al.*, 1999). Voronoi is a geometric diagram that reproduces irregular biomimetic cells that can be found in nature (Voronoi, 1908), such as on turtle shells. Voronoi tessellation has grown in popularity among scientists across a wide range of disciplines, starting from biology to mechanical design, due to its capacity to quantitatively describe natural models (Silva and Gibson, 1997; Vajjala, Kraynik and Gibson, 2000). The Voronoi tessellation approach is a good option to design stochastic cellular structures. It has been adopted by many researchers in their engineering designs, such as in B-spline fitting (Kou and Tan, 2010) or using the Voronoi diagram of ellipses to create free-support cellular structures (Lee *et al.*, 2018) due to excellence of Voronoi tessellation in technology. Because structural topologies (Alkhader and Vural, 2008; Schaedler *et al.*, 2011) have a significant influence on the mechanical behavior of cellular structures, attempts have been devoted to developing deterministic materials with novel mechanical properties.

Biomimetic patterns are created looking for ways to reduce the weight of structures while maintaining their structural integrity. Consequently, current mechanical design advancements have a strong bio-inspired influence. Meanwhile, biomimetic patterns are created by arranging either regular or irregular unit cells. Researchers used a variety of techniques to create bio-inspired lattice structures, such as Triply Periodic Minimal Surface (TPMS) (Bobbert *et al.*, 2017) and Voronoi tessellation. Voronoi tessellation is an irregular geometric shape that can create engineering structures with controllable mechanical properties. Voronoi tessellation has grown in popularity among scientists across a wide range of disciplines, starting from biology to mechanical design, due to its capability to quantitatively describe natural models (Silva and Gibson, 1997; Vajjala, Kraynik and Gibson, 2000). Voronoi tessellation is a geometric diagram that reproduces irregular biomimetic

cells that can be found in nature (Voronoi, 1908), such as on giraffes, dragonfly wings, plant leaves, and so on.

Voronoi diagram is suitable for creating 2D and 3D cellular structures. The process begins by forming the nucleation and then the growth of the bubbles. A Voronoi tessellation is obtained as a result of the random formation of all bubbles in space at the same time and growing at a similar linear rate (Klein, 1989). This means that the topology of the resulting Voronoi structure is unambiguously and totally defined by the seed points or the original distribution of the nuclei. One method for generating *n*-number of seed points is to distribute them at random over a predefined area A_0 with no constraints, as shown in Figure 1-6. This method yields the Poisson distribution. Voronoi structures built using Poisson distribution have an irregular topology with great variability in cell size. Alternatively, the constraint that the distance between the two random millennium points is greater than a minimum predetermined value, δ, can be imposed. This causes δ-distribution, which results in a somewhat more uniform cell size distribution (Alkhader and Vural, 2008). For a reminder, what was mentioned above has been approved under the name of four assumptions: i) the bubbles form in a specific region of space at the same time, ii) during the growth, the nuclei of these bubbles remain fixed in the place, iii) growth occurs at a constant pace in all directions, and iv) when adjacent bubbles come into contact with one another, the growth is halted (Tekoğlu *et al.*, 2011). A perfectly regular point pattern yields a regular Voronoi diagram, but an irregular point pattern generates a random counterpart. Natural structures are not necessarily completely regular or completely irregular, and hence their configuration might be considered as falling between these two extremes.

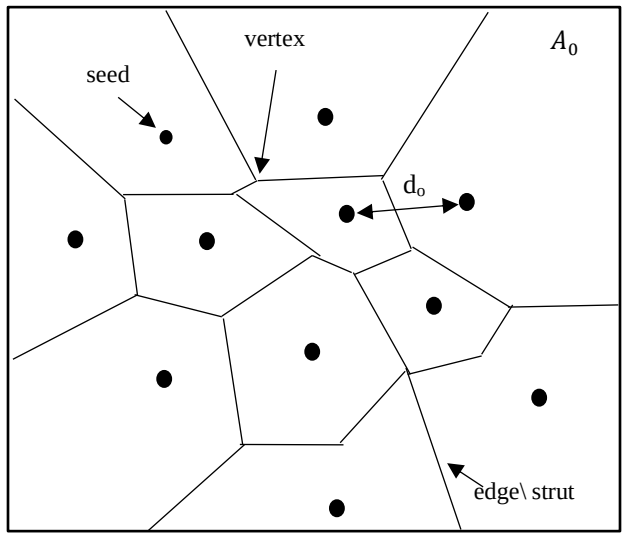

Figure 1-6 Voronoi diagram parameters.

Based on δ constraint, Zhu *et al.* (Zhu, Thorpe and Windle, 2001) put steps, as indicated in Figure 1-7 to describe parameters to determine the regularity of 2D Voronoi tessellations. To Begin with finding d_0 which is represents the constant distance between each and every two neighboring seed points if an *n*-number of regular honeycombs are formed in the square unit area A_0, then the equation to calculate the d_0 is:

$$d_0 = \left(\frac{2\,A_0}{n\,\sqrt{3}}\right)^{1/2} \tag{1-1}$$

while Eq. (1-2) is given to determine the regularity parameter α. The least distance between each two seed points in a random Voronoi tessellation with n cells in area A_0 should be less than d_0. Or else, obtaining n cells is impossible. To achieve a regular structure, the regularity parameter must be equal to 1 ($\alpha = 1$), and $\delta = d_0$. Whereas $\alpha = 0$, and $\delta = 0$ for a Poisson (fully random) Voronoi tessellation.

$$\alpha = \frac{\delta}{d_0} \tag{1-2}$$

as previously mentioned, δ is the minimum distance between any two adjacent seed points. The nucleation and then the growth of bubbles is a common process in the formation of cellular solids.

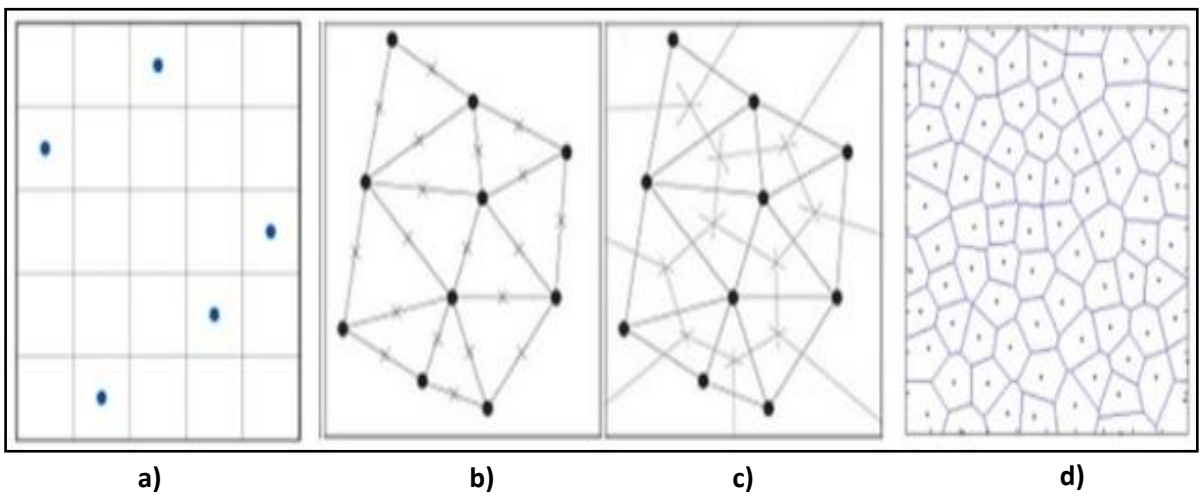

Figure 1-7 Two-dimension Voronoi tessellation generation steps. **a)** seed distribution, **b)** delauney triangulation, **c)** identification of the bisector lines, and **d)** Voronoi cellular structure (Jiao and Torquato, 2011; Angelucci and Mollaioli, 2018).

1.3 Real-life Applications of Structural Design

The world is witnessing the rapid and sudden development in the biomedical engineering curriculum. In the realm of orthopedics, bone tissue regeneration represents a major challenge. For example, osteoporosis and osteogenesis imperfecta can affect bone function, resulting in bone fractures that do not heal properly. The second most prevalent type of tissue transplantation is bone transplants (Lewandrowski *et al.*, 2000), but if the injury surpasses the critical limit then cannot

be repaired by regeneration and existing clinical treatments are ineffective. Both allograft and xenograft graftings are considered elective therapies; nonetheless, each procedure comes with its own set of drawbacks, the most significant of which is the risk of graft rejection by the immune system (Kumar, 2006). New approaches are required to resolve the drawbacks of current bone grafting methods, such as tissue engineering or regenerative medicine, which hold promise for the reconstruction of bone fractures and the treatment of bone diseases (Fernandez-Yague *et al.*, 2015). BTE techniques combine cells, scaffolds, and customized culture conditions including biochemical and physical stimulation (Hutmacher, 2006) which helps in the growth and repair of tissues and organs lost or flawed due to traumatic injuries (Vacanti and Langer, 1999).

One of the common alternatives for the repair and functional reconstruction of injured and lost tissues such as bone is biological scaffolds. Whereas most scaffolds and implants used for bone replacement or fracture treatment are comprised of robust materials that provide excellent mechanical support (Fu *et al.*, 2011; Jahani, Wang and Brooks, 2020). Where these scaffolds operate as a limited extracellular matrix to add support for cells, promoting the normal processes of tissue regeneration and evolution (Furth, Atala and Van Dyke, 2007; Habraken, Wolke and Jansen, 2007; Lee and Shin, 2007). The conventional techniques for scaffold fabrication include solvent casting, fiber bonding, particulate leaching, and melt molding (Widmer and Mikos, 1998). However, these techniques require great effort and take a lot of time, with the relatively poor quality of the product. Karp *et al.*, (2003) fabricated a scaffold by using individual molds. The beginning of industrialization was the manufacture of a macroporous scaffold block. Then a stainless-steel cutting device was used to make the pores, as shown in Figure 1-8.

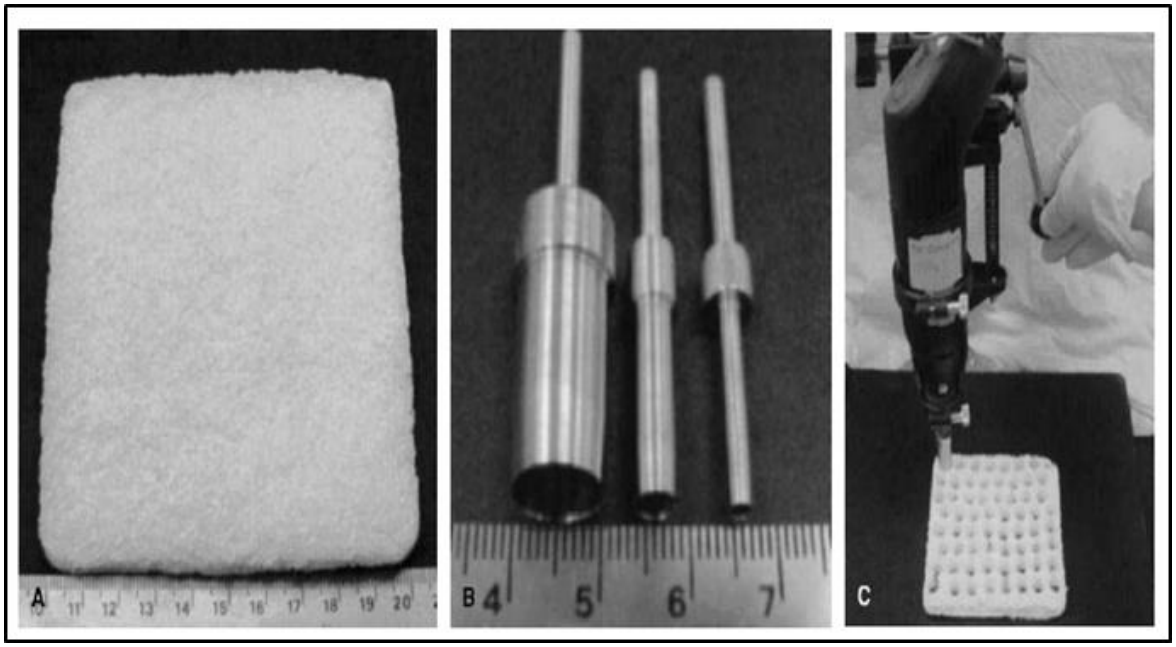

Figure 1-8 Conventional techniques for scaffold fabrication. **a)** scaffold block, **b)** cutting tools, and **c)** pores making for the scaffold (Karp *et al.*, 2003).

The advent of additive manufacturing processes facilitated the process of manufacturing scaffolds, especially those based on complex shapes such as Voronoi structures. Picking a suitable geometry structure and the correct material that can be 3D printed successfully are critical aspects of the scaffold's ability to execute its function similarly to the genuine bone. Uí Mhurchadha *et al.*, (2021) manufactured a new 3D printed scaffold structure based on Voronoi tessellation using Ti-6Al-4V ELI material. Although the results showed an improvement in mechanical properties, the use of a bio metal continues to corrode in the body to some extent, so it cannot be considered biocompatible in general. In addition, it requires secondary surgery later to remove it at the end of its functional life.

1.4 Mechanical Properties of the Natural Inspiration Designs

The researchers and designers should choose the right structure designed with precise specifications, including geometry and size, to achieve the desired properties compatible with the external load effects. In this regard, both regular and irregular structures for scaffold fabrication have gained attention in the literature.

Open-cell cellular structures have attracted a lot of interest from researchers due to their appealing mechanical characteristics, such as high stiffness, high strength, low weight, and high energy absorption (Dong, Deshpande and Wadley, 2015). Figure 1-9 demonstrate that structures based on open-cell are consisting of nodes and struts, and they typically classified according to their topology as bending-dominated or stretch-dominated, which in turn influence their mechanical properties. Mechanical properties depend on the relative density, the constituent materials characteristics, and the geometry design (architecture) of the structure. Open-cell cellular structures that are stretch-dominated have a higher modulus than of a bending-dominated structures with the same relative density. Thus, they are preferred in some engineering applications compared to those of bending-dominated cellular structures. Nonetheless, they are less desirable in lightweight and energy absorption applications in compression because they have a weakening post-yield response due to strut buckling, at variance to the structures that are bending-dominated (Deshpande, Ashby and Fleck, 2001). Hence, bending-dominated structures are preferred for applications require compression resistance.

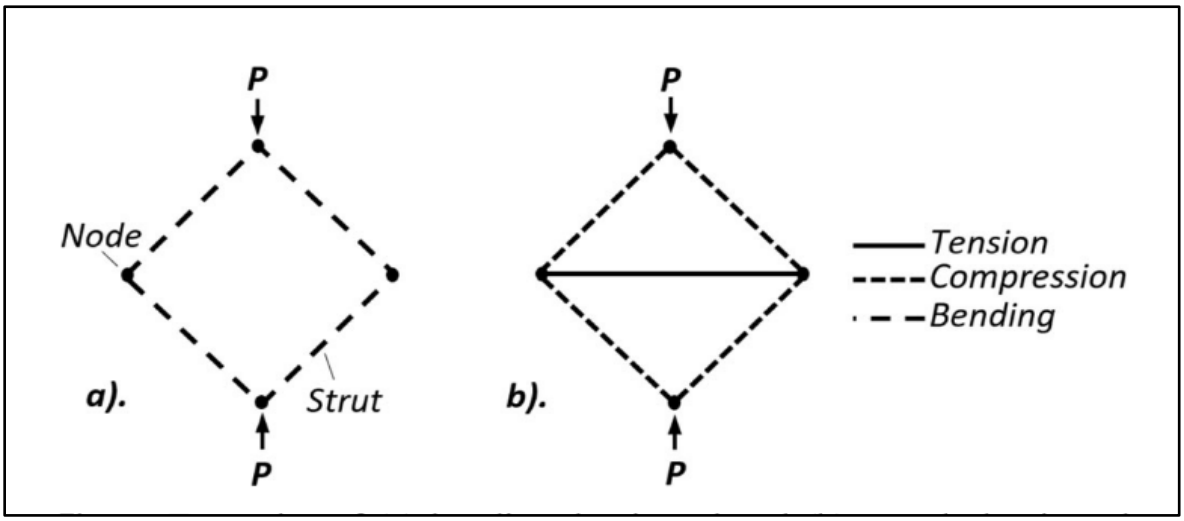

Figure 1-9 An illustration of, **a)** bending-dominated structure, and **b)** stretch-dominated structure (Alghamdi et al., 2020)**.**

1.5 Crashworthiness Parameters

According to the definition of energy absorption and the peak load obtained from a quasi-static test, the average load is described as one of the factors that determine absorbed energy capability. Crashworthiness parameters which are known as energy absorption. Energy absorption capability is classified into volumetric energy absorption (VEA), total energy absorption (TEA), and the specific energy absorption (SEA). SEA is the cross-section area where the material is in contact with the upper edge plate during the deformation (Fazita *et al.*, 2019). In general, it was concluded that the type of design has a crucial effect on the crashworthiness parameters. It can distinctively notice that the crushing force of the Voronoi structures is high, which is compatible with the fact that the Voronoi tessellation is based on the triangular lattice configuration, which is the particular stiffest geometric topology (Gibson *et al.*, 1999).

To further comprehension of the mechanical response of the Voronoi structures, the deformation patterns of the Voronoi structures are shown in Figure

1-10. The deformation shows a Y-shaped joint and an X-shaped joint. When the material was compacted, these joints revolved around the cross-center throughout the compression process until they were crushed. Ordinarily, the rotation of the X-shaped joint could absorb more energy than the rotations of the Y-shaped joint (Yin *et al.*, 2018).

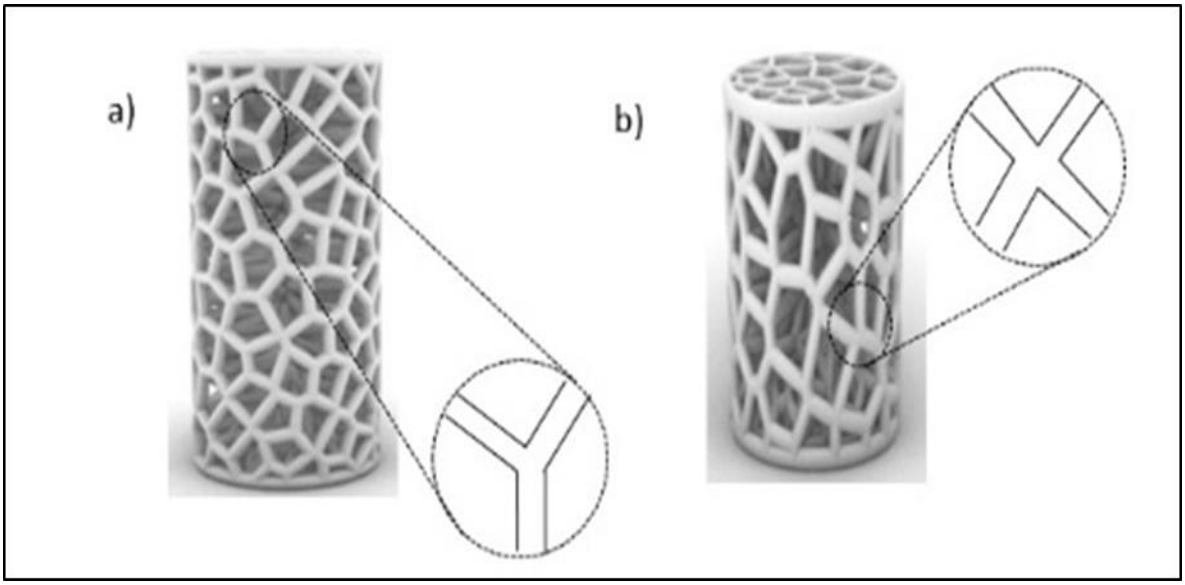

Figure 1-10 Deformation pattern of the 3D: **a)** normal Voronoi structures, and **b)** elongated Voronoi structures.

1.6 Failure Modes of Structures

The Voronoi structures' deformation mode is strictly correlated with the average crushing force (Papka *et al.*, 1998). Therefore, understanding the deformation mechanisms of Voronoi structures is essential. Failure mode involves three subsequent stages of failure starting from the fracture of the cells' strut, cell collapse, and finally, fracture growth (Sienkiewicz *et al.*, 2020).

1.7 Additive Manufacturing Techniques

AM is a kind of innovation that automatically creates physical models from CAD data which operates on a layer-by-layer basis (Ashley, 1991). One of the earliest AM processes is rapid prototyping (RP) that are not similar to subtractive processes, for example, milling, grinding, and lathing, in which material is expelled during the manufacturing process. Figure 1-11 shows the growth rate of the RP process from 1995 to the 2010 year according to the Wohlers, (2012) report. The chart clarifies that the growth rate reached 24.1 % in 2010. In addition, until 2010, the industry's annual rate of growth was 26.2 %. This indicates the wide area occupied by the RP process in the printing of 3D objects. The parts are formed by the accumulation of layers shaped in a 2-dimensional x - y axis plane in a precise manner of all commercial RP forms. Whereas the Z axis is the third dimension created by stacking individual layers on top of one another, but not as a continuous z-coordinate. As a result, the models are extremely accurate in the x - y axis plane but exhibit stair-stepping behavior in the z-direction. If the model is built up with fine layers, i.e., with less z - stepping, the model appears to be unrivaled (Puppi *et al.*, 2010).

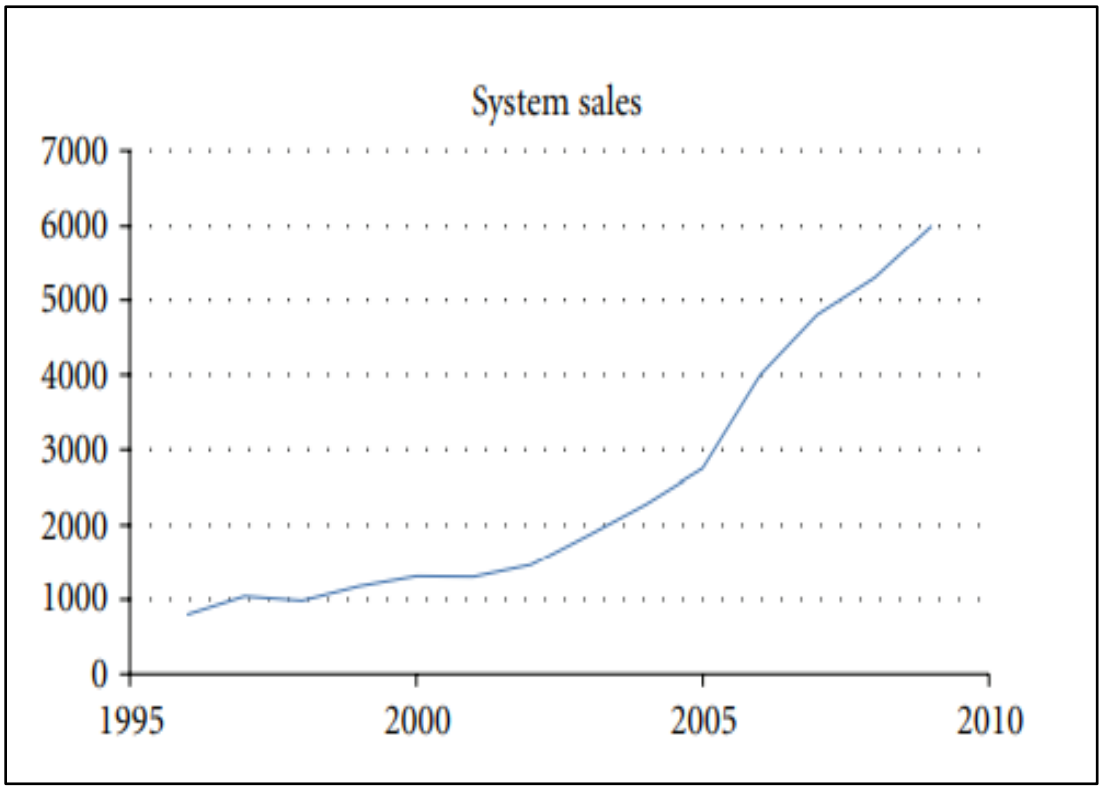

Figure 1-11 Growth of RP process (Wong and Hernandez, 2012).

RP process, as a generative manufacturing process, is divided into two chief process steps: the generation of mathematical layer information and the generation of physical layer models. In general, RP processes begin with a three-dimensional computer model of the component to be manufactured. Computer software slices this digital representation of the part into virtual layers. Each layer, which represents a cross-section of the desired part, is sent to the RP machine and constructed on top of the previous layer. This process of layering the part from the bottom up is repeated until the part is complete. RP systems combine powder, liquid, or sheet materials layer by layer to form physical objects. In addition, certain processes employ thermal energy generated by a laser or electron beams, while others employ inkjet-type printing heads to precisely spray binder or dissolvable onto powdered ceramic or polymer. These technologies are essentially similar in that they combine and link

materials in layers to create objects (Prakash, Nancharaih and Rao, 2018). The stages of the AM process are summarized in Figure 1-12. The beginning is drawing a 3D model with appropriate software with the required dimensions. Then, the drawn model file should be saved in the standard tessellation language (STL) format that can be imported into the 3D AM printer which automatically the printer program starts to slice the model to be capable of identifying by the printer. The method of creating an STL file mostly involves converting the geometry contained in a CAD file into a set of tiny triangles, or a triplet list of coordinates for x, y, and z together with the basic vector for the triangles (Wong and Hernandez, 2012).

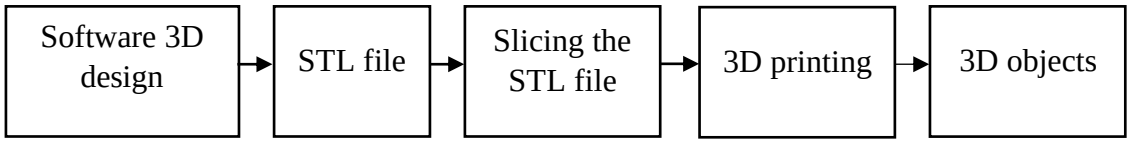

Figure 1-12 3D printing process.

1.7.1 AM Techniques

AM techniques can provide a great degree of control over the design of the manufactured structures, which is perfect for swiftly producing prototypes by AM. Because of the dependency of the 3D printing's cost on the following: printing technique, the material used, and the quantity printed; it has been described as it is both pros and cons (Martelli *et al.*, 2016; Nadagouda, Ginn and Rastogi, 2020). Additional obstacles to the widespread use of 3D printing also include the inability to create monumental structures, the presence of print defects, and a limited selection of materials that are compatible with 3D printing (Ngo *et al.*, 2018). Besides these drawbacks, there are also essential advantages and benefits such as low cost, no need for molds, parts with complex geometry can be produced easily, as well as minimum

waste material, measurement accuracy, and there is no requirement for subsequent operations. Nowadays, 3D printing technologies can be used in a variety of industries, including aerospace, implant applications, and automotive (Çevik and Kam, 2020).

Traditionally, the most widely used AM techniques for fabrication have been categorized into four types based on their manufacturing principle, as illustrated in Figure 1-13:

a) Powder based technique, including Selective Laser Sintering (SLS) and three-dimensional printing (3DP) (Hutmacher, Sittinger and Risbud, 2004; Mota *et al.*, 2015).

b) Solution extrusion-based technique, including Low Temperature Deposition Manufacturing (LTDM).

c) Melt extrusion-based technique, including Fused Deposition Modelling (FDM) (Popescu *et al.*, 2018), and (d) photosensitive based technique, such as stereolithography (SLA).

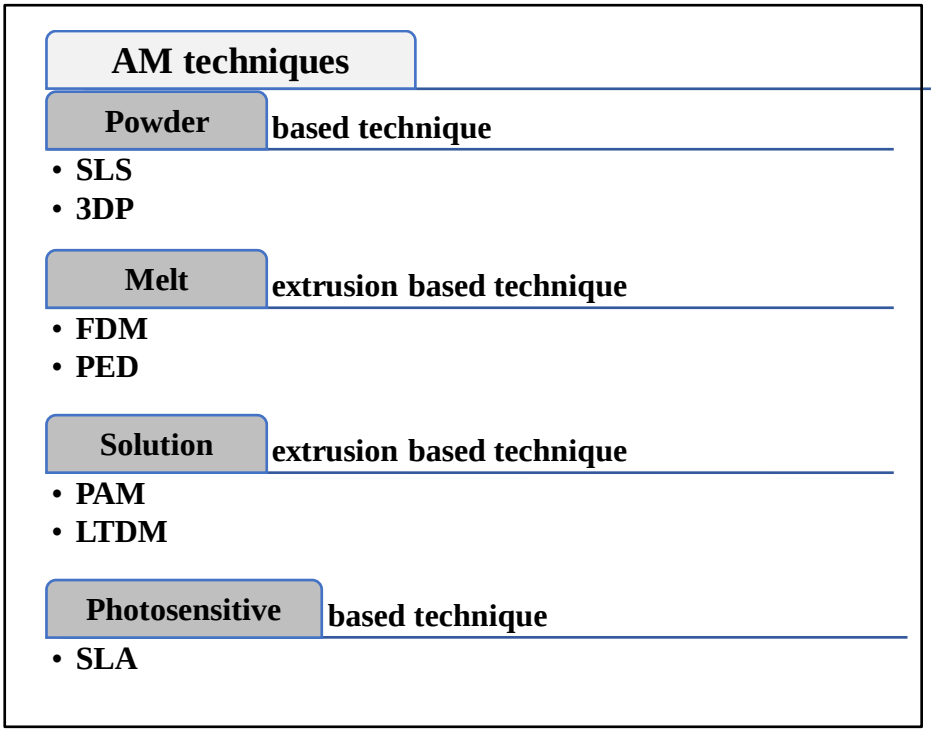

Figure 1-13 Classification of Additive Manufacturing techniques commonly used in 3D printing.

Each technology operates on a distinct principle. For instance, SLS creates three-dimensional parts by using laser energy to heat powder particles in a selectively way, which causes them to fuse together. The particles that have joined together then harden into a 3D body (Charoo *et al.*, 2020). While 3DP technique which originated at the Massachusetts Institute of Technology in the early 1990s, is focused on the controlled deposition of a binder material on a powder bed through an inkjet head (Sachs E, 1990). One of the most popular defects of these techniques is the associated high porosity for the final printed part, powdered surface, binder contamination, and expensive despite the good strength, high quality, and easy removal of support powder (Wang *et al.*, 2017).

Another common technique is LTDM based on solution extrusion. It is a 3D printing technique based on material extrusion and Thermally Induced Phase Separation (TIPS). TIPS dissolves polymer into solvents to create a homogeneous

solution. The polymer solution is then heated to a temperature higher than its melting points. Hence the solution is then cooled to the required quenching temperature. Through the cooling process, the homogeneous solution separates into two phases. Eventually, solvents are extracted using a freeze extraction method. However, there are some obvious flaws such as the limited height of printable objects (Liu et al., 2019). Therefore, a new AM process was developed which based on melting extrusion, one of these processes is the FDM technique. It is a widely viable additive manufacturing process that was created in 1992 for the quick production of industrial prototypes by (Crump, 1992) due to its simplicity of usage, low cost, and suitability for processing standard thermoplastic polymers such as ABS, PLA, and Nylon (Mohan et al., 2017). However, FDM usage is restricted with dimensions greater than 1 cm because of the principle that is built on the extrusion of a polymeric filament through a heated nozzle. In addition, the nozzle clogging and anisotropy (Wang et al., 2017). Stereolithography (SLA) is the most precise technique that is used in manufacturing a complex geometry with a small size.

1.7.1.1 Stereolithography Technique

SLA is the earliest, most developed, and most precise technique among all additive manufacturing techniques, having been adapted to a variety of applications (Melchels, Feijen and Grijpma, 2010; Chen *et al.*, 2019). SLA, as presented in Figure 1-14, is a widely viable additive manufacturing process that was created in 1986 for the quick production of industrial prototypes by Charles Hull (Charles W. Hull, Arcadia, 1986). Stereolithography is based on a process of curing liquid resin with light. The liquid resin is put into a reservoir, and a laser is moved over the surface of the resin to start photo polymerization. This hardens the resin and turns it from a liquid to a solid, usually through a chemical process called cross-linking. (Manapat

et al., 2017). A platform is dropped into the resin, causing the platform's surface to be a layer thicker than the resin's surface. After a layer of resin is hardened, the platform drops a distance with one layer, and the solidification process is performed repeatedly layer by layer until a solid 3D item is created (Wang *et al.*, 2016). The movement of the laser beam controls the pattern generation of each layer (Quan *et al.*, 2020). Which makes it precise enough to print items with intricate structures and tiny dimensions.

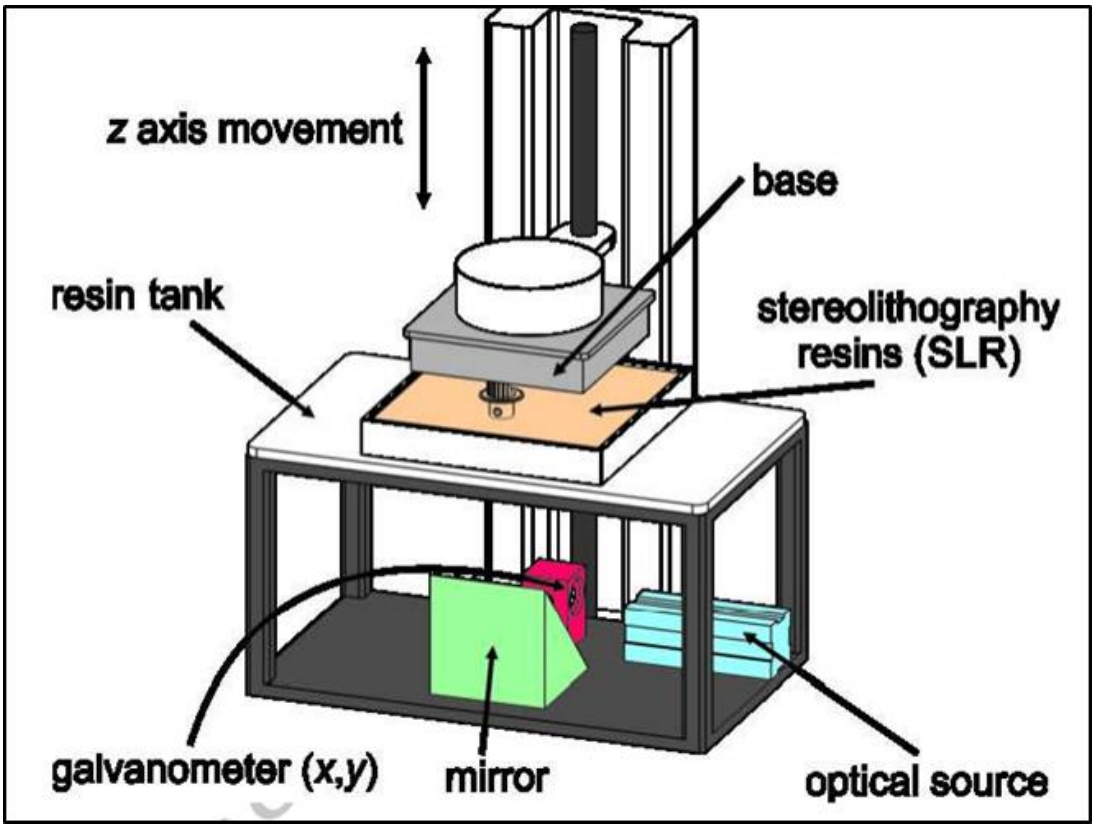

Figure 1-14 The main principle of stereolithography (SLA) (Gross, Lockwood and Spence, 2017).

SLA was employed in a wide range of applications, from consumer goods prototyping to printing living tissues. SLA is still a significant printing process that has applications in numerous fields, including dentistry, automotive, toys, aerospace,

etc. (Asif, 2017). Additionally, SLA has been applied in a variety of bioanalytical applications such as microfluidic devices and BTE including implants and scaffolds (Lee *et al.*, 2015; Alessandri *et al.*, 2016). The road was paved for researchers to print nanocomposites using 3D SLA technology by (Weng *et al.*, 2016).

In addition, SLA ensures fabricating objects based on very small dimensions with complex shapes such as biological scaffolds that form in a specific geometry and include a high percentage of tiny porosities. Recently, researchers depend on the Voronoi tessellation in designing and fabricating scaffolds because it can provide the required porosity with high resolution that easily deals with SLA technique.

SLA 3D printing is preferred by engineers due to its final part precision, smooth surface finish, and mechanical characteristics such as isotropy and material adaptability. One of the best benefits of the SLA method is that it has the smoothest surface finish among of all AM methods, as illustrated in Figure 1-15, and can make pretty accurate measurements within ∓ 0.1 mm (Chua, Leong and Lim, 2010). However, it requires a great deal of time for post-processing, shrinkage inaccuracy due to hardening, supporting structural requirements, and the printing speed decreases as the sample size is larger (Liou, 2007; Manoharan *et al.*, 2013). Moreover, specific types of materials that fit the requirements and limitations of 3D printing.

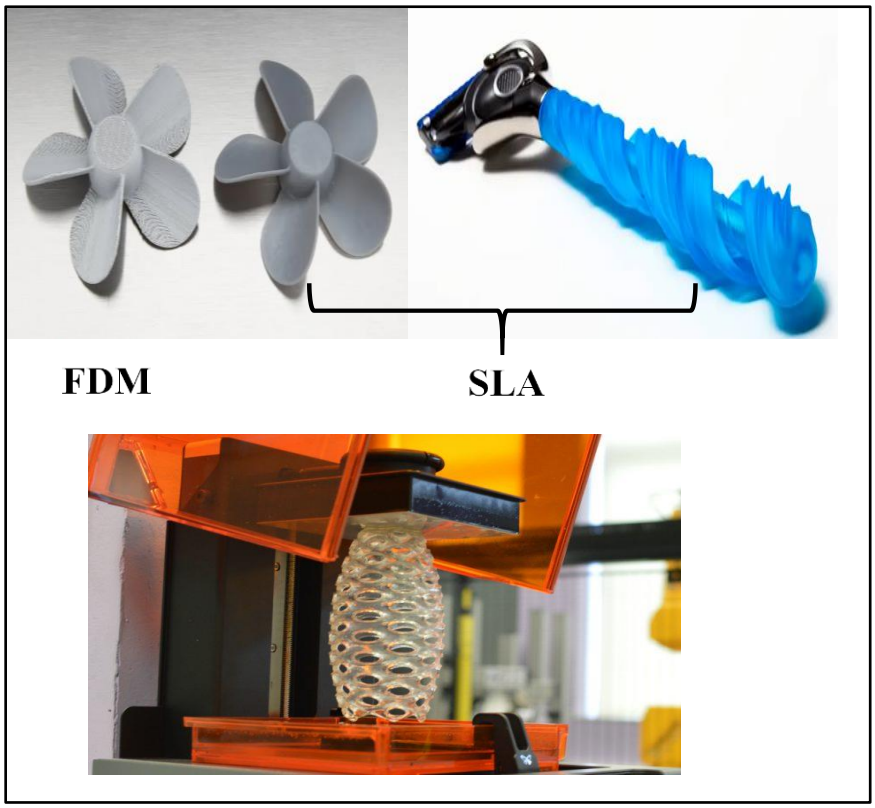

Figure 1-15 An illustration of the difference in surface roughness of the final 3D printed part between the SLA and FDM technique (Formlabs, 2022).

Despite the widespread use of additive manufacturing in many fields due to the aforementioned advantages, choosing this process to manufacture a product is not a trivial task. Closely related to the choice of the type of material used in the manufacture, since not all materials can be compatible with the selected AM technique. Polymer resins are commonly preferred in the SLA additive manufacturing technique for easy compatibility.

1.8 AM Printing Materials

Biopolymers are polymers made or obtained from living creatures such as plants and microorganisms and most (not all) of them are biodegradable. Renewable

resources make up the bulk of biopolymer production (Kandola, 2012). Mechanical behavior, compatibility, cost, stability, and availability are all factors to consider when selecting a biopolymer for 3D printing (Christian, 2016). Biopolymers can be categorized on different scales as shown in Figure 1-16.

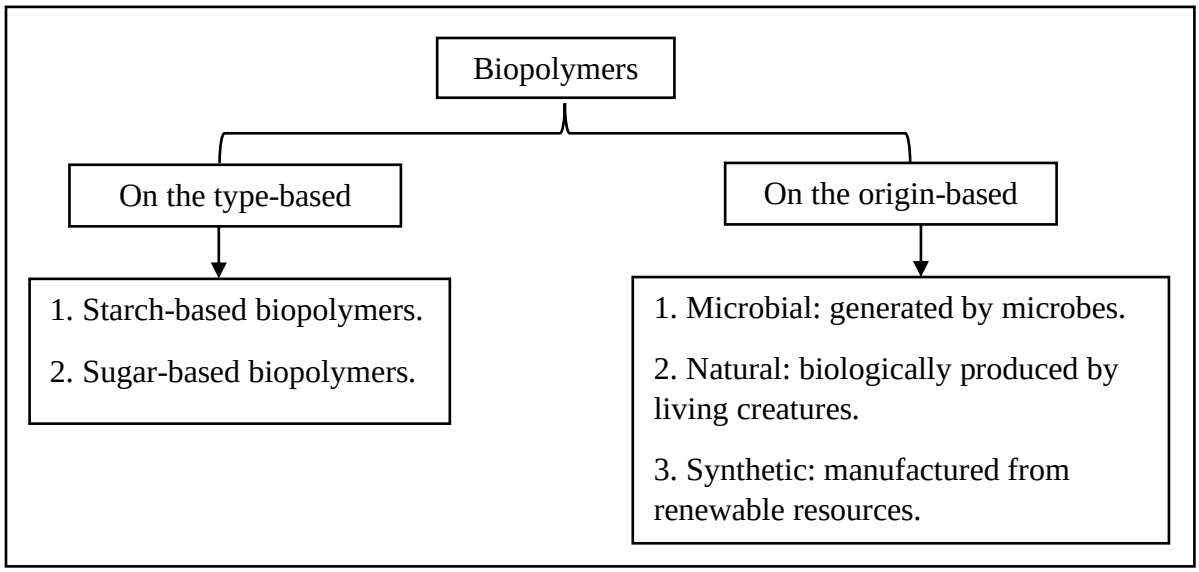

Figure 1-16 Categorization of biopolymers (Vedantu, 1800).

Synthetic biopolymers are the most popular used biopolymers in additive manufacturing. They are divided into non-degradable and degradable polymers. Reddy, Misra and Mohanty, (2012) reported that to manufacture higher-grade polymers, researchers have begun to use genetically engineered crops. Conventional petro-polymers are increasingly being replaced by polymers made from renewable resources due to environmental anxieties, including pollution, the depletion of fossil resources, greenhouse gases, and gas emissions (Jenck, Agterberg and Droescher, 2004; Kümmerer, 2007). Microorganisms break down biodegradable polymers into water and CO_2, and they can be composted and will decompose within a half year.

While the film of the biopolymer must not exceed 20 μm such as Polylactide acid (PLA) (NNFCC, 1945).

PLA has been a leader in these biopolymers that deal with AM because of its favorable mechanical qualities, renewable, easily 3D fabricated with complex geometries, and biodegradability (Tokiwa *et al.*, 2009). In addition, it is a thermoplastic that has a high Young's modulus and strength (Garlotta, 2001; Auras, Harte and Selke, 2004; Raquez *et al.*, 2013). Despite the wide uses and features required by engineers, the high price is the biggest challenge facing synthetic biopolymers (Reddy, 2013).

Therefore, lately, scientists tend to use naturally produced biopolymers widely. Because of their non-toxicity, environmentally friendly features, wide variety, and low cost. Bio-degradable-based materials have been presented as an efficient alternative (Sadeghi *et al.*, 2018). Natural biopolymers can be produced from vegetable oils and proteins, for instance, soybean oil and linseed oil (Khot *et al.*, 2001; Netravali, Huang and Mizuta, 2007). Recently, researchers are seeking to introduce natural plant-based resins into the additive manufacturing field for easy compatibility with 3D printers, and low cost. The main component of plant-based resin is soybean oil.

1.9 Problem Statement

3D structural engineering are oftentimes used to resist the external load in numerous applications due to their desirable mechanical properties such as compression resistance and high strength-to-weight ratio (Zenkert, 1997). However, the usage of these structures is restricted in a few engineering applications such as biomedical due to their rather low compression Young's modulus and stiffness.

Hence, the improvement of these compression resistance has been the subject of an extensive investigation by researchers.

Several solutions have been proposed to enhance compression resistance, the most important of which is topology and geometry modification. Many topologies were investigated such as non-stochastic-lattice (McShane *et al.*, 2006) and stochastic foam (Martínez, Dumas and Lefebvre, 2016; Liu *et al.*, 2021). Foams are classified into several groups, Voronoi tessellation is the most recent popular group. Voronoi-based structures have received a wide attention from researchers in various fields, especially in lightweight applications. Numerous studies have been conducted on traditional Voronoi tessellation. Soro et al., (2022) investigated 3D fabricated biomedical implants based on 3D Voronoi lattice. Their work demonstrated the effectiveness of the Voronoi structure in improving the compression properties, particularly in elastic admissible strain. However, it failed when subjected to buckling, demonstrating the structure's inherent weakness. In addition, the theoretical and numerical blast responses of 3D Voronoi-based with a graded density cellular materials were investigated by (Lan *et al.*, 2018). The results indicated an obvious improvement in compression properties. Nonetheless, the improvement in compression properties remains insufficient to balance strength to weight ratio. Furthermore, the state of the studies has proven that the majority of conventional Voronoi structures lack of mechanical properties such as compression strength (Liu, Lim and Teoh, 2013). Previous studies commend that researchers have conducted research on irregular porous structures in an effort to develop engineering structures with medicinal efficacy. However, the design strategy for precisely managing the mechanical properties of the structure has flaws.

Therefore, choosing an appropriate topology to enhance the mechanical characteristics of a structure is a crucial matter. The cell geometry of the normal

Voronoi-based tessellation has been slightly modified in the current work, and the new structure was named Irregular Elongated Voronoi-based tessellation. The cell struts of the new design interconnect with each other in the form of (X) joints more than in normal Voronoi-based tessellation, which is characterized by high energy absorption (Yin *et al.*, 2018). Correspondingly, a great enhancement in mechanical properties is expected. The modification of the cell topology is carried out by several 3D software such as nTopology (NTopology, 2022), MATLAB (Pelanconi *et al.*, 2020), Voxel-mesh (Owen *et al.*, 2017), and Rhinoceros 7\Grasshopper (Wang *et al.*, 2018). Nowadays, Rhinoceros 7\Grasshopper is the most used software in generating Voronoi tessellation-based objects, because it focuses on creating computer graphics that accurately portray Voronoi curves and uses fewer plugins to facilitate the 3D printing process. González *et al.*, (2023) used it in their work in designing a cylindrical scaffold to assure optimum mesh. Accordingly, choosing Rhinoceros 7\Grasshopper to design the proposed models in the current research will be the most appropriate choice.

1.10 Research Aim and Objectives

The main aim of the current study is to design a lightweight and meantime less dense structure having a geometry that provides improved mechanical properties such as compression resistance. Following is the objective of this research:

- Topology modification of the normal Voronoi structure by making a modification to the cell geometry.

- Propose and design three different 3D models for each normal and elongated Voronoi structure by using a suitable 3D software based on the cell geometry optimization.
- Manufacturing the proposed 3D Voronoi structures by 3D printing, using bio polymeric material.
- Defines the best structural design which achieves the highest compressive and energy absorption properties.

1.11 Thesis Plan

The research plan has been summarized in Figure 1-17. The work of the study can be broken down into three stages: bio-inspiration, sample preparation, and mechanical testing. In the first stage, the engineering design was inspired by existing natural designs due to their high strength and rigidity.

In the second stage, the samples are prepared, which in turn is divided into two parts: firstly, design the models through using the 3D Rhinoceros software, in which the challenge was to design six samples having similar volume and density. Secondly, is the manufacturing part, where the six samples were manufactured by the method of SLA 3D additive manufacturing.

In the third stage, the samples are ready to be subjected to compression testing in order to investigate their mechanical properties and thus select and recommend the best design to be used for lightweight applications.

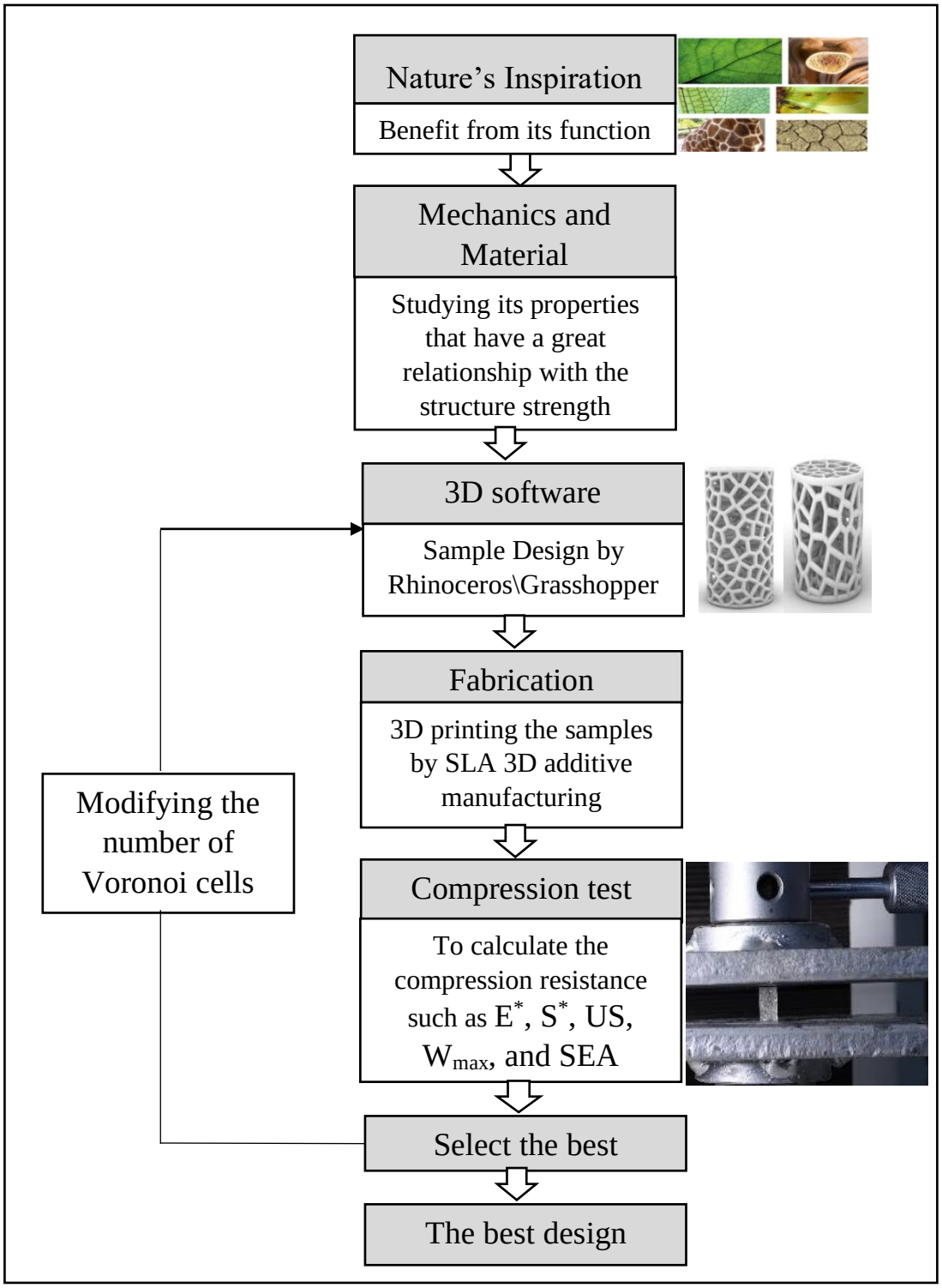

Figure 1-17 Research objective.

1.12 Limitations

AM technology was used to fabricate the designed samples to be subjected to the experimental testing in order to study the mechanical properties. The most significant limitations of this research are the lengthy time required to obtain highly acutely three-dimensional samples (which can take up to 3 days). In addition, a 3D printing printer, the material, and compression test apparatus availability.

1.13 Thesis Outline

Chapter one provided an overview of the study, problems and gaps, and the main goals and objectives of this research. Followed by chapter two, a comprehensive review of previous studies has been conducted for the main determinants of the current research in terms of the methodology used, the composition and mechanism of action of biopolymer 3D printing, as well as many indications of their use in engineering applications.

Chapter three includes the research methodology, as well as the testing procedures that were conducted, including the sample preparation process from the design stage to the printing, and finally toward mechanical testing.

Chapter four discusses the results obtained theoretically and practically from the experimental testing and analyzes and compares the data. Finally, in chapter five, the conclusion of this research work and recommended ideas for future work are presented.

CHAPTER 2

LITERATURE REVIEW

2.1 Introduction

This chapter deals with a summary of the previous conducted studies on the basic terms and expressions of this research. Section 2.2 addresses an overview of the nature inspiration designs and discusses the varieties of designs that found their way into engineering applications. The most important is the topic of Voronoi structures which is explained in section 2.3. In addition, most importantly, the compression properties achieved from nature inspired designs are explained in section 2.4. A brief overview of additive manufacturing and techniques explained in section 2.5, followed by the basic material used in this research in section 2.6. Eventually, the failure modes of the cellular structures are mentioned in section 2.7 followed by the summary of this chapter in section 2.8.

2.2 Bio-inspiration

The development of a unit cell model utilizing dissimilar regular polyhedrons is involved in rule-based geometry design. Chua *et al.*, (2003) used the regular form in the manufacture of scaffolds of different shapes. Where it was found that some of these geometries have poor compression properties and others have complex surfaces that are difficult to fabricate. This lead Gómez *et al.*, (2016) to be inspired to use the Voronoi diagram polygon approach to create a 3D porous scaffold model with internal connectivity. It was observed that the irregular-based design has the benefit over a wide range of geometric shapes and can be utilized to build a parameterized

mathematical model. As a result, it is being used in the creation of cellular models (Kapfer *et al.*, 2011).

Because structural topologies have a significant influence on the mechanical behavior of cellular structures, attempts have been devoted to developing deterministic materials with novel mechanical properties (Alkhader and Vural, 2008; Schaedler et al., 2011). Do, Nguyen and Choi, (2021) highlighted the great effectiveness of the Voronoi structure in cases of structural stability with variable load directions and durability with local flaws. Bone, by its nature, has a high strength in order to withstand sudden shocks and stresses, and from microscopic studies, it was found that this force is widely distributed on the edges, which is what inspired us to design scaffolds that are graded in the structure in terms of stress distribution. Zhao et al., (2021) proposed a gradient scaffold structure based on the Voronoi tessellation method. The results showed that a structure with an irregular and gradient design has better performance in mechanical properties, where all density gathers at the edges, providing optimum structural support for the structures (Jang *et al.*, 2014; Xu *et al.*, 2014) and it provides a stiffer geometry which is confirmed by Finite Element Analysis (FEA) (Öncel and Yaman, 2019).

2.3 Voronoi Tessellation

Numerous studies have been conducted by researchers using two-dimensional (2D) (Zhu, Thorpe and Windle, 2001, 2006; Tekoğlu *et al.*, 2011; Bouakba, Bezazi and Scarpa, 2012) and 3D (Li and Tanaka, 2018; Kladovasilakis, Tsongas and Tzetzis, 2020; Uí Mhurchadha *et al.*, 2021) Voronoi cellular structures. Sotomayor and Tippur, (2014) investigated the effect of both cell irregularity and relative density variation on the mechanical properties of random honeycombs using Voronoi

diagrams. An improvement in stiffness of 66% was recorded when the irregular Voronoi structure replaced the regular one. Contrarily, the plastic collapse strength is directly related to the regularity. Nevertheless, with the increase in relative density, a similar collapse strength was observed for irregular and regular structures. These results were further confirmed by Do, Nguyen and Choi, (2021) when they observed a 150% increase in the stiffness when they replaced a regular Voronoi structure with an irregular substructure. In addition, they highlighted the great effectiveness of the Voronoi structure in cases of structural stability with variable load directions and durability with local flaws. In addition, Lei *et al.*, (2020) proposed an innovative parametric approach for designing Voronoi-based lattice structures is presented to control the porosity. In another work, Deering *et al.*, (2021) studied the anisotropy and durability of the struts for a structure selective Voronoi tessellation-based. Additionally, Voronoi-based structures provide a lower mass that desired in lightweight applications (Piros et al., 2023).

Nonetheless, the mechanical properties of the Voronoi tessellation structures are poorly studied which most of these studies based on finite element simulation due to difficulties in the 3D printing fabrication and cost of testing. Fantini, Curto and De Crescenzio, (2016) proposed a method to design 3D scaffolds for Bone Tissue Engineering (BTE) based on Voronoi lattice structure utilizing Rhinoceros 7\Grasshopper software. However, their method is restricted to cubic shape geometry. While a numerical evaluation of the biomimetic capabilities of the Voronoi-based cellular microstructure was presented by (Frayssinet, Colabella and Cisilino, 2022). Researchers and designers are always looking for ways to reduce the weight of structures while maintaining their structural integrity. Consequently, current mechanical design advancements have a strong bio-inspired influence.

2.4 Compression Properties

The irregular open-cell porous structure ensures uniform stress distribution over regular porous structures (Wu *et al.*, 2022). Open-cell foam structures are based on bending-dominated. Therefore, they have been used extensively lately as enable the creation of structures with low weight and high energy absorption (Pan, Han and Lu, 2020). Numerous application requirements can be met by adjusting the topology of the unit cells (Sigmund, 2000; Bendsoøe and Sigmund, 2007).

One common way to modify the topology is to change the degree of regularity of the standard honeycomb until the desired Voronoi cell is obtained which can enhance some mechanical property; for instance, Young's modulus and stiffness (Lakes *et al.*, 1987). The advent of a range of new manufacturing techniques that permit topology control has accelerated the evolution of cellular core panel structures. Few attempts were being carried out with the goal of developing cellular structures that can actively modify their mechanical characteristics. For example, Niknam and Akbarzadeh (2020) fabricated gradient-type cellular structures with different topologies to study and evaluate the response of the 3D printed cellular structures exposed to a compressive force. Beyond a noticeable improvement in the stiffness and strength, cellular structures offered a decrease in the weight of the structure that required in some applications. Simultaneously, a 69 % increase in energy absorption for an open-cell cellular structure was observed compared to the other designs by (Ghazlan *et al.*, 2020).

Ahmadi et al., (2015) investigated the relationship between the relative density and compressive properties for six kinds of regular scaffolds structures based on different unit cell configurations (cubic, diamond, truncated cuboctahedron, truncated cube, rhombic dodecahedron, and rhombi cuboctahedron). In their study, the geometry of the cell has an obvious influence on the compressive strength and stiffness of 3D-printed samples. Similarly, the work done by Kantaros, Chatzidai and

Karalekas, (2016) clearly shows the dependence of the mechanical properties of scaffolds on the type of unit cell and the unit cell dimensions. Additionally, the 3D truss architecture of the regular scaffold was designed by Shirzad et al., (2021) and they optimized their mechanical and physical properties by the Response Surface Methodology (RSM). In other work, Babaee et al., (2012) studied the role of irregularity of the open-cell Voronoi structure by finite element models. They found that the effective elastic modulus of the Voronoi structure increases with increasing the level of irregularity. Furthermore, an irregular Voronoi structure of about 66 % is stiffer than a regular one under compression response. Additionally, the strength collapse of the regular structure is higher than that of the irregular structure by about 50 % with the same relative density of 3 % (Sotomayor and Tippur, 2014).

Van *et al.*, (2021) reported that the extensions of cell struts enhance the microstructures in addition to the moderate spacing of the cells from each other Wang and Han, (2016). Nevertheless, more stretching of the cells will show low levels of anisotropy (Frayssinet, Colabella and Cisilino, 2022). Furthermore, the increase in the number of seed points, the total surface area increases, hence the average shear stress of the Voronoi cells' walls increases (Paz *et al.*, 2022).

On the other hand, porosity is an essential parameter during design, as previous studies showed the extent to which mechanical properties are related to porosity. In this regard, Zhu *et al.*, (2021) conducted a study on the effect of porosity, as they designed irregular scaffolds structures with different porosities. The results demonstrated that the mechanical property especially elastic modulus decreases as the porosity increases, as illustrated in Figure 2-1. While Du *et al.*, (2019) compared the regular and irregular structures. In their study, the results showed that the irregular structure has superior development potential compared to the regular structure. Certainly, a simple change in the cell geometry of a regular structure leads

to an overall change in structure and an opportunity to improve mechanical properties. Studies in the literature revealed that in addition to the aforementioned parameters, mechanical properties are greatly affected by the way of fabricating the required specimens. Recently, scientists around the world are taking an interest in the recent field of 3D additive manufacturing for its countless benefits.

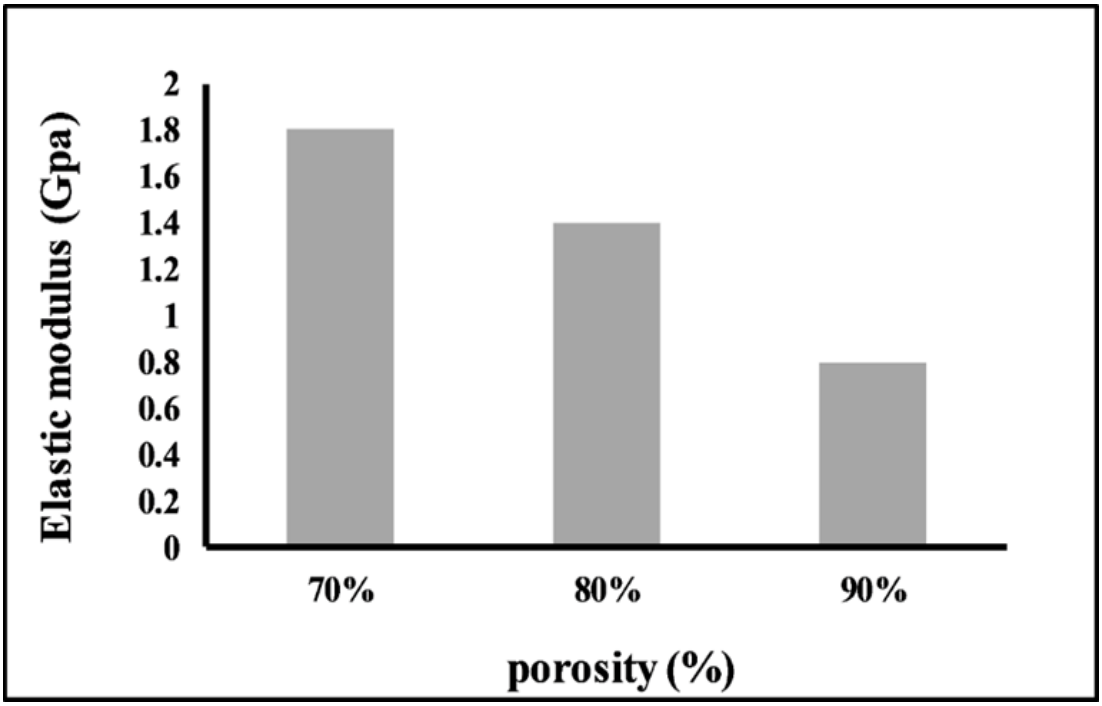

Figure 2-1 Variation of the elastic modulus with porosity (Zhu *et al.*, 2021).

2.5 Additive Manufacturing

Studies in the literature have shown that in addition to the aforementioned factors, the method used to fabricate the required specimens has a significant impact

on mechanical characteristics. The recent field of 3D AM has piqued the curiosity of experts all around the world due to its numerous advantages and its ability to improve mechanical quality.

AM, more commonly referred to as three-dimensional (3D) printing, is one of the most studied techniques today. It is an important technique that has the potential to significantly reduce the cost of manufacturing conventional components made of very expensive materials (Szost *et al.*, 2016). Meantime, AM has generated a generation of amateurs and evolved into a common technology with several uses across various industries. This involves, but is not limited to, aerospace (Murr, 2016), automotive (Gibson *et al.*, 2021), biomedical (Godoi *et al.*, 2018), and manufacturing (Paolini, Kollmannsberger and Rank, 2019). There are numerous additive manufacturing techniques, based on the type of application, the control system, and the size of the pattern to be printed, for instance, stereolithography (SLA). One of the most common techniques in additive manufacturing is SLA, due to its capacity to print complex geometrical pieces cleanly and safely in a friendly environment. SLA technique has been used in manufacturing the structures with very complex and precise designs such as those based on Voronoi tessellation.

2.5.1 SLA Technique

As a first try, three-dimensional antennas of the Sierpinski Triangle (ST) and Voronoi tessellation with high accuracy were achieved by using 3D SLA technology (Bahr *et al.*, 2017). Almonti *et al.*, (2020) produced customized structures based on Voronoi tessellation made from metal foams. The results showed better mechanical properties for 3D SLA printed structures with high precision. In addition, Pasquale

and Barra, (2022) introduced the design and 3D SLA manufacturing of modified orthopedic insoles based on Voronoi tessellation.

In an attempt, a 3D porous scaffold and biodegradable with high porosity, interconnectivity, and uniformity of pore distribution, is designed and processed by the FDM technique (Hutmacher, 2000). However, from Figure 2-2, it can be concluded that the sample has a poor resolution and is anisotropic of the printed sample behavior because of the layer-by-layer FDM process (Chacón *et al.*, 2017). Whilst in another work, Kim *et al.*, (2011) reported that using the SLA technique reduced the roughness of the fabricated scaffold and improved its stiffness, as shown in Figure 2-3.

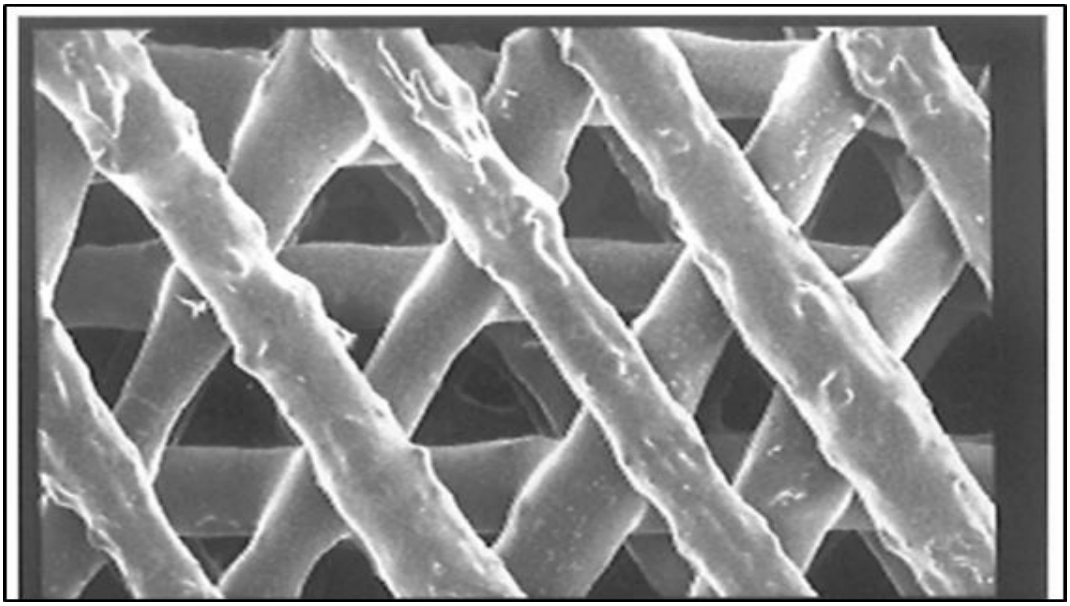

Figure 2-2 3D scaffold fabricated by FDM (Hutmacher, 2000).

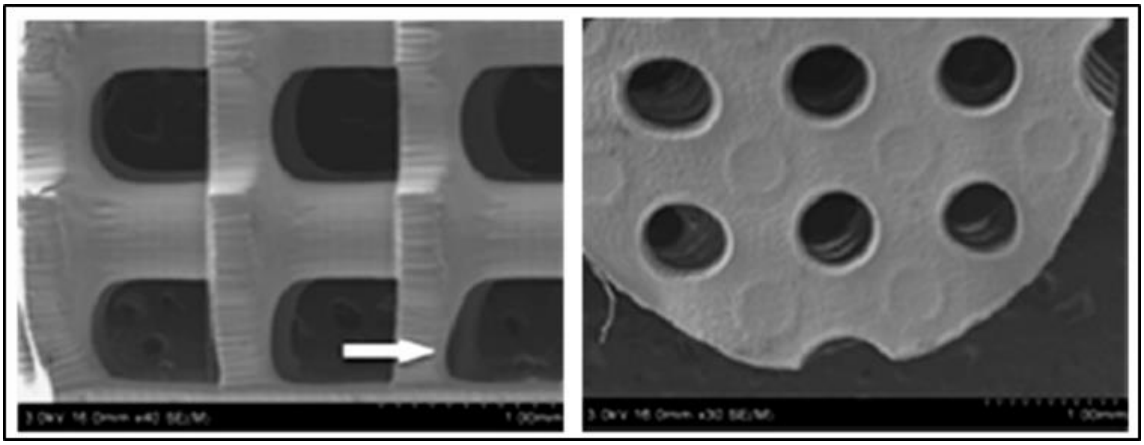

Figure 2-3 The morphology of a fabricated SLA scaffold by SEM (Kim *et al.*, 2011).

There are numerous AM techniques for printing the required samples. Nevertheless, the selection of appropriate and optimal techniques is the most crucial matter. For example, the design that is based on Voronoi tessellation, which can be found in biomedical scaffolds, is based on small pores; hence, a technique that satisfies the fabrication of the smallest details with the highest accuracy is a critical issue in addition to the materials that are compatible with the technique. These requirements can be satisfied by the SLA technique. Therefore, it is selected for the printing of samples in the current research.

2.6 Plant-based Biopolymer

In the last six years, soybean oil products have been widely used in industries, where in 2016 it was used as an important resin in SLA additive manufacturing (Miao *et al.*, 2016). Mondal *et al.*, (2021) used a resin based on soybean oil in the fabrication of biological materials as a prototype and then applied it in the manufacture of bone grafts to repair bone defects. They reported that this resin provides high printability in printing complex shapes with high accuracy. Moreover, it showed a significantly

increase in Young's modulus up to 660 % which is promising for biomedical applications (Noè *et al.*, 2022). In addition, the biodegradability of these resins reaches 19.6 % within 60 days and they have a high potential to be a competitor replacement for traditional petroleum-derived ones while also reducing environmental impact (Lebedevaite *et al.*, 2022).

2.7 Failure Mode

When the cellular structures are exposed under compressive load, the cell begins to collapse gradually. This is due to the fact that the cellular structures contain struts and nodes. Du *et al.*, (2019) reported that stress was mainly concentrated at the joints connected by the struts in a cubic scaffold. Works of literature reveal in most structures, stress was severely concentrated at the sharp edges (Gao *et al.*, 2021). A similar phenomenon of failure was detected in the breaking behavior of lattice structures for diverse additively manufactured materials using the same technique (Pawlak *et al.*, 2015; Liu *et al.*, 2020). Moreover, Chao *et al.*, (2021) studied the failure nature of a Voronoi structure with different porosity levels (70, 80, and 90 %.) using the Finite Element Method (FEM). They found that the maximum Mises stress in porous Voronoi structures is mainly concentrated at the nodes where the connecting rods of the porous structure are connected. They observed that the randomly distributed pores were helpful to promote fragile and brittle pore edges, which led to the concentration of more stresses. The most obvious finding in their study is that the average pore size has a crucial influence on the stress distribution on the connecting rod edges. The smaller the pore size, the higher the stress concentration, which leads to an easier fracture. They suggested that when designing

the Voronoi structure, the appropriate average cell size should be considered more than the porosity percentage.

2.8 Summary

Cellular structures are porous materials that have a high strength-to-weight ratio (Chen, McKittrick and Meyers, 2012). They can be in a regular or irregular geometry. Cellular structures are also divided into two classes: closed-cell where each pore is totally isolated, and open-cell where the liquid can pass through it. Therefore, it is preferred for the fabrication of biological scaffolds. Cellular structures are further classified based on their mechanical properties into stretch-dominated and bending-dominated structures.

Irregular open-cell structures such as those based on Voronoi tessellation offer highly enhanced mechanical properties due to their microstructure topology. In biomedical applications, inevitably, the regular structure with a small change to the unit cell will lead to a global change in the entire structure, and it is difficult to apply local control to the pore shape and the pore size distribution. Thence, the irregular scaffold structure approach has gained attention to overcome these challenges. Numerous irregular designs naturally exist in nature which inspired researchers for adopting them for improved mechanical properties of biomedical applications. Thus, by mimicking nature can get the best design and benefit from its microstructure geometry.

In a conclusion from the aforementioned studies, nature-inspired and Voronoi-based structures are expected to improve mechanical properties in terms of strength and meantime have a lightweight that is much needed in the world of modern manufacturing in many fields, especially structures, aerospace as well as biomedical.

For these reasons, many 3D Voronoi structures will be designed and then fabricated through additive manufacturing. Then, their mechanical properties will be compared, and on the basis of this, the best design will be recommended. Due to its capacity to produce functional parts with complicated shapes, the 3D additive manufacturing stereolithography technique (SLA) is a fast-developing additive manufacturing technology, it will be used in printing the samples of this research.

CHAPTER 3

METHODOLOGY

3.1 Introduction

This chapter deals with the experimental procedures, techniques, materials, software used for designing and fabricating samples of the current work, and experimental testing that is used to evaluate the mechanical properties of the samples. A detailed description of the 3D printing technique, SLA, was given in detail. additionally, the production of six models and designs was explained and presented.

3.2 Used Material

A commercial biopolymer (Plant-based resin is shown in Figure 3-1) made from soybean oil, it is an ultraviolet (UV-curable) liquid used in SLA additive manufacturing because it is truly eco-friendly, biocompatible, has no volatile organic compounds (VOCs), has no harmful chemicals, optimized low shrinkage to provide better printing quality, is sensitive to 355 nm-410 nm UV light, low density 1.39 g/cm^3, and complied with EN 71-3:2013 safety standard. The commercial Plant-based resin (made in China, Shenzhen, Guangdong Anycubic 3D technology company) was purchased from Orange 3D company and its properties are given in Table 3-1.

Figure 3-1 Biopolymer used in samples 3D printing (Anycubic, 2022).

Table 3-1 Biopolymer/Plant-based resin properties (Anycubic, 2022).

Property	Unit	Value
Elongated break	%	8-12
Bending strength	MPa	40-50
Extension strength	MPa	35-45
Vitrification temp	℃	60 ∓5
Viscosity (25℃)	MPa.s	150-350
Shrinkage	%	1.88-2.45
Hardness	D	89

3.3 Used Equipment

3.3.1 SLA 3D Printer

Figure 3-2 shows the ELFIN 3 Mini by NOVA3D printer (Orange 3D printing, Baghdad) which it was used to print the test samples for the current study. Parameters were identified and controlled by NOVA printing control software as follows: layer thickness of 0.06 mm, printing speed of 50 mm/h, 119.8x 67.8x 149.9 mm printing area size, and a 90° printing angle with ± 0.1 mm model tolerance.

Figure 3-2 SLA 3D printer.

3.3.2 Compression Test Machine

The uniaxial compression tests were conducted on six Voronoi-based models with low density specimens using a GOTECH AI-3000 universal testing machine (Mechanics and Civil Testing, Erbil) with a total height of 1570 mm, as shown in Figure 3-3. The speed was kept constant at 5 mm/min. The test was performed in quasi-static condition at a strain rate of 0.001/sec. The applied load and displacement were measured by a digital board, and compression tests were conducted at least four times for each sample. Then, the stress-strain curve was by taking the average of several curves. The apparent stress and apparent strain can be calculated from Eq. (3-1) and Eq. (3-2), respectively (Rychlewski, 1984).

$$\sigma^* = F/A = F/\pi R^2 \tag{3-1}$$

$$\varepsilon^* = \Delta L/L_i = \frac{(L_i - L_f)}{L_i} \tag{3-2}$$

where σ^* is the apparent stress in MPa, F is the applied load in N, A is the cross section area in mm^2, R is the radius of the sample in mm, ε^* is the apparent strain, L_i is the initial length of the porous sample in mm, L_f is the length of the sample after the deformation in mm, and ΔL representing the compressive displacement (mm), based on the concept that the apparent stress is constant over the cross-sectional area and throughout the gauge length.

Figure 3-3 GOTECH AI-3000 controlled testing machine for micro samples.

3.4 Experiment Plan

3.4.1 Constant Factors

In the current work, two shapes of cylinder were designed. The first is the homogeneous coreless cylinder with diameter R of 3.27 mm and height H of 12 mm. Second, is the hollow cylinder with R of 3.27 mm and core diameter r of 1 mm, and H of 12 mm, as shown in Figure 3-4. The thickness was set at 0.1 mm. plant-based biopolymer resin was used to print the samples by SLA 3D printing technique.

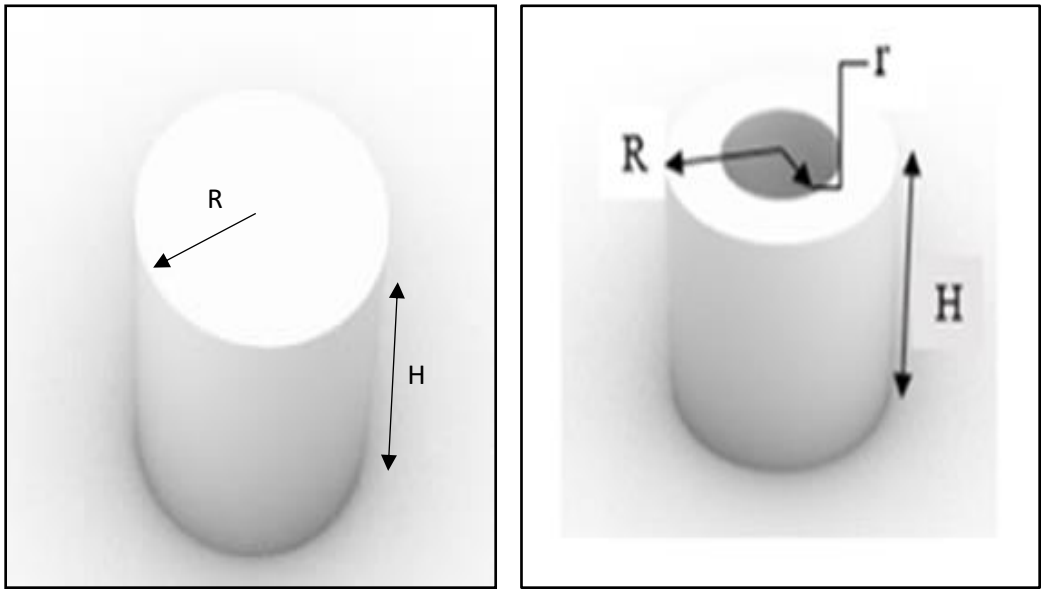

Figure 3-4 The designed cylinder details.

3.4.2 Variables and Levels

The irregular-based design has the benefit of a wide range of geometric shapes and can be utilized to build a parameterized mathematical model. As a result, it is being used in the creation of cellular models. In this work, a new topology bio-inspired was proposed based on three-dimensional Voronoi tessellation to be used in lightweight applications. The new design involved replacing the normal Voronoi (N_v) cell struts with longitudinally elongated Voronoi (E_v) struts in the Z-direction based on bending-dominated properties. Rhinoceros 7/Grasshopper software (version 7.17.22102, Robert McNeel & Associates company, North America, and Pacific) was used to design two groups of 3D irregular cylindrical structure:

1. Irregular Elongated Voronoi Structures (IEVSs).
2. Irregular Normal Voronoi Structures (INVSs).

Each group contained three models; homogeneous cylinder E1 and N1, hollow (with core) cylinder (gradient I) E2 and N2, and filled core cylinder (gradient II) E3 and N3, as shown in Figure 3-5, and their details are presented in Table 3-2.

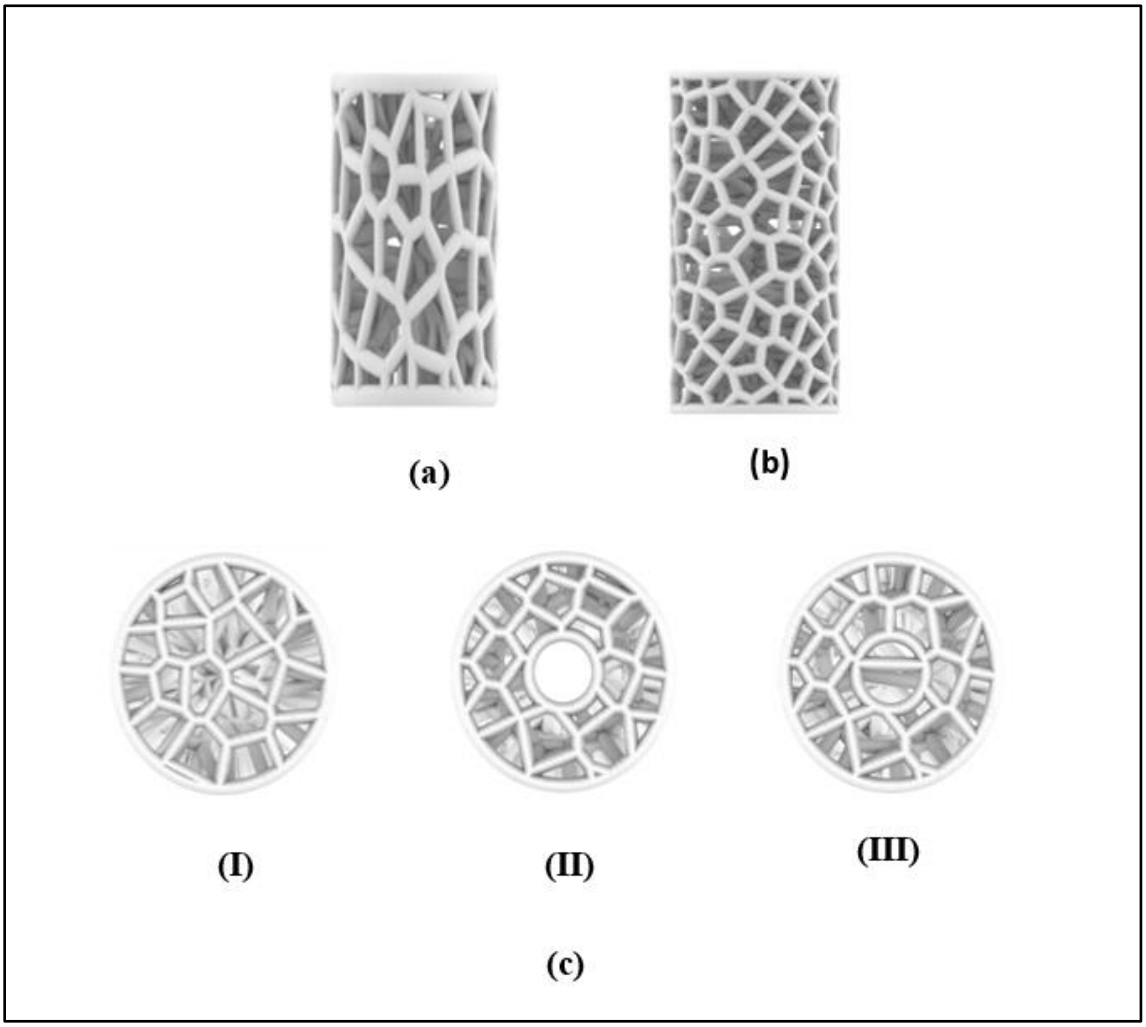

Figure 3-5 An illustration of designed irregular structures. **a)** elongated Voronoi, **b)** normal Voronoi, **c)** the top view of the three models; **I)** homogenous cylinder, **II)** hollow (with core) cylinder (gradient I), and **(III)** filled core cylinder (gradient II).

Table 3-2 The details of the designed models.

Cell strut design	Irregular Voronoi structure	Sample shape	Seed number
Elongated	E1	Coreless cylinder	110
	E2	Hollow (with core) cylinder	125
	E3	Filled core cylinder	100+20 in the core
Normal	N1	Coreless cylinder	200
	N2	Hollow (with core) cylinder	250
	N3	Filled core cylinder	215+20 in the core

3.4.3 Design Limitations

The volume of the structures was controlled by the number of Voronoi cells and thus the density distribution of the sample structure was controlled. All models were kept at the same volume of about 95 mm^3 and 0.0005 g/mm^3 density with a thickness of 0.1 mm and mass of 0.20 g.

3.4.4 Response Data

3.4.4.1 Stress-Strain Curve

The apparent stress and apparent strain are obtained by applying a load to a test specimen progressively and monitoring the resulting deformation. In addition, the form of this deformation can be compression, torsion, and stretching. Numerous properties of a material are revealed through this curve, including the apparent Young's modulus E^*, apparent stiffness S^*, maximum deformation W_{max}, and ultimate strength US.

3.4.4.2 Total Energy Absorption

Energy Absorption is a key parameter in lightweight engineering, especially for structure design in the event of a bone crash. For different geometrical designs, various responses for energy absorption are expected. Hence, TEA is considered an important parameter for the comparison of abilities for these structures based on energy absorption. Usually, the TEA is obtained from the area under the load–displacement curve. Moreover, it is calculated from Eq. (3-3) (Al-Qrimli, 2011):

$$TEA = \int P_{ave}\, d_s \equiv P_{ave}\,(d_f - d_i) \qquad (3\text{-}3)$$

where P_{ave} is the mean crushing force, d_i is the initial crushing distance, and d_f is the final crushing distance. Commonly, TEA is measured with (J) according to the SI.

3.4.4.3 Specific Energy Absorption

Since our proposed models are designed to be used in the manufacture of engineering structures, they require a light weight. Therefore, it is necessary to calculate the SEA of the models. SEA is defined as the total energy absorbed divided by the mass of the sample (AL-Qrimli, Khalid and Mahdi, 2015). As a consequence, this can be determined based on Eq. (3-4):

$$SEA = TEA/MASS \qquad (3\text{-}4)$$

3.4.4.4 Porosity

The porosity has a great effect on the mechanical properties. For the bone scaffold, it was suggested the porosity should be over 50 % and pore size larger than 300 µm (Hollister, 2006; Mantila Roosa *et al.*, 2010; Li *et al.*, 2016). The microstructures of bone are diverse; therefore, the porosity was set around 64 % for all samples, as given in Table 3-3. The porosity was determined by the gravimetric method as shown in Eq. (3-5) and Eq. (3-6) (Hollinger *et al.*, 2002; Maspero *et al.*, 2002; Guarino *et al.*, 2008; Qiu Li Loh; Cleo Choong, 2012).

$$\rho_s = \text{mass/volume} \tag{3-5}$$

$$\text{Total porosity} = 1 - (\rho_s/\rho_{\text{material}}) \tag{3-6}$$

where ρ_{material} is the density of the material, and ρ_s is the apparent density of the structure. It is noteworthy the term of (apparent) accompanies the description for all mechanical properties throughout this thesis due to the fact that our designed samples refer to the Voronoi lattices, not to the base of the material.

Table 3-3 The porosity of the designed models.

Model	E1	E2	E3	N1	N2	N3
Porosity (%)	64 (±1.87)	60 (±1.23)	64 (±0.92)	64 (±0.84)	60 (±1.02)	64 (±0.78)

3.5 Samples Fabrication

3.5.1 Designing the Samples

Rhinoceros 7\Grasshopper software was implemented to generate topologies for the six designs for Voronoi structures. Two groups of irregular cylindrical scaffolds, IEVSs and INVSs, were generated through seeding throughout the fixed volume and density of six models. Figure 3-6 shows the Rhino file of all Voronoi structures.

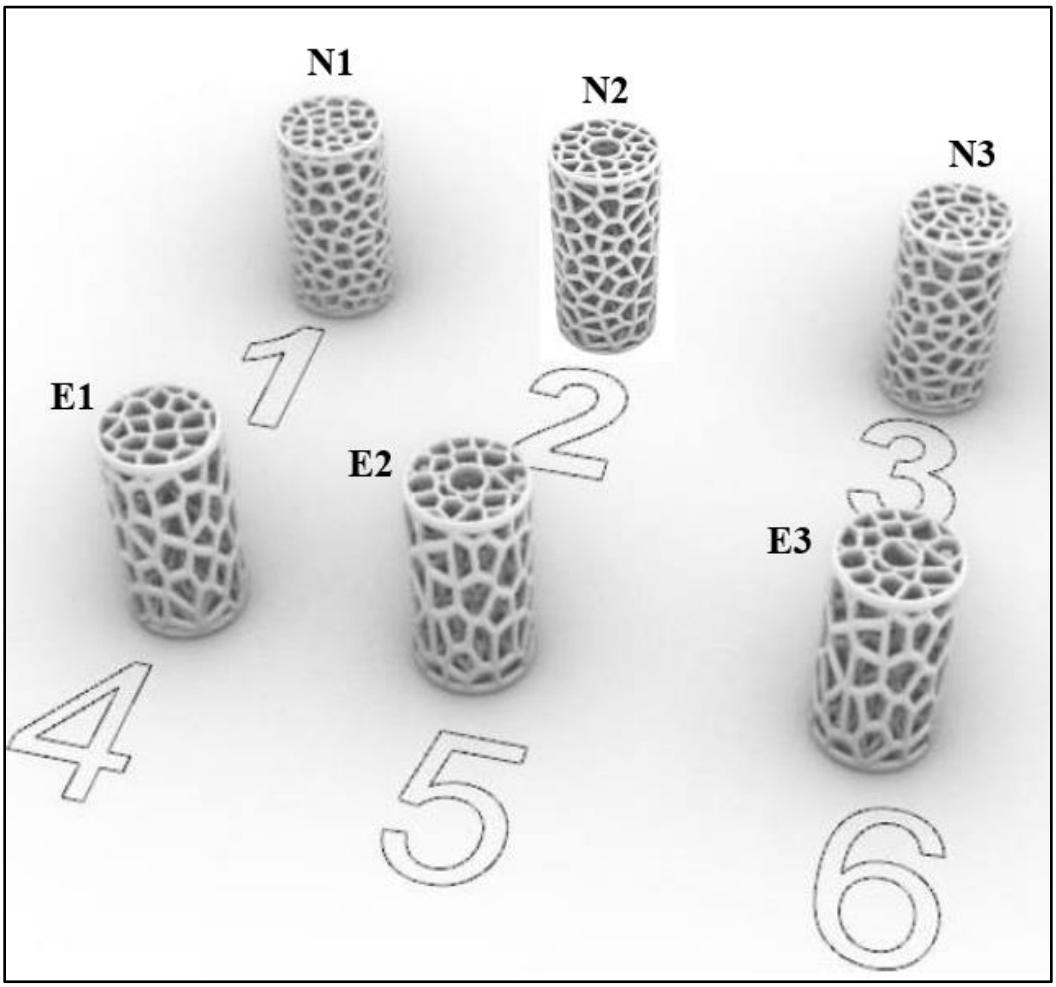

Figure 3-6 3dm Rhinoceros file.

The process of designing the models by software, as indicated in Figure 3-7, began by distributing several points randomly in the 3D cylindrical normal Voronoi structure to obtain a specific volume with defined dimensions. Then, the scale command was applied to create the 3D cylindrical elongated Voronoi structure.

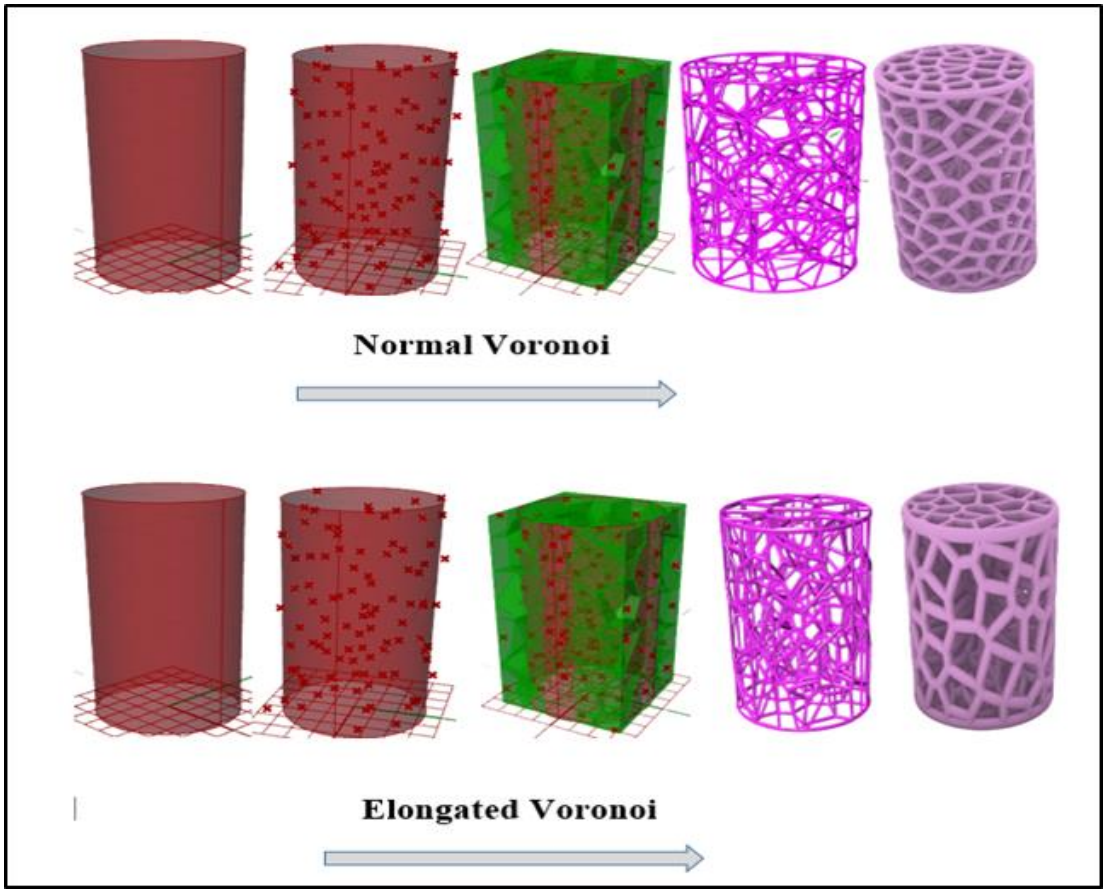

Figure 3-7 Steps of designing the models in Rhinoceros 7/Grasshopper software.

There are several steps to obtaining a normal Voronoi-based design using Rhinoceros 7\Grasshopper software. Firstly, the (cylinder) plugin is used to form a cylindrical shape to the sample model. Then, by using the (3D populate geometry) plugin, a number of seeds are distributed within the cylinder perimeter, and then should be connected to the (3D Voronoi) plugin to create the polygons of the cells.

Subsequently, the (solid intersection) and (deconstruct brep) plugins are used to intersect the Voronoi cells within the center of the cylinder. In addition, the thickness of the cells is controlled by the (cull duplicates) and (smaller than) plugins. Eventually, all plugins must be baked to obtain the final 3D design. The number of seeds was chosen according to the volume balance between all models.

Figure 3-8a shows the Grasshopper file for the homogeneous elongated Voronoi structure, while Figure 3-8b presents Grasshopper file for the homogeneous normal Voronoi structure.

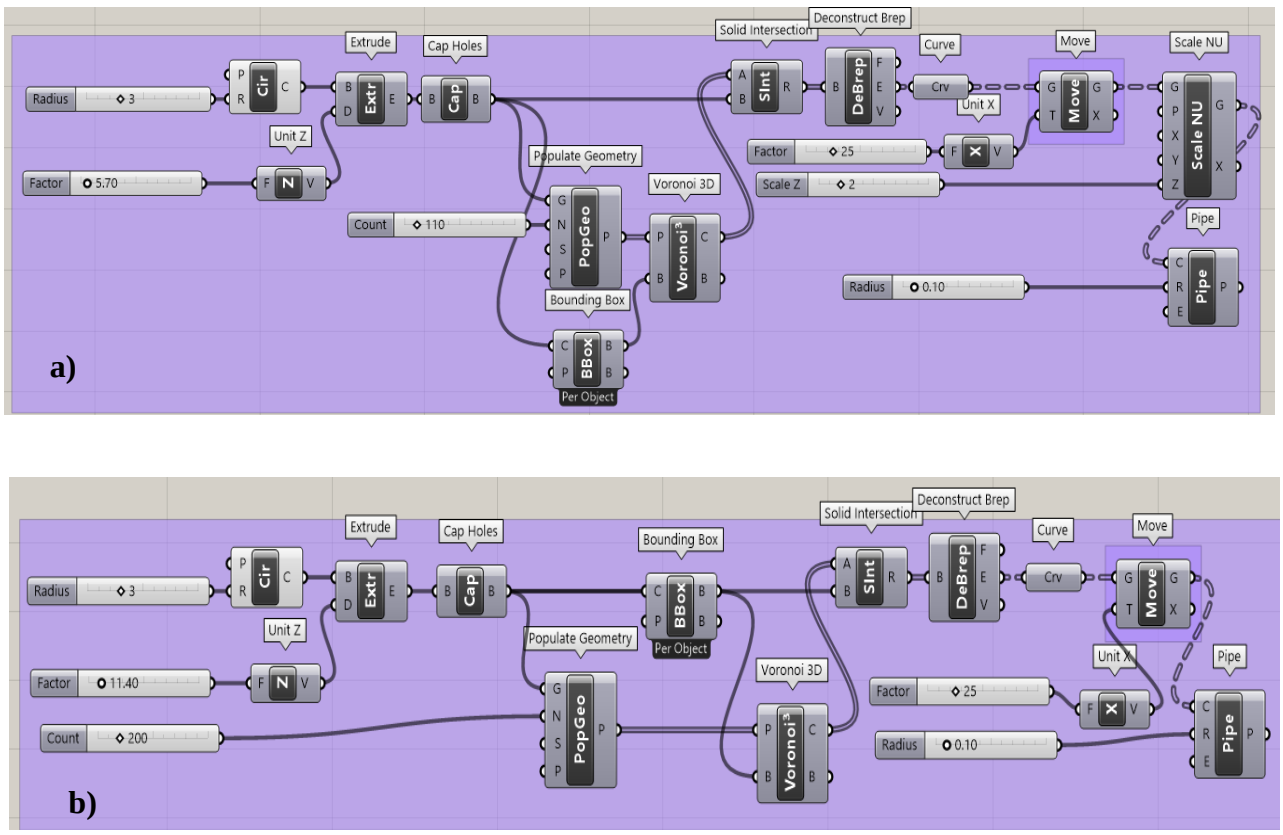

Figure 3-8 The Grasshopper file for the **a)** homogeneous elongated Voronoi structure (E1), and **b)** homogeneous normal Voronoi structure (N1).

Then, the Grasshopper file of each 3D model is saved in the STL format, as shown in Figure 3-9a. While Figure 3-9b indicates the format was imported into the slicing software (Siddique *et al.*, 2019) that divides the CAD model file into tiny data stored in the STL file into horizontal two-dimensional sections that can be addressed by a 3D printer (Gross *et al.*, 2014).

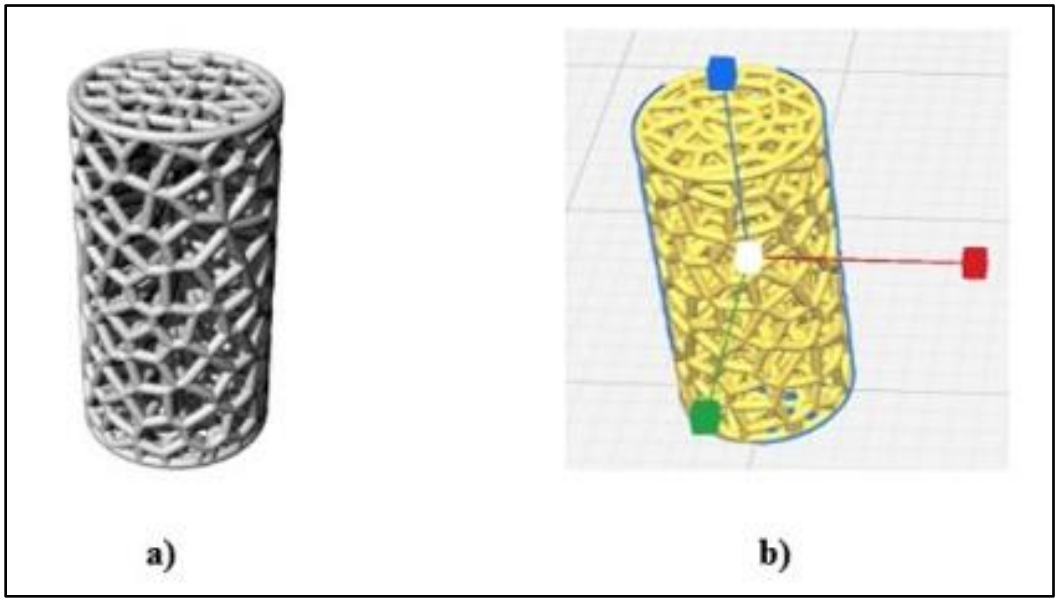

Figure 3-9 Illustration of **a)** STL file, and **b)** slicing software file.

3.5.2 3D Printing of the Samples

The Voronoi tessellation of all 3D models was implemented in Rhinoceros 7\Grasshopper 3D software. The CAD model was used to refer to the designed model. Following the design steps, six samples were saved as an STL file before being sent for printing. The SLA technique was used to print the samples, because of its common use in printing geometric shapes with precise and complex details. The SLA printer contains a build platform which is the place where the part is created. Underneath there is a resin tank, and a clear glass allows the UV laser to

cure the resin. In order to begin the printing, the model file must first be uploaded, and then the tank must be filled with resin up to the limited level. The laser passes back and forth inside, eventually solidifying the liquid plastic. Finally, the printed part is taken out to be washed in rubbing alcohol to remove the excess resin, as indicated in Figure 3-10.

Figure 3-10 An illustrative of the printed samples.

3.6 Compression Test

Numerous compression properties of a material are revealed through the stress-strain curve, including the apparent Young's modulus E^*, apparent stiffness S^*, maximum deformation W_{max}, and ultimate strength US. There are two ways to draw this curve: the conventional stress-strain diagram and the true stress-strain diagram (Goodno, 2013). In the current study, the conventional method was used in which the engineering stress can be calculated by dividing the applied load by the cross-sectional area of the sample (Eq. (3-3)). In order to compare the mechanical properties of the models, the apparent Young's modulus and stiffness were calculated from Eq. (3-7) and Eq. (3-8), respectively, while ultimate strength could be determined precisely from the apparent stress-strain curve.

$$E^* = \sigma^*/\varepsilon^* \tag{3-7}$$

$$S^* = F/\Delta L \tag{3-8}$$

CHAPTER 4

RESULTS AND DISCUSSION

4.1 Introduction

This chapter deals with the results obtained from experimental testing to respond to the statement of the problem of the current research. Section 4.2 presents the numerous results obtained from experimental testing to explore the Voronoi structures' compression properties, and how the manufactured samples' cell geometry modification influences the apparent Young's modulus and the apparent stiffness. The relationship between the amount of energy absorbed with the modification and the total energy absorbed per the mass of the sample are showed in section 4.3. Eventually, the deformation behavior of the Voronoi structures under the load is discussed in section 4.4.

4.2 Compression Resistance

Sufficient compressive strength is a primary and prominent requirement for structures in lightweight applications. Hence, a compressive strength test was essential for evaluating the compression resistance of different Voronoi designs. The compressive test was repeated four times for each sample, and the average value of these four tests is reported here. Figure 4-1 illustrates the stiffness of the Voronoi structures' with different designs. The stiffness of the structures can be determined by the load–displacement curve. Both E1 and N1 broke at similar displacements with a stiffness of 352.5 ± 0.98 N/mm for E1 and a stiffness of 380.3 ± 1.02 N/mm for N1. Similarly, E2 and N2 fractured at similar approximate displacements: E2 with a stiffness of about 286.9 ± 1.06 N/mm and N2 with 272.8 ±1.04 N/mm stiffness. It is

noteworthy that the gradient I Voronoi structure for both E2 and N2 shows the lowest stiffness among the three designs. However, the gradient II Voronoi structures (E3 and N3) showed a different trend, E3 recorded a maximum displacement which is the highest among all samples with a stiffness of 302.8 ±0.95 N/mm, while N3 recorded a stiffness of 336 ±0.94 N/mm. It reveals that it is stiffer than the gradient I Voronoi structure due to the improved geometric design with the filled core which made it bear the load with a higher displacement. It is noticeable that the normal Voronoi structures are stiffer than the normal Voronoi structures

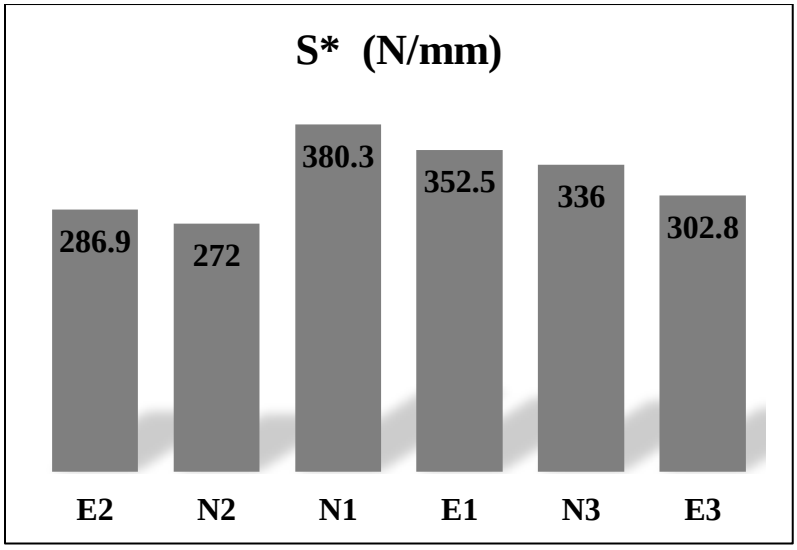

Figure 4-1 Stiffness of the Voronoi structures.

On the other hand, Figure 4-2 displays the Young's modulus of the various designs. It is clear that the elongated Voronoi structure gradient I type (E2) has the highest apparent Young's modulus of about 142 ±0.66 MPa, this is due to the microstructure and design features where all density gathers at the edges, providing optimum structural support for the structures. While, the gradient II Voronoi structure (E3 and N3) has the lowest record of Young's modulus of about 115 MPa and 112 MPa, respectively. This is due to the highest porosity which leads to break

under the influence of lesser stress. Whereas structures with high porosity are typically weaker because the pores cause Voronoi cells to be separated by a greater distance, structures with low porosity are stronger (Paz *et al.*, 2022). Furthermore, it is significant to mention that the value of Young's modulus for both the homogeneous and gradient of the elongated Voronoi structure obtained in this work is superior to that obtained from Shirzad *et al.*, (2021) study of 94% for the cubic non-stochastic truss-based scaffold structures with a porosity of 56.45%.

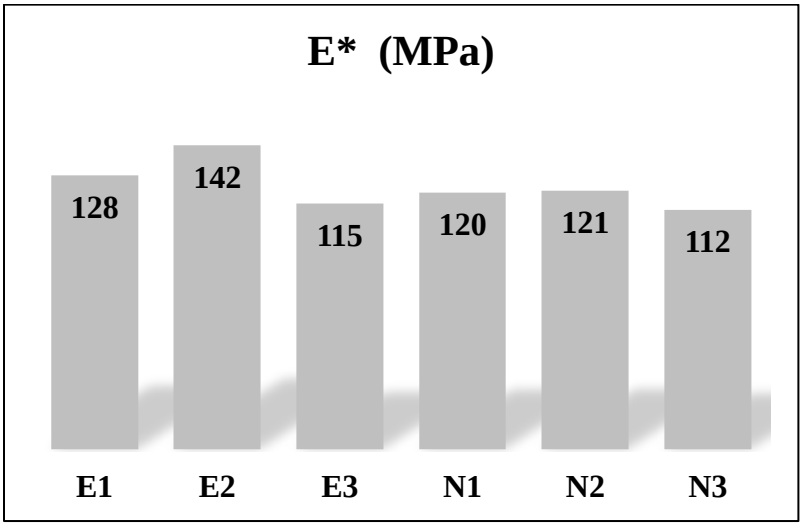

Figure 4-2 Young's modulus of the various Voronoi structures design.

In regard to the other properties, Figure 4-3 demonstrates the ultimate strength and the maximum deformation of the designed Voronoi structures. It is clear that the greatest ultimate strength is achieved by the elongated Voronoi structure homogeneous type (E1) with 29.00 ±0.12 MPa, this is due to the fact that when homogeneous structures are subjected to a load that will be distributed largely evenly over all parts of the structure, and thus the structure absorbs the largest amount of energy. Moreover, the normal Voronoi structure of homogeneous type (N1) shows a maximum stiffness of about 380.30 ±1.02 N/mm, it has to be mentioned, that there

was no significant difference between the two types of designs (elongated and normal Voronoi) in terms of maximum deformation. The ratios are either very close or exactly equal, as in (E1 and N1) and (E2 and N2), respectively, except for the designs (E3 and N3) in which there is a colossal difference, where the gradient II elongated Voronoi structure is 43 % superior to the normal Voronoi structure.

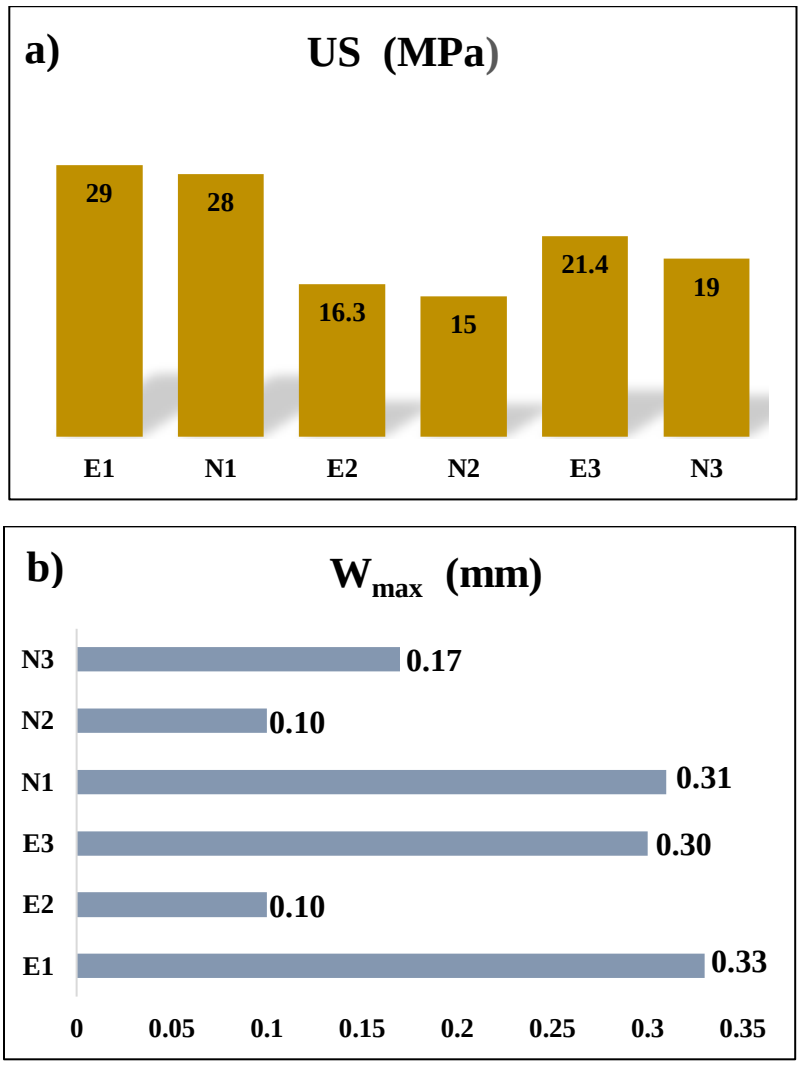

Figure 4-3 Compression properties of the six Voronoi structures. **a)** the ultimate strength, and **b)** the maximum deformation.

The experimental results indicate changes in the cell geometry of Voronoi structures could lead to a completely different mechanical performance. Figure 4-4a,

b, and c displays the apparent stress-strain curve of all the 3D Voronoi structures ((E1 and N1), (E2 and N2), and (E3 and N3)). It is evident from the data that apparent strain increases with increasing load, and all designs exhibited a linear increase in apparent stress up to a specific apparent strain value, after which it shifted to a more moderate relationship between these two parameters. Figure 4-4a clarifies the apparent stress-strain comparison for both homogeneous designs (elongated and normal Voronoi structures). It is clear a that both have linear behavior until they reach the same apparent strain of 0.1. Nevertheless, E1 has higher apparent stress than N1 of about 19.2 MPa and 18.8 MPa, respectively, because the extensions of cell struts enhance the microstructures. The apparent stress then begins to rise by gradually increasing the apparent strain until the samples reach maximum deformation and are fractured at an apparent strain of 0.3 for both E1 and N1 with apparent stresses of 28.2 MPa and 27.0 MPa, respectively. Although E1 appears to withstand more apparent stress than N1, the difference is very small, and its effect is negligible when used in applications that are based on pressure. Unlike the homogeneous design, the gradient Voronoi structures show a noticeable difference in withstanding the applied load. Figure 4-4b illustrates that the maximum apparent stress of E2 (16.1 MPa) outperformed that for N2 (15.3 MPa) due to the moderate spacing of the cells from each other. However, they broke at a lower apparent strain (around 0.1). This indicates that, despite the fact that the gradient I E2 begins to deform at higher apparent stresses than the gradient I N2, they do not withstand the high apparent stresses achieved by homogenous designs (E1 and N1). Furthermore, their maximum apparent stress is also lower than the gradient II Voronoi structures (E3 and N3), which in turn is lower than the homogeneous Voronoi structures, as shown in Figure 4-4c. In addition, the maximum deformation reached 0.33 for E1 and 0.31 for N1, respectively, which is higher than gradient I Voronoi structures and somehow similar to those for the homogeneous Voronoi structures.

The experiment results and analyzes indicated that the elongated Voronoi structures achieved high results and outperformed the normal Voronoi structures in achieving improved compression properties because the elongated Voronoi structures were designed with a lower number of seed points than the normal Voronoi structures. It is noteworthy that different kinds of homogeneous and gradient Voronoi structures record considerable variation in several compression properties despite the little difference in porosity among them. This is due to the microstructure and cell geometry design features. In conclusion, the relatively high improvement in mechanical properties of the IEVSs compared to the INVSs can be justified by the geometry optimization of the cell struts to the Z-direction, which provides direct support for the applied load.

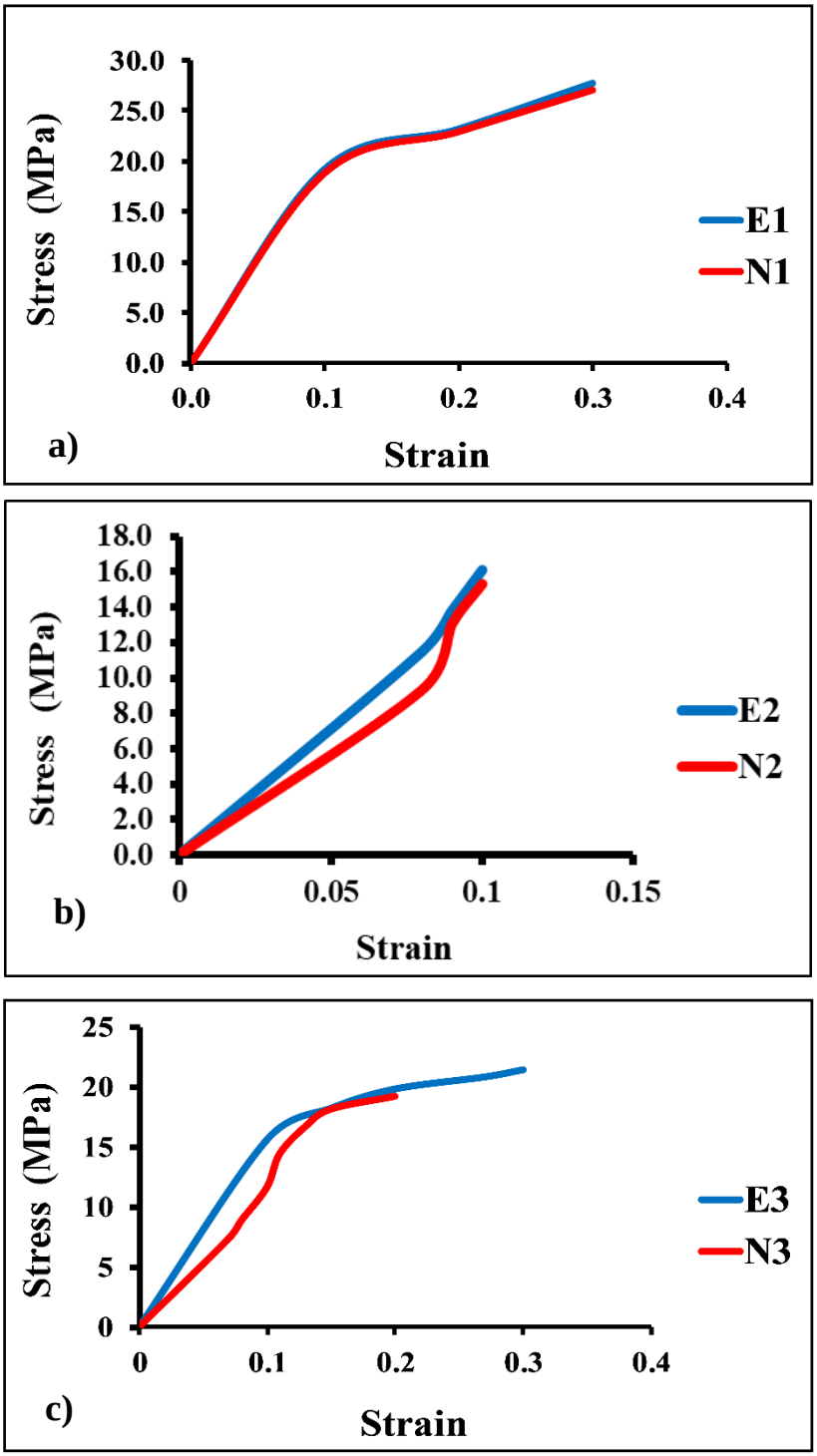

Figure 4-4 Stress-strain curve for the six samples under uniaxial compression load. **a)** homogeneous model for elongated (E1) and normal (N1) Voronoi structures, **b)** gradient I model for elongated (E2) and normal (N2) Voronoi structures, and **c)** gradient II model for elongated (E3) and normal (N3) Voronoi structures.

4.3 Energy Absorption

Figure 4-5a, b, and c shows the comparison between the energy absorption and displacement for 3D Voronoi structures (E1 and N1), (E2 and N2), and (E3 and N3), respectively. It is noticeable that the relationship between energy and displacement demonstrates an increasing trend for both structures (elongated and normal Voronoi). From Figure 4-5a, it is clear that for the homogeneous structures (E1 and N1), the rate of increase in displacement up to 1.0 mm results in a minor rise in energy absorption. However, a further rise in displacement (more than the mentioned rate) results in a ramping up of energy absorption reaching a plateau at 4.0 mm. This result reveals that further displacement is beneficial for both structures to improve their energy absorption, and it indicates that the two designs show similar behavior in energy absorption improvement. Meanwhile, Figure 4-5b presents the comparison between the energy absorption and displacement for the gradient I (E2 and N2) structures, similarly, the increment of the displacement up to a certain value 0.8 mm results in a moderate improvement in energy absorption for both models. Nonetheless, when these samples are subjected to a higher rate of displacement, it causes an abrupt enhancement of energy absorption reaching the maximum of 0.55 J at a displacement of 2.0 mm for E2, and 0.37 J at a displacement of about 2.0 mm for N1. Yet, the gradient II structures (E3 and N3) show better performance in terms of energy absorption than the previous design (gradient I). This can be seen from Figure 4-5c that the greatest energy absorption was obtained at 4.0 mm displacement with approximately 1.79 J for E3, and displacement of 2.2 mm with an energy absorption of about 0.80 J for N1. It is noteworthy that despite the similar displacement trend of both designs, the elongated Voronoi structure resists fracture at a higher displacement rate than the normal Voronoi structure. Hence, considerable energy absorption is presented when the elongated Voronoi structures replaced the

normal Voronoi structures. Whereas, the homogeneous design achieved the highest values, followed by gradient type I and finally gradient type II which has a core in the middle with fewer seeds point that made it weaker. To compare the elongated Voronoi and the normal Voronoi, it can be noticed that the elongated structure provides higher values than the normal in all models due to the fact that the stress was severely concentrated at the sharp edges, and a normal Voronoi structure has a higher number of sharp edges compared to elongated Voronoi which can lead to the earlier failure in normal Voronoi structures.

The current study paved away for designers and researchers to optimize the cell geometry by seeds distribution, irregularity, porosity variation and other parameters for elongated Voronoi structures. It is clear that changing parameters for the elongated Voronoi structures can significantly alter several mechanical properties based on the desired application.

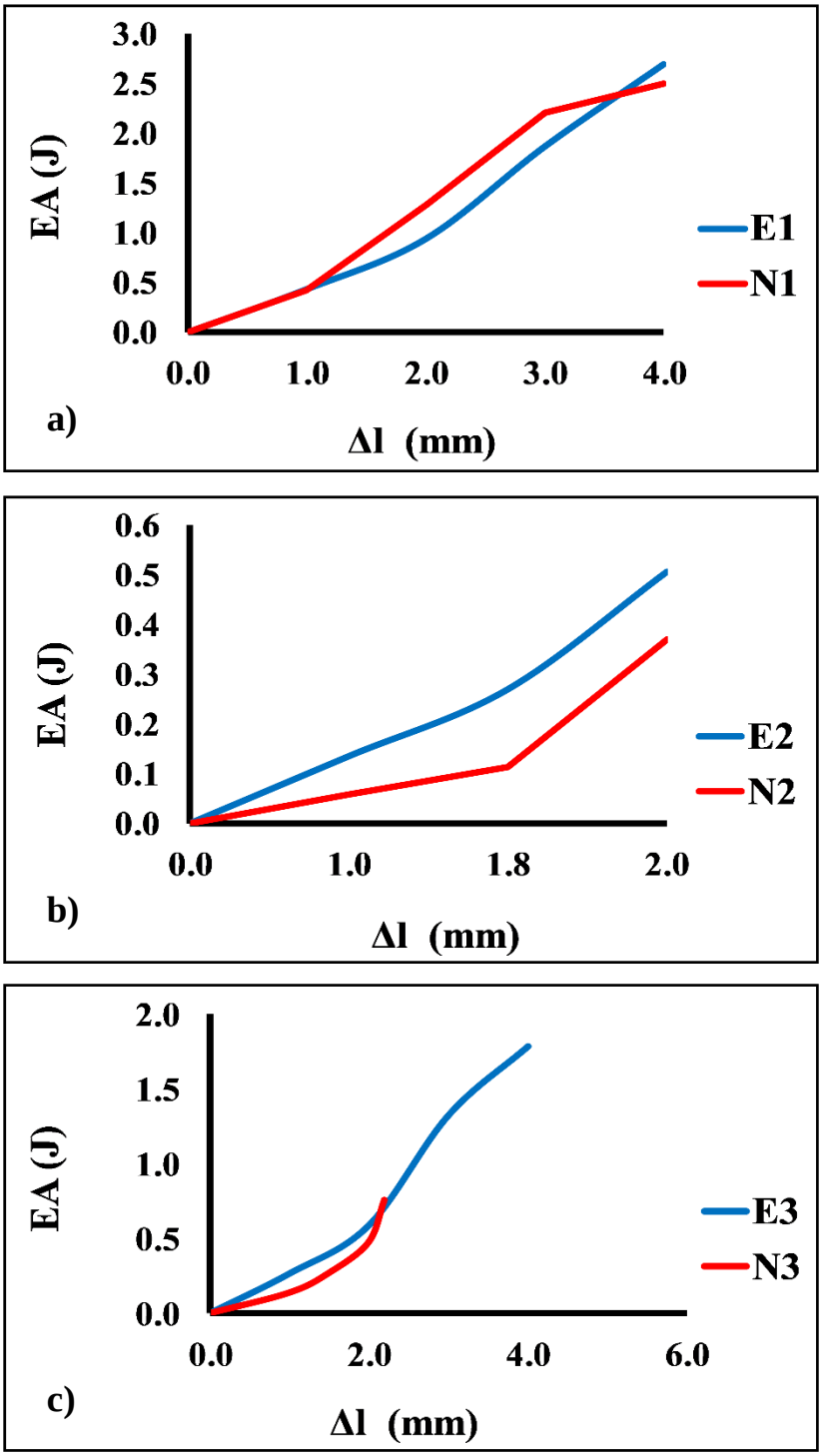

Figure 4-5 Variation in energy absorption (EA) as a function of displacement for the six Voronoi structures. **a)** homogeneous model for elongated (E1) and normal (N1) Voronoi structures, **b)** gradient I model for elongated (E2) and normal (N2) Voronoi structures, and **c)** gradient II model for elongated (E3) and normal (N3) Voronoi structures.

Moreover, the SEA for all six designs is illustrated in Figure 4-6. It is noticeable that comparing the two types of designs, the elongated Voronoi structures achieved a higher rate of specific energy absorption, as they outperformed the normal Voronoi structures with the same relative density at constant crushing velocity. It is important to mention that there are more X-shaped joints in elongated Voronoi structures than in normal Voronoi structures. This might be the reason, why the elongated Voronoi structure has a higher energy absorption capacity than the normal Voronoi structure. The homogeneous design (E1) features have the best performance among the six Voronoi topologies with a specific energy absorption of 52.45 J/g, followed by N1 with a specific energy absorption of 45.74 J/g. On the contrary, the lowest performance is provided by the gradient I (N2) with a specific energy absorption of about 6.27 J/g.

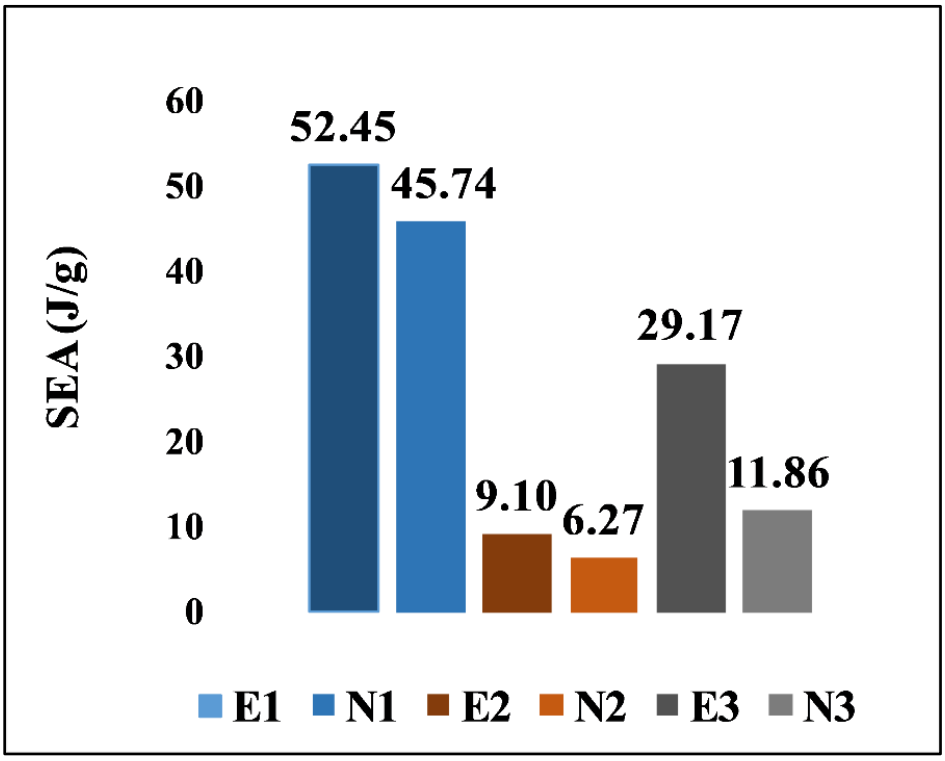

Figure 4-6 Specific energy absorption of the six models.

4.4 Failure Modes

Figure 4-7 shows the failure mode for a homogeneous elongated Voronoi structure. The failure mode is the same for all samples. The cylindrical Voronoi cells all collapsed completely due to a failure mode incorporating three successive stages of failure beginning with strut fracture, followed by the collapse of the cell, and finally fracture growth. Works of literature reveal in most structures, stress was severely concentrated at the sharp edges, and a normal Voronoi structure has a higher number of sharp edges compared to elongated Voronoi which can lead to the earlier failure in normal Voronoi structures. Moreover, the elongated Voronoi structures in the current study have larger pore sizes, they can carry larger apparent stresses and loading before they start to be fractured. This is a reason for the compression properties' improvement in the current study. In addition, no buckling behavior was observed in the structures because the Voronoi cells consist of inclined struts, which provide support for the structure to tolerate the buckling load. Thus, they are desirable for load-bearing applications because they provide stability and easy predictability of the mechanical response.

It is evident that the enhanced mechanical properties such as stiffness, energy absorption, and progressive failure mode in the Voronoi structures are all associated with the introduction of the internal triangular lattice of Voronoi tessellation.

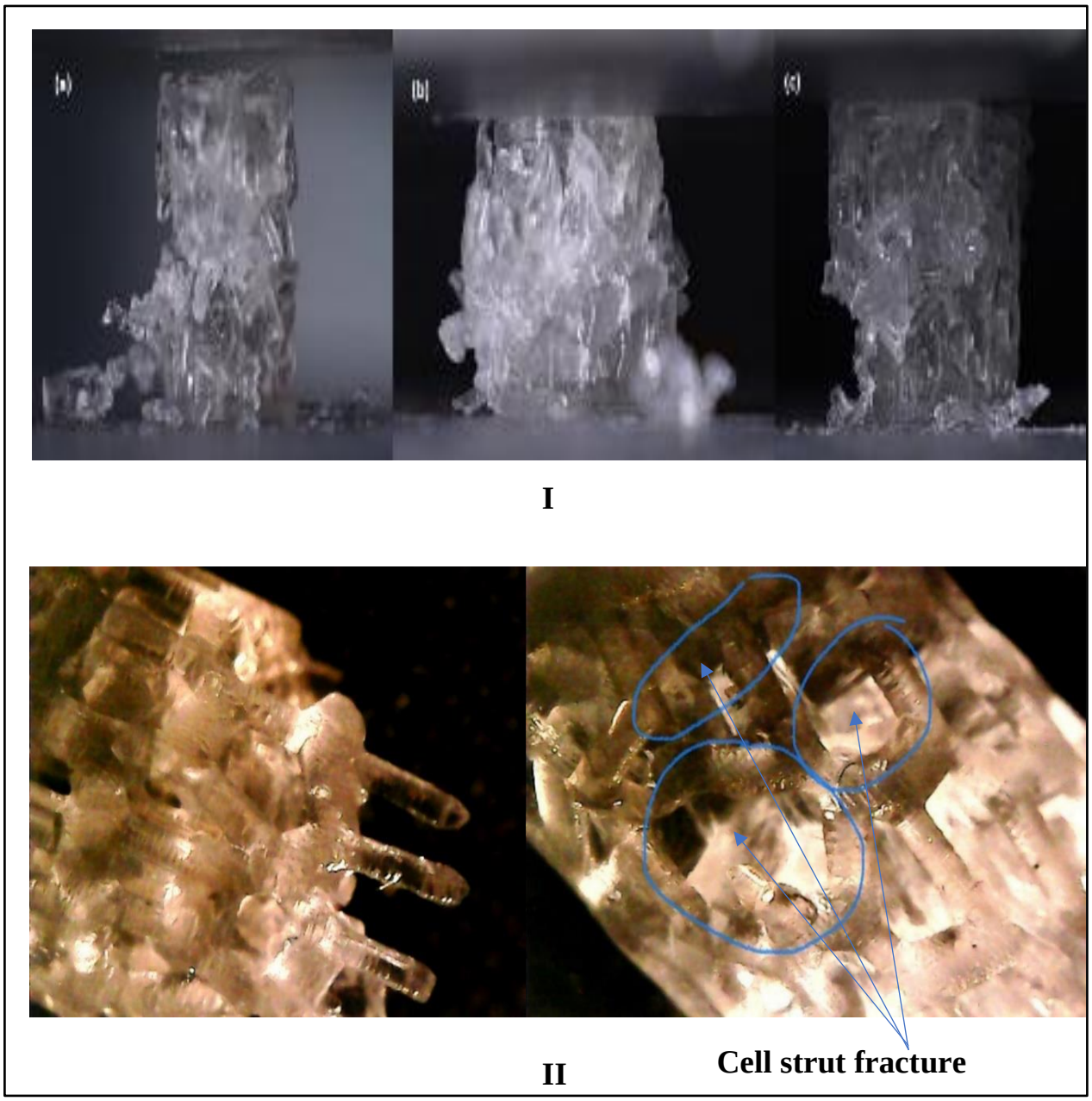

Figure 4-7 Failure mode of homogeneous elongated Voronoi structure. **I)** failure mode under compression machine; **a)** fracture prediction starts, **b)** collapse, and **c)** fracture propagation, and **II)** microscopic illustration of the fracture mode.

CHAPTER 5

CONCLUSION AND FUTURE RECOMMENDATIONS

5.1 Conclusion

Irregular Voronoi structures demonstrated that they are efficient to govern several mechanical properties of additive manufactured products. These structures ensure both improvements of mechanical properties, and simultaneously lightweight structures. Changing the geometric structure of the normal Voronoi N_v through changing the direction of cell struts and stretching them in Z-direction using Rhinoceros 7\Grasshopper software proved further significant to achieve appropriate mechanical properties. The major conclusions are formulated as follows:

i. IEVSs were proven to bear higher stress than the INVSs as well as outperformed in terms of energy absorption.

ii. IEVSs showed better performance in terms of resistance to fracture with a higher displacement rate than INVSs, which explains their high energy absorption.

iii. In terms of the three designed models: the gradient I Voronoi structures model presented a higher apparent Young's modulus than the gradient II Voronoi structures and the homogeneous structure. Thus, it is preferred for strength-to-weigh applications. While the homogeneous structures exhibited greater stiffness and absorbed more energy than the rest. Therefore, it is preferred for energy absorption and crashworthiness applications.

iv. In general, the mechanical properties are greatly affected by the geometric design of the 3D Voronoi structures as well as by the porosity. The lower the porosity, the stronger the structures.

5.2 Future Recommendations

The uniaxial compression test of 3D Voronoi structures was addressed in the current study. The stress-strain curve of the six Voronoi structures was analyzed. It was found that there is a relationship between the mechanical properties and the geometric structure of the samples; based on this, the following is recommended:

- To obtain more accurate data, DIC (Digital Image Correlation) techniques can be utilized to detect the strain of the samples during the experiment.

- Results may differ noticeably when using a biopolymer material with higher mechanical characteristics.

- Irregular elongated Voronoi structures IEVs with varying parameters show a change in irregularity, and density variation, which should have an obvious impact on mechanical properties.

REFRENCES

Ahmadi, S. M. *et al.* (2015) 'Additively manufactured open-cell porous biomaterials made from six different space-filling unit cells: The mechanical and morphological properties', *Materials*, 8(4), pp. 1871–1896. doi: 10.3390/ma8041871.

Al-Qrimli, F. A. M. (2011) 'The effect of composite tubes subjected to axial loading comparing with the number of layers and geometry', *Australian Journal of Basic and Applied Sciences*, 5(11), pp. 607–616.

AL-Qrimli, H., Khalid, K. and Mahdi, F. (2015) 'The effect of cone angle on composite tubes subjected to axial loading', *British Journal of Applied Science & Technology*, 7(4), pp. 351–363. doi: 10.9734/bjast/2015/15385.

Alessandri, K. *et al.* (2016) 'A 3D printed microfluidic device for production of functionalized hydrogel microcapsules for culture and differentiation of human Neuronal Stem Cells (hNSC)', *Lab on a Chip*, 16(9), pp. 1593–1604. doi: 10.1039/c6lc00133e.

Alghamdi, A. *et al.* (2020) 'Effect of additive manufactured lattice defects on mechanical properties: an automated method for the enhancement of lattice geometry', *International Journal of Advanced Manufacturing Technology*, 108(3), pp. 957–971. doi: 10.1007/s00170-020-05394-8.

Alkhader, M. and Vural, M. (2008) 'Mechanical response of cellular solids: Role of cellular topology and microstructural irregularity', *International Journal of Engineering Science*, 46(10), pp. 1035–1051. doi: 10.1016/j.ijengsci.2008.03.012.

Almonti, D. *et al.* (2020) 'Design and mechanical characterization of voronoi structures manufactured by indirect additive manufacturing', *Materials*, 13(5), pp. 1–12. doi: 10.3390/ma13051085.

Alomarah, A. *et al.* (2020) 'Compressive properties of 3D printed auxetic structures: experimental and numerical studies', *Virtual and Physical Prototyping*, 15(1), pp. 1–21. doi: 10.1080/17452759.2019.1644184.

Angelucci, G. and Mollaioli, F., (2018). Voronoi-like grid systems for tall buildings. *Frontiers in Built Environment, 4,* p.78. doi: 10.3389/fbuil.2018.00078.

Anycubic, C. (2022) 'Anycubic Plant-based UV Resin', *https://www.anycubic.com/products/anycubic-plant-based-uv-resin*, p. 17.

Aref Soltani, Reza Noroozi, Mahdi Bodaghi, and R. H. (2020) '3D Printing On-Water Sports Boards with Bio-Inspired Core Designs', *polymers Article*, 12(250),

pp. 1–18.

Ashley, S. (1991) ‘Rapid prototyping systems’, *Mechanical engineering*, 113(4), p. 34.

Asif, M. (2017) ‘A New 3D Printing Technique Using Extrusion of Photopolymer' School of Engineering , Auckland University of Technology Ramezani , Maziar School of Engineering.

Auras, R., Harte, B. and Selke, S. (2004) ‘An overview of polylactides as packaging materials’, *Macromolecular Bioscience*, 4(9), pp. 835–864. doi: 10.1002/mabi.200400043.

Azzouz, L. *et al.* (2019) ‘Mechanical properties of 3-D printed truss-like lattice biopolymer non-stochastic structures for sandwich panels with natural fibre composite skins’, *Composite Structures*, 213, pp. 220–230. doi: 10.1016/j.compstruct.2019.01.103.

Babaee, S. *et al.* (2012) ‘Mechanical properties of open-cell rhombic dodecahedron cellular structures’, *Acta Materialia*, 60(6–7), pp. 2873–2885. doi: 10.1016/j.actamat.2012.01.052.

Bahr, R. A. *et al.* (2017) ‘Novel uniquely 3D printed intricate Voronoi and fractal 3D antennas’, *IEEE MTT-S International Microwave Symposium Digest*, pp. 1583–1586. doi: 10.1109/MWSYM.2017.8058934.

Bandyopadhyay, A., Traxel, K. D. and Bose, S. (2021) ‘Nature-inspired materials and structures using 3D Printing’, *Materials Science and Engineering R: Reports*, 145, p. 100609. doi: 10.1016/j.mser.2021.100609.

Bendsoøe, M. P. and Sigmund, O. (2007) ‘Topology optimization’, *Optimization of Structural and Mechanical Systems*, pp. 161–194. doi: 10.1142/9789812779670_0006.

Bobbert, F.S.L., Lietaert, K., Eftekhari, A.A., Pouran, B., Ahmadi, S.M., Weinans, H. and Zadpoor, A.A. (2017). Additively manufactured metallic porous biomaterials based on minimal surfaces: A unique combination of topological, mechanical, and mass transport properties. *Acta biomaterialia*, *53*, pp.572-584.

Bonatti, C. and Mohr, D. (2017) ‘Large deformation response of additively-manufactured FCC metamaterials: From octet truss lattices towards continuous shell mesostructures’, *International Journal of Plasticity*, 92, pp. 122–147. doi: 10.1016/j.ijplas.2017.02.003.

Bouakba, M., Bezazi, A. and Scarpa, F. (2012) ‘FE analysis of the in-plane

mechanical properties of a novel Voronoi-type lattice with positive and negative Poisson's ratio configurations', *International Journal of Solids and Structures*, 49(18), pp. 2450–2459. doi: 10.1016/j.ijsolstr.2012.05.007.

Cao, X. *et al.* (2018) 'Mechanical properties of an improved 3D-printed rhombic dodecahedron stainless steel lattice structure of variable cross section', *International Journal of Mechanical Sciences*, 145, pp. 53–63. doi: 10.1016/j.ijmecsci.2018.07.006.

Çevik, Ü. and Kam, M. (2020) 'A Review Study on Mechanical Properties of Obtained Products by FDM Method and Metal/Polymer Composite Filament Production', *Journal of Nanomaterials*, 2020, pp. 1-9. doi: 10.1155/2020/6187149.

Chacón, J. M. *et al.* (2017) 'Additive manufacturing of PLA structures using fused deposition modelling: Effect of process parameters on mechanical properties and their optimal selection', *Materials and Design*, 124, pp. 143–157. doi: 10.1016/j.matdes.2017.03.065.

Chao, L. *et al.* (2021) 'Analysis of Mechanical Properties and Permeability of Trabecular-Like Porous Scaffold by Additive Manufacturing', *Frontiers in Bioengineering and Biotechnology*, 9, pp. 1–13. doi: 10.3389/fbioe.2021.779854.

Charles W. Hull, Arcadia, C. (1986) 'Apparatus for production of three-dimensional objects by stereolithography', *US patent: 4,575,330*, 716(1). doi: 10.1088/1757-899X/716/1/012012.

Charoo, N. A. *et al.* (2020) 'Selective laser sintering 3D printing–an overview of the technology and pharmaceutical applications', *Drug Development and Industrial Pharmacy*, 46(6), pp. 869–877. doi: 10.1080/03639045.2020.1764027.

Chen, P. Y., McKittrick, J. and Meyers, M. A. (2012) 'Biological materials: Functional adaptations and bioinspired designs', *Progress in Materials Science*, 57(8), pp. 1492–1704. doi: 10.1016/j.pmatsci.2012.03.001.

Chen, S. *et al.* (2020) 'Simulation of the forming process for curved composite sandwich panels', *International Journal of Material Forming*, 13(6), pp. 967–980. doi: 10.1007/s12289-019-01520-4.

Chen, Y., Li, T., Jia, Z., Scarpa, F., Yao, C.W. and Wang, L., (2018) '3D printed hierarchical honeycombs with shape integrity under large compressive deformations' *Materials & Design*, *137*, pp.226-234.

Chen, Z. *et al.* (2019) '3D printing of ceramics: A review', *Journal of the European Ceramic Society*, 39(4), pp. 661–687. doi: 10.1016/j.jeurceramsoc.2018.11.013.

Christian, S. J. (2016) *Natural fibre-reinforced noncementitious composites (biocomposites), Nonconventional and Vernacular Construction Materials*. Elsevier. doi: 10.1016/b978-0-08-100038-0.00005-6.

Chua, C. K. *et al.* (2003) 'Development of a tissue engineering scaffold structure library for rapid prototyping. Part 1: Investigation and classification', *International Journal of Advanced Manufacturing Technology*, 21(4), pp. 291–301. doi: 10.1007/s001700300034.

Chua, C. K., Leong, K. F. and Lim, C. S. (2010) *Rapid prototyping: principles and applications (with companion CD-ROM).* World Scientific Publishing Company.

Crump, S. S. (1992) 'Apparatus and method for creating three-dimensional objects'. Google Patents.

Deering, J. *et al.* (2021) 'Selective Voronoi tessellation as a method to design anisotropic and biomimetic implants', *Journal of the Mechanical Behavior of Biomedical Materials*, 116(January). doi: 10.1016/j.jmbbm.2021.104361.

Deshpande, V. S., Ashby, M. F. and Fleck, N. A. (2001) 'Foam topology: Bending versus stretching dominated architectures', *Acta Materialia*, 49(6), pp. 1035–1040. doi: 10.1016/S1359-6454(00)00379-7.

Do, Q. T., Nguyen, C. H. P. and Choi, Y. (2021) 'Homogenization-based optimum design of additively manufactured Voronoi cellular structures', *Additive Manufacturing*, 45, p. 102057. doi: 10.1016/j.addma.2021.102057.

Dong, L., Deshpande, V. and Wadley, H. (2015) 'Mechanical response of Ti-6Al-4V octet-truss lattice structures', *International Journal of Solids and Structures*, 60, pp. 107–124. doi: 10.1016/j.ijsolstr.2015.02.020.

Dossi, M., Brennan, M. and Moesen, M. (2017) 'A Multi-Physics Study of the Wave Propagation Problem in Open Cell Polyurethane Foams', (October), pp. 18–20.

Du, Y. *et al.* (2019) 'Finite element analysis of mechanical behavior, permeability of irregular porous scaffolds and lattice-based porous scaffolds', *Materials Research Express*, 6(10), pp. 0–13. doi: 10.1088/2053-1591/ab3ac1.

Ekiert, M., Mlyniec, A. and Uhl, T. (2015) 'The influence of degradation on the viscosity and molecular mass of poly(lactide acid) biopolymer', *Diagnostyka*, 16(4), pp. 63–70.

Fantini, M., Curto, M. and De Crescenzio, F. (2016) 'A method to design biomimetic scaffolds for bone tissue engineering based on Voronoi lattices', *Virtual and Physical Prototyping*, 11(2), pp. 77–90. doi: 10.1080/17452759.2016.1172301.

Fazita, M.N., Khalil, H.A., Izzati, A.N.A. and Rizal, S. (2019). Effects of strain rate on failure mechanisms and energy absorption in polymer composites. In *Failure Analysis in Biocomposites, Fibre-Reinforced Composites and Hybrid Composites* (pp. 51-78). Woodhead Publishing.

Fernandez-Yague, M. A. *et al.* (2015) 'Biomimetic approaches in bone tissue engineering: Integrating biological and physicomechanical strategies', *Advanced Drug Delivery Reviews*, 84, pp. 1–29. doi: 10.1016/j.addr.2014.09.005.

Formlabs, F. (2022) 'Guide to Stereolithography (SLA) 3D Printing What is Stereolithography 3D Printing ? Request a Free Sample The SLA 3D Printing A Brief History of Desktop SLA Printers Disrupt the Market The Next Chapter of SLA : Why Choose SLA 3D Printing ?', *formlabs company.com*.

Frayssinet, E., Colabella, L. and Cisilino, A. P. (2022) 'Design and assessment of the biomimetic capabilities of a Voronoi-based cancellous microstructure', *Journal of the Mechanical Behavior of Biomedical Materials*, 130, p. 105186. doi: 10.1016/j.jmbbm.2022.105186.

Fu, Q. *et al.* (2011) 'Bioactive glass scaffolds for bone tissue engineering: State of the art and future perspectives', *Materials Science and Engineering C*, 31(7), pp. 1245–1256. doi: 10.1016/j.msec.2011.04.022.

Furth, M. E., Atala, A. and Van Dyke, M. E. (2007) 'Smart biomaterials design for tissue engineering and regenerative medicine', *Biomaterials*, 28(34), pp. 5068–5073. doi: 10.1016/j.biomaterials.2007.07.042.

Gao, H. *et al.* (2021) 'Porous tantalum scaffolds: Fabrication, structure, properties, and orthopedic applications', *Materials and Design*, 210, p. 110095. doi: 10.1016/j.matdes.2021.110095.

Garlotta, D. (2001) 'A literature review of poly(lactic acid)', *Journal of Polymers and the Environment*, 9(2), pp. 63–84. doi: 10.1023/A:1020200822435.

Ghazlan, A. *et al.* (2020) 'Performance of a 3D printed cellular structure inspired by bone', *Thin-Walled Structures*, 151, p. 106713. doi: 10.1016/j.tws.2020.106713.

Gibson, I. *et al.* (2021) 'Additive manufacturing technologies', Springer.

Gibson, L. J., Ashby, M. F. and Harley, B. A. (2010) 'Cellular materials in nature and medicine', Cambridge University Press.

Gibson, L.J. and Ashby, M.F., (1999) 'Cellular Solids: Structure and Properties', Cambridge Univ Press. *Cambridge, UK*.

Gibson LJ, A. M. (1997) 'Cellular solids: Structure and properties', *Cambridge*

University Press, pp. 282–283. doi: 10.1016/0921-5093(90)90295-e.

Godoi, F. C. *et al.* (2018) 'Fundamentals of 3D food printing and applications', Academic press.

Gómez, S. *et al.* (2016) 'Design and properties of 3D scaffolds for bone tissue engineering', *Acta Biomaterialia*, 42, pp. 341–350. doi: 10.1016/j.actbio.2016.06.032.

González, S.G., Vlad, M.D., López, J.L. and Aguado, E.F., (2023). Novel bio-inspired 3D porous scaffold intended for bone-tissue engineering: Design and in silico characterisation of histomorphometric, mechanical and mass-transport properties. *Materials & Design*, *225*, p.111467.

Goodno, J. M. G. and B. J. (2013) 'Mechanics of Materials', Eighth Edi, *Damascus University Publications*. Eighth Edi. Edited by J. M. G. and B. J. Goodno. USA: Cengage Learning. Global Engineering: Christopher M. Shortt.

Gordelier, T. J. *et al.* (2019) 'Optimising the FDM additive manufacturing process to achieve maximum tensile strength: a state-of-the-art review', *Rapid Prototyping Journal*, 25(6), pp. 953–971. doi: 10.1108/RPJ-07-2018-0183.

Gross, B. C. *et al.* (2014) 'Evaluation of 3D printing and its potential impact on biotechnology and the chemical sciences', *Analytical Chemistry*, 86(7), pp. 3240–3253. doi: 10.1021/ac403397r.

Gross, B., Lockwood, S. Y. and Spence, D. M. (2017) 'Recent advances in analytical chemistry by 3D printing', *Analytical Chemistry*, 89(1), pp. 57–70. doi: 10.1021/acs.analchem.6b04344.

Guarino, V. *et al.* (2008) 'Polylactic acid fibre-reinforced polycaprolactone scaffolds for bone tissue engineering', *Biomaterials*, 29(27), pp. 3662–3670. doi: 10.1016/j.biomaterials.2008.05.024.

Habraken, W. J. E. M., Wolke, J. G. C. and Jansen, J. A. (2007) 'Ceramic composites as matrices and scaffolds for drug delivery in tissue engineering', *Advanced Drug Delivery Reviews*, 59(4–5), pp. 234–248. doi: 10.1016/j.addr.2007.03.011.

Herath, B. *et al.* (2021) 'Mechanical and geometrical study of 3D printed Voronoi scaffold design for large bone defects', *Materials and Design*, 212, p. 110224. doi: 10.1016/j.matdes.2021.110224.

Hollinger, J. O. *et al.* (2002) 'Fabrication of poly(α-hydroxy acid) foam scaffolds using multiple solvent systems', *Journal of Biomedical Materials Research*, 59(3), pp. 563–572. doi: 10.1002/jbm.1269.

Hollister, S. J. (2006) ‘Porous scaffold design for tissue engineering’. *Nature Materials*, 5(7), p. 590.

Hutmacher, D. W. (2000) ‘Scaffolds in tissue engineering bone and cartilage’, *The Biomaterials: Silver Jubilee Compendium*, 21, pp. 175–189. doi: 10.1016/B978-008045154-1.50021-6.

Hutmacher, D. W. (2006) ‘Regenerative medicine will impact, but not replace, the medical device industry’, *Expert Review of Medical Devices*, 3(4), pp. 409–412. doi: 10.1586/17434440.3.4.409.

Hutmacher, D. W., Sittinger, M. and Risbud, M. V. (2004) ‘Scaffold-based tissue engineering: Rationale for computer-aided design and solid free-form fabrication systems’, *Trends in Biotechnology*, 22(7), pp. 354–362. doi: 10.1016/j.tibtech.2004.05.005.

Jahani, B., Wang, X. and Brooks, A. (2020) ‘Additive Manufacturing Techniques for Fabrication of Bone Scaffolds for Tissue Engineering Applications’, *Recent Progress in Materials*, 2(3), pp. 1–41. doi: 10.21926/rpm.2003021.

Jang, D. W. *et al.* (2014) ‘Fabrication of porous hydroxyapatite scaffolds as artificial bone preform and its biocompatibility evaluation’, *ASAIO Journal*, 60(2), pp. 216–223. doi: 10.1097/MAT.0000000000000032.

Jenck, J. F., Agterberg, F. and Droescher, M. J. (2004) ‘Products and processes for a sustainable chemical industry: A review of achievements and prospects’, *Green Chemistry*, 6(11), pp. 544–556. doi: 10.1039/b406854h.

Jiang, Q. *et al.* (2014) ‘Mechanical anisotropy of columnar jointed basalts: An example from the Baihetan hydropower station, China’, *Engineering Geology*, 175, pp. 35–45. doi: 10.1016/j.enggeo.2014.03.019.

Jiao, Y. and Torquato, S. (2011) ‘Emergent behaviors from a cellular automaton model for invasive tumor growth in heterogeneous microenvironments’, *PLoS Computational Biology*, 7(12), pp. 10–12. doi: 10.1371/journal.pcbi.1002314.

Kandola, B. K. (2012) ‘Flame retardant characteristics of natural fibre composites’, *Natural polymers*, 1, pp. 86–117.

Kantaros, A., Chatzidai, N. and Karalekas, D. (2016) ‘3D printing-assisted design of scaffold structures’, *International Journal of Advanced Manufacturing Technology*, 82(1–4), pp. 559–571. doi: 10.1007/s00170-015-7386-6.

Kapfer, S. C. *et al.* (2011) ‘Minimal surface scaffold designs for tissue engineering’, *Biomaterials*, 32(29), pp. 6875–6882. doi: 10.1016/j.biomaterials.2011.06.012.

Karp, J. M. *et al.* (2003) 'Fabrication of Precise Cylindrical Three-Dimensional Tissue Engineering Scaffolds for In Vitro and In Vivo Bone Engineering Applications', *Journal of Craniofacial Surgery*, 14(3), pp. 317–323. doi: 10.1097/00001665-200305000-00009.

Khot, S. N. *et al.* (2001) 'Development and application of triglyceride-based polymers and composites', *Journal of Applied Polymer Science*, 82(3), pp. 703–723. doi: 10.1002/app.1897.

Kim, H. S., Chen, W. and Wierzbicki, T. (2002) 'Weight and crash optimization of foam-filled three-dimensional "S" frame', *Computational Mechanics*, 28(5), pp. 417–424. doi: 10.1007/s00466-002-0306-2.

Kim, K. *et al.* (2011) 'The influence of stereolithographic scaffold architecture and composition on osteogenic signal expression with rat bone marrow stromal cells', *Biomaterials*, 32(15), pp. 3750–3763. doi: 10.1016/j.biomaterials.2011.01.016.

Kladovasilakis, N., Tsongas, K. and Tzetzis, D. (2020) 'Finite element analysis of orthopedic hip implant with functionally graded bioinspired lattice structures', *Biomimetics*, 5(3). doi: 10.3390/BIOMIMETICS5030044.

Klein, R. (1989) *Concrete and abstract Voronoi diagrams*. Springer Science & Business Media.

Kou, X. Y. and Tan, S. T. (2010) 'A simple and effective geometric representation for irregular porous structure modeling', *CAD Computer Aided Design*, 42(10), pp. 930–941. doi: 10.1016/j.cad.2010.06.006.

Kumar, C. S. S. R. (2006) *Tissue, cell and organ engineering*. Wiley-VCH.

Kümmerer, K. (2007) 'Sustainable from the very beginning: Rational design of molecules by life cycle engineering as an important approach for green pharmacy and green chemistry', *Green Chemistry*, 9(8), pp. 899–90. doi: 10.1039/b618298b.

Lakes, R. *et al.* (1987) 'Lakes1987-1', *Science*, 235(1987), pp. 1038–1041.

Lan, X. ke *et al.* (2018) 'Blast response of continuous-density graded cellular material based on the 3D Voronoi model', *Defence Technology*, 14(5), pp. 433–440. doi: 10.1016/j.dt.2018.06.003.

Lebedevaite, M. *et al.* (2022) 'Development and optical 3D printing of acrylated epoxidized soybean oil-based composites with functionalized calcium silicate hydrate filler derived from aluminium fluoride production waste', *Composites Part A: Applied Science and Manufacturing*, 157, p. 106929. doi: 10.1016/j.compositesa.2022.106929.

Lee, M. *et al.* (2018) ‘Support-free hollowing for 3D printing via Voronoi diagram of ellipses’, *CAD Computer Aided Design*, 101, pp. 23–36. doi: 10.1016/j.cad.2018.03.007.

Lee, S. H. and Shin, H. (2007) ‘Matrices and scaffolds for delivery of bioactive molecules in bone and cartilage tissue engineering’, *Advanced Drug Delivery Reviews*, 59(4–5), pp. 339–359. doi: 10.1016/j.addr.2007.03.016.

Lee, W. *et al.* (2015) ‘3D-Printed micro fluidic device for the detection of pathogenic bacteria using size-based separation in helical channel with trapezoid cross-section’, *Scientific Reports*, 5, pp. 1–6. doi: 10.1038/srep07717.

Lei, H. Y. *et al.* (2020) ‘Parametric design of Voronoi-based lattice porous structures’, *Materials and Design*, 191. doi: 10.1016/j.matdes.2020.108607.

Lewandrowski, K. U. *et al.* (2000) ‘Bioresorbable bone graft substitutes of different osteoconductivities: A histologic evaluation of osteointegration of poly(propylene glycol-co-fumaric acid)-based cement implants in rats’, *Biomaterials*, 21(8), pp. 757–764. doi: 10.1016/S0142-9612(99)00179-9.

Li, G. *et al.* (2016) ‘In vitro and in vivo study of additive manufactured porous Ti6Al4V scaffolds for repairing bone defects’, *Scientific Reports*, 6, pp. 1–11. doi: 10.1038/srep34072.

Li, J. and Tanaka, H. (2018) ‘Feasibility study applying a parametric model as the design generator for 3D–printed orthosis for fracture immobilization’, *3D Printing in Medicine*, 4(1), pp. 1–15. doi: 10.1186/s41205-017-0024-1.

Li, S. *et al.* (2020) ‘Compressive properties and collapse behavior of additively-manufactured layered-hybrid lattice structures under static and dynamic loadings’, *Thin-Walled Structures*, 157(May), p. 107153. doi: 10.1016/j.tws.2020.107153.

Lin, K. *et al.* (2019) ‘3D printing of bioceramic scaffolds-barriers to the clinical translation: From promise to reality, and future perspectives’, *Materials*, 12(7). doi: 10.3390/ma12172660.

Liou, F. W. (2007) *Rapid prototyping and engineering applications: a toolbox for prototype development*. Crc Press.

Liu, B. *et al.* (2021) ‘Adaptive anisotropic porous structure design and modeling for 2.5D mechanical parts’, *Materials and Design*, 206. doi: 10.1016/j.matdes.2021.109786.

Liu, C. *et al.* (2019) ‘Low-Temperature Deposition Manufacturing: A Versatile Material Extrusion-Based 3D Printing Technology for Fabricating Hierarchically

Porous Materials', *Journal of Nanomaterials*. doi: 10.1155/2019/1291067.

Liu, F. *et al.* (2020) 'Additively manufactured continuous cell-size gradient porous scaffolds: Pore characteristics, mechanical properties and biological responses in vitro', *Materials*, 13(11). doi: 10.3390/ma13112589.

Liu, Y., Lim, J. and Teoh, S. H. (2013) 'Review: Development of clinically relevant scaffolds for vascularised bone tissue engineering', *Biotechnology Advances*, 31(5), pp. 688–705. doi: 10.1016/j.biotechadv.2012.10.003.

Manapat, J. Z. *et al.* (2017) '3D Printing of Polymer Nanocomposites via Stereolithography', *Macromolecular Materials and Engineering*, 302(9), pp. 1–13. doi: 10.1002/mame.201600553.

Manoharan, V. *et al.* (2013) 'Application of additive manufacturing techniques in sports footwear: This paper suggests a five-point scoring technique to evaluate the performance of four AM techniques, namely, stereolithography (SLA), PolyJet (PJ), selective laser sintering (SLS) and t', *Virtual and Physical Prototyping*, 8(4), pp. 249–252. doi: 10.1080/17452759.2013.862958.

Mantila Roosa, S. M. *et al.* (2010) 'The pore size of polycaprolactone scaffolds has limited influence on bone regeneration in an in vivo model', *Journal of Biomedical Materials Research - Part A*, 92(1), pp. 359–368. doi: 10.1002/jbm.a.32381.

Martelli, N. *et al.* (2016) 'Advantages and disadvantages of 3-dimensional printing in surgery: A systematic review', *Surgery (United States)*, 159(6), pp. 1485–1500. doi: 10.1016/j.surg.2015.12.017.

Martínez, J., Dumas, J. and Lefebvre, S. (2016) 'Procedural voronoi foams for additive manufacturing', *ACM Transactions on Graphics*, 35(4). doi: 10.1145/2897824.2925922.

Maspero, F. A. *et al.* (2002) 'Resorbable defect analog PLGA scaffolds using CO2 as solvent: Structural characterization', *Journal of Biomedical Materials Research*, 62(1), pp. 89–98. doi: 10.1002/jbm.10212.

McShane, G. J. *et al.* (2006) 'The response of clamped sandwich plates with lattice cores subjected to shock loading', *European Journal of Mechanics, A/Solids*, 25(2), pp. 215–229. doi: 10.1016/j.euromechsol.2005.08.001.

Melchels, F. P. W., Feijen, J. and Grijpma, D. W. (2010) 'A review on stereolithography and its applications in biomedical engineering', *Biomaterials*, 31(24), pp. 6121–6130. doi: 10.1016/j.biomaterials.2010.04.050.

Miao, S. *et al.* (2016) '4D printing smart biomedical scaffolds with novel soybean

oil epoxidized acrylate', *Scientific Reports*, 6, pp. 1–10. doi: 10.1038/srep27226.

Mohan, N. *et al.* (2017) 'A review on composite materials and process parameters optimisation for the fused deposition modelling process', *Virtual and Physical Prototyping*, 12(1), pp. 47–59. doi: 10.1080/17452759.2016.1274490.

Mondal, D. *et al.* (2021) 'mSLA-based 3D printing of acrylated epoxidized soybean oil - nano-hydroxyapatite composites for bone repair', *Materials Science and Engineering C*, 130, p. 112456. doi: 10.1016/j.msec.2021.112456.

Mota, C. *et al.* (2015) 'Additive manufacturing techniques for the production of tissue engineering constructs', *Journal of tissue engineering and regenerative medicine*, 9(3), pp. 174–190.

Mullen, L. *et al.* (2009) 'Selective laser melting: A regular unit cell approach for the manufacture of porous, titanium, bone in-growth constructs, suitable for orthopedic applications', *Journal of Biomedical Materials Research - Part B Applied Biomaterials*, 89(2), pp. 325–334. doi: 10.1002/jbm.b.31219.

Mullen, L. *et al.* (2010) 'Selective laser melting: A unit cell approach for the manufacture of porous, titanium, bone in-growth constructs, suitable for orthopedic applications. II. Randomized structures', *Journal of Biomedical Materials Research - Part B Applied Biomaterials*, 92(1), pp. 178–188. doi: 10.1002/jbm.b.31504.

Murr, L. E. (2016) 'Frontiers of 3D Printing/Additive Manufacturing: from Human Organs to Aircraft Fabrication', *Journal of Materials Science and Technology*, 32(10), pp. 987–995. doi: 10.1016/j.jmst.2016.08.011.

Nadagouda, M. N., Ginn, M. and Rastogi, V. (2020) 'A review of 3D printing techniques for environmental applications', *Current Opinion in Chemical Engineering*, 28, pp. 173–178. doi: 10.1016/j.coche.2020.08.002.

Nazir, A., Arshad, A. Bin and Jeng, J. Y. (2019) 'Buckling and post-buckling behavior of uniform and variable-density lattice columns fabricated using additive manufacturing', *Materials*, 12(21), pp. 1–15. doi: 10.3390/ma12213539.

Netravali, A. N., Huang, X. and Mizuta, K. (2007) 'Advanced "green" composites', *Advanced Composite Materials: The Official Journal of the Japan Society of Composite Materials*, 16(4), pp. 269–282. doi: 10.1163/156855107782325230.

Ngo, T. D. *et al.* (2018) 'A review of 3D printing techniques for environmental applications and challenges', *Composites Part B: Engineering*, 143, pp. 172–196. doi: 10.1016/j.compositesb.2018.02.012.

Nikkhah, H., Crupi, V. and Baroutaji, A. (2020) 'Crashworthiness analysis of bio-

inspired thin-walled tubes based on Morpho wings microstructures', *Mechanics Based Design of Structures and Machines*, 50(10), pp. 1–18. doi: 10.1080/15397734.2020.1822184.

Niknam, H. and Akbarzadeh, A. H. (2020) 'Graded lattice structures: Simultaneous enhancement in stiffness and energy absorption', *Materials and Design*, 196, p. 109129. doi: 10.1016/j.matdes.2020.109129.

NNFCC (1945) 'Forestry and agriculture', *Nature. https://www.nnfcc.co.uk/*, 155(3933), pp. 311–313. doi: 10.1038/155311a0.

Noè, C. *et al.* (2022) 'DLP-printable fully biobased soybean oil composites', *Polymer*, 247. doi: 10.1016/j.polymer.2022.124779.

NTopology (2022) 'nTopology software', *nTopology Help Centre*, (Online). Available at: https://ntopology.com/.

van Nuland, T. F. W., van Dommelen, J. A. W. and Geers, M. G. D. (2021) 'An anisotropic Voronoi algorithm for generating polycrystalline microstructures with preferred growth directions', *Computational Materials Science*, 186, p. 109947. doi: 10.1016/j.commatsci.2020.109947.

Öncel, A. C. and Yaman, U. (2019) 'Generation of optimized voronoi based interior structures for improved mechanical properties', *Procedia Manufacturing*, 38(2019), pp. 42–51. doi: 10.1016/j.promfg.2020.01.006.

Owen, S. J. *et al.* (2017) 'Hexahedral Mesh Generation for Computational Materials Modeling', *Procedia Engineering*, 203, pp. 167–179. doi: 10.1016/j.proeng.2017.09.803.

Pan, C., Han, Y. and Lu, J. (2020) 'Design and optimization of lattice structures: A review', *Applied Sciences (Switzerland)*, 10(18), pp. 1–36. doi: 10.3390/APP10186374.

Paolini, A., Kollmannsberger, S. and Rank, E. (2019) 'Additive manufacturing in construction: A review on processes, applications, and digital planning methods', *Additive Manufacturing*, 30. doi: 10.1016/j.addma.2019.100894.

Papka, S.D. and Kyriakides, S., (1998) 'Experiments and full-scale numerical simulations of in-plane crushing of a honeycomb', *Acta materialia*, *46*(8), pp.2765-2776.

Park, K. M., Min, K. S. and Roh, Y. S. (2022) 'Design Optimization of Lattice Structures under Compression: Study of Unit Cell Types and Cell Arrangements', *Materials*, 15(1). doi: 10.3390/ma15010097.

Pasquale, G. De and Barra, D. (2022) ‘Voronoi lattice-based orthotics with modular stiffness for additive manufacturing’, *Transactions on Additive Manufacturing Meets Medicine*, 4(1), pp. 1–5. doi: 10.18416/AMMM.2022.2209668.

Pawlak, A. *et al.* (2015) ‘Fabrication of microscaffolds from Ti-6Al-7Nb alloy by SLM’, *Rapid Prototyping Journal*, 21(4), pp. 393–401. doi: 10.1108/RPJ-10-2013-0101.

Paz, C. *et al.* (2022) ‘Numerical modelling of osteocyte growth on different bone tissue scaffolds’, *Computer Methods in Biomechanics and Biomedical Engineering*, 25(6), pp. 641–655. doi: 10.1080/10255842.2021.1972290.

Pelanconi, M., Rezaei, E. and Ortona, A. (2020) ‘Cellular ceramic architectures produced by hybrid additive manufacturing: a review on the evolution of their design’, *Journal of the Ceramic Society of Japan*, 128(9). Available at: https://www.jstage.jst.go.jp/article/jcersj2/128/9/128_20071/_article.

Piros, A. and Trautmann, L., (2023). Creating interior support structures with Lightweight Voronoi Scaffold. *International Journal on Interactive Design and Manufacturing (IJIDeM)*, pp.1-9.

Popescu, D. *et al.* (2018) ‘FDM process parameters influence over the mechanical properties of polymer specimens: A review’, *Polymer Testing*, 69, pp. 157–166. doi: 10.1016/j.polymertesting.2018.05.020.

Prakash, K. S., Nancharaih, T. and Rao, V. V. S. (2018) ‘Additive Manufacturing Techniques in Manufacturing -An Overview’, *Materials Today: Proceedings*, 5(2), pp. 3873–3882. doi: 10.1016/j.matpr.2017.11.642.

Puppi, D. *et al.* (2010) ‘Polymeric materials for bone and cartilage repair’, *Progress in Polymer Science (Oxford)*, 35(4), pp. 403–440. doi: 10.1016/j.progpolymsci.2010.01.006.

Qiu Li Loh; Cleo Choong (2012) ‘Three-dimensional Scaffolds for Tissue Engineering Applications: Role of Porosity and Pore Size’, *Tissue Engineering Part B : Reviews*, (3), pp. 1–61.

Quan, H. *et al.* (2020) ‘Photo-curing 3D printing technique and its challenges’, *Bioactive Materials*, 5(1), pp. 110–115. doi: 10.1016/j.bioactmat.2019.12.003.

Raquez, J. M. *et al.* (2013) ‘Polylactide (PLA)-based nanocomposites’, *Progress in Polymer Science*, 38(10–11), pp. 1504–1542. doi: 10.1016/j.progpolymsci.2013.05.014.

Reddy, M. M. (2013) ‘Bio-Based Materials in the New Bio-Economy. Pdf’.

Reddy, M. M., Misra, M. and Mohanty, A. K. (2012) 'Bio-based materials in the new bio-economy', *Chemical Engineering Progress*, 108(5), pp. 37–42.

Rehme, O. (2010) 'Cellular Design for Laser Freeform Fabrication 1 Introduction', 4(0), pp. 0–8. Available at: https://cuvillier.de/uploads/preview/public_file/1820/9783869552736.pdf.

Rhea, M. (2022) 'Diabse Rock in nature, the Strongest Rock in the World', *Rockhound Resource. https://rockhoundresource.com/the-strongest-rock-in-the-world/*.

Rychlewski, J. (1984) 'On Hooke's law', *Journal of Applied Mathematics and Mechanics*, 48(3), pp. 303–314. doi: 10.1016/0021-8928(84)90137-0.

Sachs, E., Cima, M. and Cornie, J. (1990). Three-dimensional printing: rapid tooling and prototypes directly from a CAD model. *CIRP annals*, *39*(1), pp.201-204.

Sadeghi-Varkani, A., Emam-Djomeh, Z. and Askari, G. (2018) 'Physicochemical and microstructural properties of a novel edible film synthesized from Balangu seed mucilage', *International Journal of Biological Macromolecules*, 108, pp. 1110–1119. doi: 10.1016/j.ijbiomac.2017.11.029.

Saito, K. *et al.* (2021) 'Insect wing 3D printing', *Scientific Reports*, 11(1), pp. 1–8. doi: 10.1038/s41598-021-98242-y.

Schaedler, T. A. *et al.* (2011) 'Ultralight metallic microlattices', *Science*, 334(6058), pp. 962–965.

Shirzad, M. *et al.* (2021) 'Design, evaluation, and optimization of 3D printed truss scaffolds for bone tissue engineering', *Journal of the Mechanical Behavior of Biomedical Materials*, 120(May), p. 104594. doi: 10.1016/j.jmbbm.2021.104594.

Siddique, T. H. M. *et al.* (2019) 'Low cost 3D printing for rapid prototyping and its application', *2019 2nd International Conference on Latest Trends in Electrical Engineering and Computing Technologies, INTELLECT 2019*, pp. 1–5. doi: 10.1109/INTELLECT47034.2019.8954983.

Sienkiewicz, J. *et al.* (2020) 'Investigations on the mechanical response of gradient lattice structures manufactured via slm', *Metals*, 10(2). doi: 10.3390/met10020213.

Sigmund, O. (2000) 'Topology optimization: A tool for the tailoring of structures and materials', *Philosophical Transactions of the Royal Society A: Mathematical, Physical and Engineering Sciences*, 358(1765), pp. 211–227. doi: 10.1098/rsta.2000.0528.

Silva, M. J. and Gibson, L. J. (1997) 'The effects of non-periodic microstructure and

defects on the compressive strength of two-dimensional cellular solids', *International Journal of Mechanical Sciences*, 39(5), pp. 549–563. doi: 10.1016/s0020-7403(96)00065-3.

Soro, N. *et al.* (2022) 'Additive manufacturing of biomimetic Titanium-Tantalum lattices for biomedical implant applications', *Materials and Design*, 218, p. 110688. doi: 10.1016/j.matdes.2022.110688.

Sotomayor, O. E. and Tippur, H. V. (2014) 'Role of cell regularity and relative density on elasto-plastic compression response of random honeycombs generated using Voronoi diagrams', *International Journal of Solids and Structures*, 51(21–22), pp. 3776–3786. doi: 10.1016/j.ijsolstr.2014.07.009.

Sun, Y. *et al.* (2012) 'Degradable amorphous scaffolds with enhanced mechanical properties and homogeneous cell distribution produced by a three-dimensional fiber deposition method', *Journal of Biomedical Materials Research - Part A*, 100(10), pp. 2739–2749. doi: 10.1002/jbm.a.34210.

Sun, Z. P., Guo, Y. B. and Shim, V. P. W. (2021) 'Characterisation and modeling of additively-manufactured polymeric hybrid lattice structures for energy absorption', *International Journal of Mechanical Sciences*, 191, p. 106101. doi: 10.1016/j.ijmecsci.2020.106101.

Szost, B. A. *et al.* (2016) 'A comparative study of additive manufacturing techniques: Residual stress and microstructural analysis of CLAD and WAAM printed Ti-6Al-4V components', *Materials and Design*, 89, pp. 559–567. doi: 10.1016/j.matdes.2015.09.115.

Tee, Y. L. *et al.* (2021) 'From nature to additive manufacturing: Biomimicry of porcupine quill', *Materials and Design*, 210, p. 110041. doi: 10.1016/j.matdes.2021.110041.

Teimouri, M. and Asgari, M. (2021) 'Mechanical performance of additively manufactured uniform and graded porous structures based on topology-optimized unit cells', *Proceedings of the Institution of Mechanical Engineers, Part C: Journal of Mechanical Engineering Science*, 235(9), pp. 1593–1618. doi: 10.1177/0954406220947119.

Tekoğlu, C. *et al.* (2011) 'Size effects in foams: Experiments and modeling', *Progress in Materials Science*, 56(2), pp. 109–138. doi: 10.1016/j.pmatsci.2010.06.001.

Tokiwa, Y. *et al.* (2009) 'Biodegradability of plastics', *International Journal of Molecular Sciences*, 10(9), pp. 3722–3742. doi: 10.3390/ijms10093722.

Uí Mhurchadha, S.M., Marques, S., Givet, L. and Raghavendra, R., (2021). Effect of Voronoi Lattice Geometry on the Fatigue Performance of Ti-6Al-4V. In *2021 International Solid Freeform Fabrication Symposium*. University of Texas at Austin.

Vacanti, J.P. and Langer, R., (1999). Tissue engineering: the design and fabrication of living replacement devices for surgical reconstruction and transplantation. *The lancet*, 354, pp.32-34. doi: 10.1016/s0140-6736(99)90247-7.

Vajjala, S., Kraynik, A. M. and Gibson, L. J. (2000) 'A cellular solid model for modulus reduction due to resorption of trabeculae in bone', *Journal of Biomechanical Engineering*, 122(5), pp. 511–515. doi: 10.1115/1.1289996.

Vedantu, L. courses for (1800) 'Biopolymers - Definition, Types, Examples and Applications.', *vedantu webpage: https://www.vedantu.com/chemistry/biopolymers*, 2456, p. 2456.

Voronoi, G. (1908) 'Nouvelles applications des parametres continus a la theorie des forms quadratiques', *J. Reine Angew. Math.*, 133, pp. 97–178.

Wadley, H. N. G., Fleck, N. A. and Evans, A. G. (2003) 'Fabrication and structural performance of periodic cellular metal sandwich structures', *Composites Science and Technology*, 63(16), pp. 2331–2343. doi: 10.1016/S0266-3538(03)00266-5.

Wagner, M. A. *et al.* (2019) 'Programmable, active lattice structures: Unifying stretch-dominated and bending-dominated topologies', *Extreme Mechanics Letters*, 29, p. 100461. doi: 10.1016/j.eml.2019.100461.

Wang, G. *et al.* (2018) 'Design and Compressive Behavior of Controllable Irregular Porous Scaffolds: Based on Voronoi-Tessellation and for Additive Manufacturing', *ACS Biomaterials Science and Engineering*, 4(2), pp. 719–727. doi: 10.1021/acsbiomaterials.7b00916.

Wang, J. *et al.* (2016) 'Stereolithographic (SLA) 3D printing of oral modified-release dosage forms', *International Journal of Pharmaceutics*, 503(1–2), pp. 207–212. doi: 10.1016/j.ijpharm.2016.03.016.

Wang, K., Wang, D. and Han, F. (2016) 'Effect of crystalline grain structures on the mechanical properties of twinning-induced plasticity steel', *Acta Mechanica Sinica/Lixue Xuebao*, 32(1), pp. 181–187. doi: 10.1007/s10409-015-0513-7.

Wang, X. *et al.* (2017) '3D printing of polymer matrix composites: A review and prospective', *Composites Part B: Engineering*, 110, pp. 442–458. doi: 10.1016/j.compositesb.2016.11.034.

Weng, Z. *et al.* (2016) 'Structure-property relationship of nano enhanced

stereolithography resin for desktop SLA 3D printer', *Composites Part A: Applied Science and Manufacturing*, 88, pp. 234–242. doi: 10.1016/j.compositesa.2016.05.035.

Widmer, M. S. and Mikos, A. G. (1998) 'Fabrication of Biodegradable Polymer Scaffolds for Tissue Engineering', *Frontiers in Tissue Engineering*, pp. 107–120. doi: 10.1016/b978-008042689-1/50008-x.

Wohlers, T. (2012) 'Additive Manufacturing Advances', *Manufacturing Engineering*, 148(4), pp. 55–56. Available at: https://wohlersassociates.com/wohlers-report-2016-downloads/.

Wong, K. V. and Hernandez, A. (2012) 'A Review of Additive Manufacturing', *ISRN Mechanical Engineering*, 2012, pp. 1–10. doi: 10.5402/2012/208760.

Wu, H. *et al.* (2022) 'Design and 3D printing of ceramic maxillofacial prosthesis with gradient pores based on Voronoi-Tessellation principle', *Materials Today Communications*, 33, p. 104559. doi: 10.1016/j.mtcomm.2022.104559.

Xu, N. *et al.* (2014) '3D artificial bones for bone repair prepared by computed tomography-guided fused deposition modeling for bone repair', *ACS Applied Materials and Interfaces*, 6(17), pp. 14952–14963. doi: 10.1021/am502716t.

Yan, C. *et al.* (2015) 'Ti-6Al-4V triply periodic minimal surface structures for bone implants fabricated via selective laser melting', *Journal of the Mechanical Behavior of Biomedical Materials*, 51, pp. 61–73. doi: 10.1016/j.jmbbm.2015.06.024.

Yin, H. *et al.* (2018) 'In-plane crashworthiness of bio-inspired hierarchical honeycombs', *Composite Structures*, 192, pp. 516–527. doi: 10.1016/j.compstruct.2018.03.050.

Zenkert, D., 1997. *The handbook of sandwich construction*. Engineering Materials Advisory Services. pp. 442.

Zhao, H. *et al.* (2021) 'Design and mechanical properties verification of gradient voronoi scaffold for bone tissue engineering', *Micromachines*, 12(6), pp. 1–23. doi: 10.3390/mi12060664.

Zhu, H. X., Thorpe, S. M. and Windle, A. H. (2001) 'The geometrical properties of irregular two-dimensional Voronoi tessellations', *Philosophical Magazine A: Physics of Condensed Matter, Structure, Defects and Mechanical Properties*, 81(12), pp. 2765–2783. doi: 10.1080/01418610010032364.

Zhu, H. X., Thorpe, S. M. and Windle, A. H. (2006) 'The effect of cell irregularity on the high strain compression of 2D Voronoi honeycombs', *International Journal*

of Solids and Structures, 43(5), pp. 1061–1078. doi: 10.1016/j.ijsolstr.2005.05.008.

Zhu, L. *et al.* (2021) 'Design and Compressive Fatigue Properties of Irregular Porous Scaffolds for Orthopedics Fabricated Using Selective Laser Melting', *ACS Biomaterials Science and Engineering*, 7(4), pp. 1663–1672. doi: 10.1021/acsbiomaterials.0c01392.

APPENDIX

The core of this research has been published in a highly reputed journal indexed in Clarivate Analytics. Journal of Functional Biomaterials (JFB) by Multidisciplinary Digital Publishing Institute (MDPI), Basel, Switzerland on 16 December 2022. JFB has an impact factor of 4.901 and it is a leading platform for enhancement in biomedical engineering.

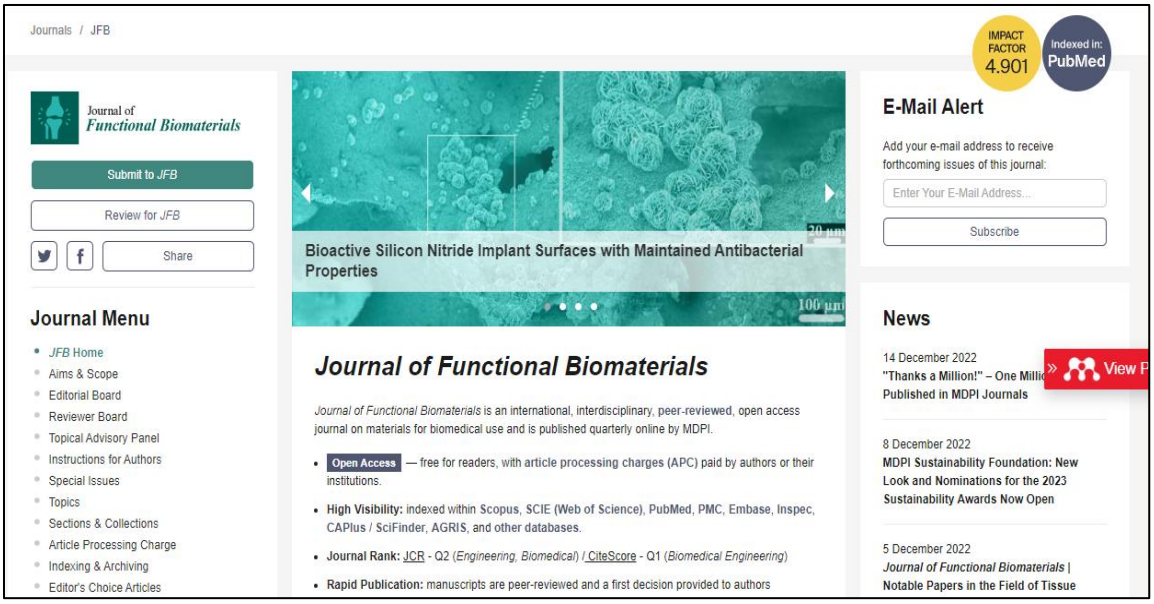

Figure A1: Cover page of the JFB.

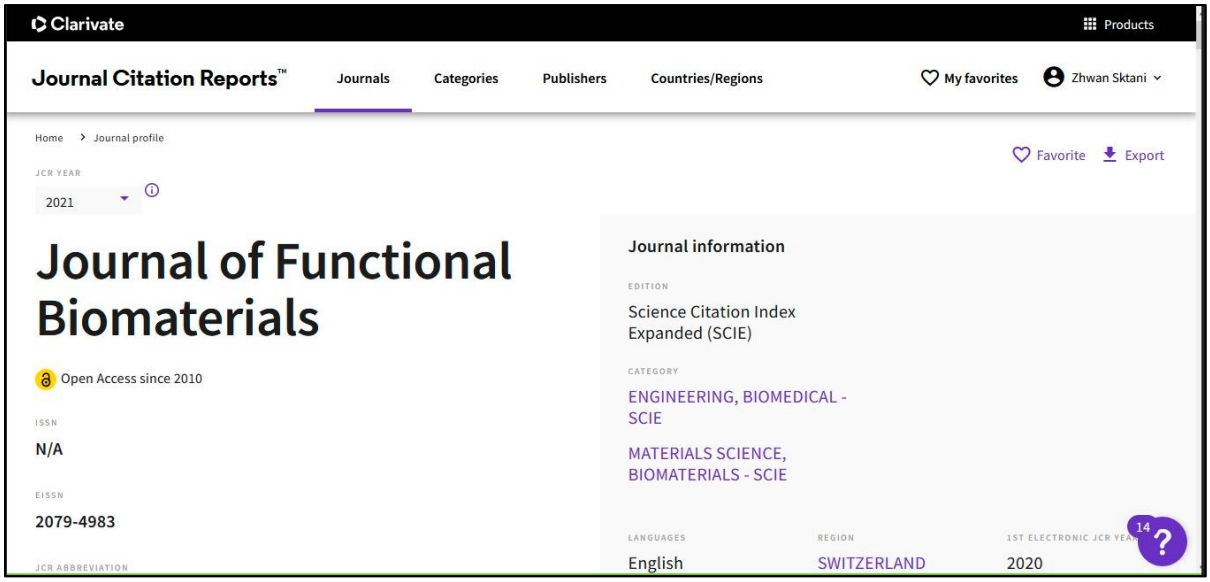

Figure A2: Indexing of JFB in Clarivate Analytics.

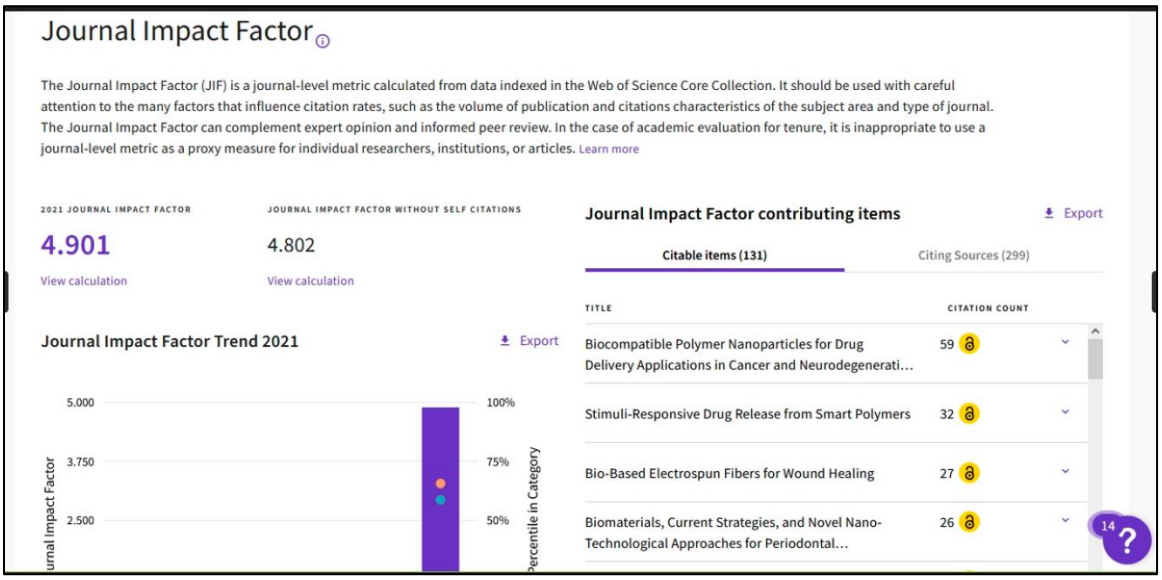

Figure A3: Impact factor (IF) information of JFB in Clarivate Analytics.

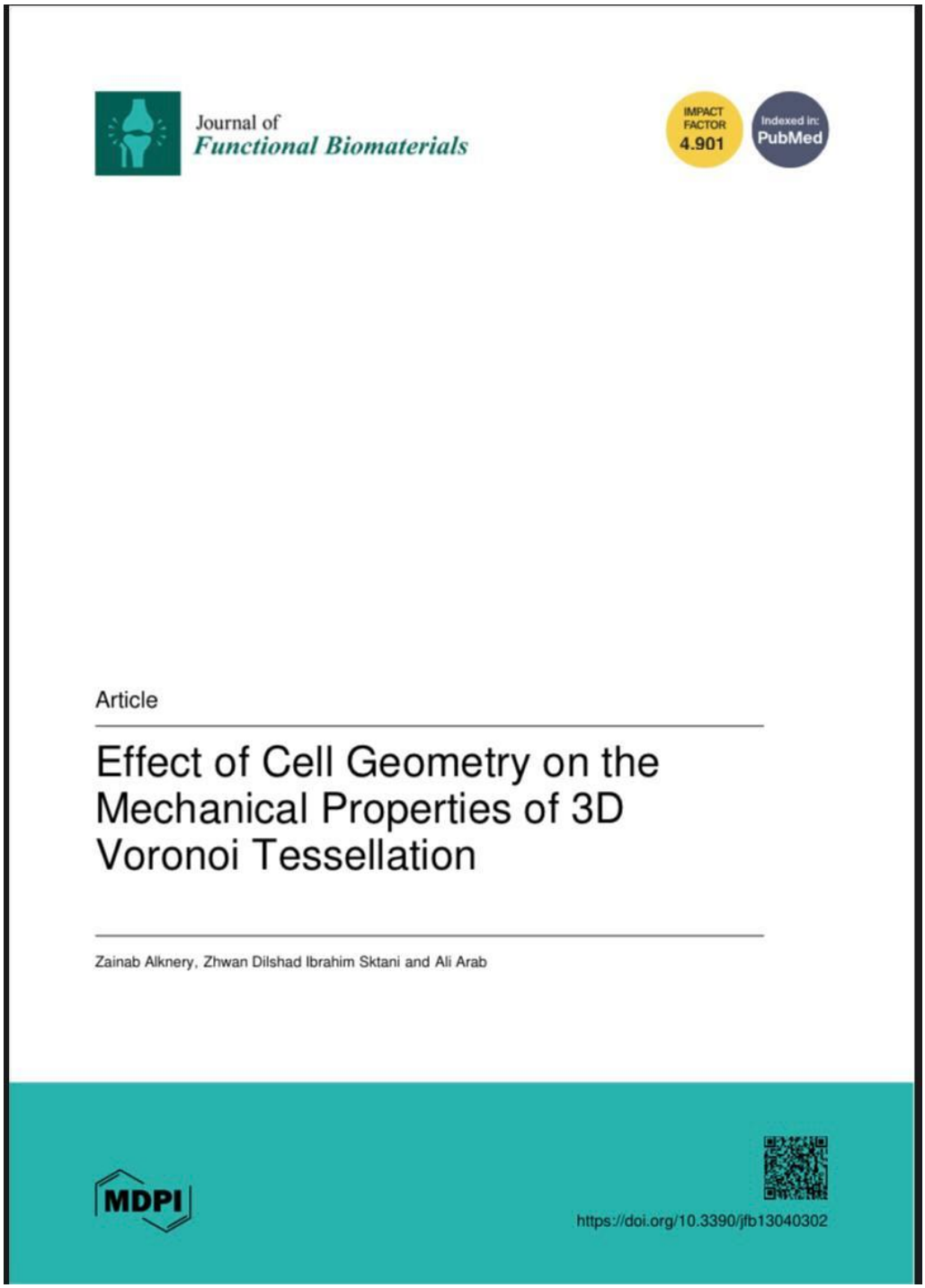

Journal of
Functional Biomaterials

IMPACT FACTOR 4.901

Indexed in: PubMed

Article

Effect of Cell Geometry on the Mechanical Properties of 3D Voronoi Tessellation

Zainab Alknery, Zhwan Dilshad Ibrahim Sktani and Ali Arab

MDPI

https://doi.org/10.3390/jfb13040302

Figure A4: Cover page of JFB including our published manuscript.

Rank by Journal Impact Factor

Journals within a category are sorted in descending order by Journal Impact Factor (JIF) resulting in the Category Ranking below. A separate rank is shown for each category in which the journal is listed in JCR. Data for the most recent year is presented at the top of the list, with other years shown in reverse chronological order. Learn more

EDITION
Science Citation Index Expanded (SCIE)

CATEGORY
ENGINEERING, BIOMEDICAL
34/98

JCR YEAR	JIF RANK	JIF QUARTILE	JIF PERCENTILE
2021	34/98	Q2	65.82
2020	N/A	N/A	N/A

EDITION
Science Citation Index Expanded (SCIE)

CATEGORY
MATERIALS SCIENCE, BIOMATERIALS
19/45

JCR YEAR	JIF RANK	JIF QUARTILE	JIF PERCENTILE
2021	19/45	Q2	58.89
2020	N/A	N/A	N/A

Figure A5: Quartile (Q) information of JFB in Clarivate Analytics.

SPECIAL GRATITUDE

Ali Arab, Ph.D.

Senior Researcher at BIT, China

All words cannot express my thanks and appreciation to Dr. Ali and his distinguished effort for what he is doing with the great personal effort that is appreciated and grateful. He is a perfect example of someone who performs a sublime message that reflects a respected and conscious personality.

I wish to express my gratitude for his support and generosity in all aspects. In addition to the extensive guidance and providing outstanding research, giving a lot of his time is greatly appreciated.

الإهـــــداء

قال تعالـى (وَمَن يَشْكُرْ فَإِنَّمَا يَشْكُرُ لِنَفْسِهِ) (لقمان:12)

أحمِد الله تعالى حمداً كثيراً طيباً على ما أكرمني بهِ من إتمام هذهِ الرســــــالـة.

أَهـدي ثَمَــرة جُهـدي المتـــواضع الى مـن وَهبوني الحيـــاة والأمـــل والنشـــأة على شغَـف التَعَـلم. ومَـنْ عَلَموني أن أرتَقي سُلـم الحيـاة بِقـــوة وَصَبَـــر ؛ بِـــرًّا، وإحســـانـاً، ووفـــاءً لهُما: والـدّي العـزيزيـــن.

إلى مَـــنْ وَهَبَـني الله نِعمَـــة وجودَهُـم في حيـــاتي، مَنْ كانـوا عَونـاً لـــي في رحلـــة بحـثي: إخـــواني، أَخَواتـــي، وإبنَـتي.

إلـــى مَـــنْ كاتفتـــني ونحـنُ نَشـــق الطـريـــق معـــاً نحـــو النجـــاح، إلـــى رَفيقـــة دَربي: نيـــــان زيـــن الديـــن.

ثُـــمَّ إلى كُـــل مَنْ ساندني سَـــواء بدوره مِن قريـــب او بعيـــد في إتمـــام هذهِ الرســـــالـــة، سائله الله ﷻ أن يجـــزي الجميع خَيرَ الجـــزاء في الدنيـــا والأخـــرة.

وأخيـراً إلى كل طالـب علـــم يسعى لكَسب المعرفـــة وتَزويـــد رَصيـــده المعرفي العلمـــــي والثقـــافي.

پوختـه

دیزاینه هاوشـــیوەکانی ســـروشـــت ئیلهامبەخش بوو بۆ ئەوەی لە بەکارهێنانی ژیانی راســـتەقینەدا بیانگونجێنن بەهۆی بەهێزی و تایبەتمەندییە میکانیکییە گونجاوەکانیانەوە. پێکهاتە ناڕێکەکانی ڤۆرۆنۆی کە لە ڕێگەی بەکارهێنانی Rhinoceros 7\Grasshopper درووســـت کراون. هەردوو دیزاینی ئاسایی وە درێژکراوەی ڤۆرۆنۆی (بە پشتبەستن بەو جومگە ستوونیانەی کە بە شـــێوەیەکی ســـروشـــتی بوونیان هەیە) دیزاین کران، کە ســـێ مۆدێلی جیاوازیان هەیە بۆ هەریەکەیان، ڕێک، لار I، وە لار II لەســـەر بنەمای یەکســـانی وە هەبوونی core لە ناو نمونەکاندا هەیە. چـــاپـــی (3D) three-dimensional (SLA) Stereolithography بەکـــارهـــات بـــۆ دروســـتکردنی مادەی بایۆپۆلیمر لەســـەر بنەمای ڕووەک بۆ ئەوەی ئامادە بکرێت بۆ تاقیکردنەوەی میکانیکی. بەگشـــتی ئەنجامە تاقیکارییەکان دەریانخســـت کە دیزاینە پێشـــنیار کراوەکانی درێژکراو ڤۆرۆنۆی تایبەتمەندی میکانیکی باشـــتریان هەیە. درێژکراوی ڤۆرۆنۆی نزیکەی 21% لە ڤۆرۆنۆی ئاسایی باشترن لە ڕووی بەرگریکردن لە شێواندن و نزیکەی 30% لە هەڵمژینی وزە. لێرەوە ئەم دیزاینانە تۆپۆلۆژیای جاوەروانی بۆ بەکارهێنانەکانی داهاتوو. جگە لەوەش دۆخی شـکسـتی شـەش پێکهاتەکە بەهۆی دارمانەوە لە سـێ قۆناغدا ڕوویدا؛ شـکانی سـترۆتی خانەکان، دارمانی خانەکان و لە کۆتاییدا، تەشـــەســـەندنی درزی خانەکان کە دەبیتە هوی شـــکان. ســـەبارەت بە مۆدێلە دیزاینکراوەکان، جۆری مۆدێلی ڕێک ڕەقبوونی بەرزتر وە ultimate strength ی بەرزتر نیشـان دا بەڵام مۆدێلی لار I بەهای Young's modulus بەرزتری نیشان دا. جگە لەوەش مۆدێلی لار II خاوەنی کەمترین تایبەتمەندی میکانیکی بوو بەهۆی دیزاینی ئەندازەیی لاوازەکەیەوە. لێرەوە ئەم مۆدێلە لە کارپێکردنە سووکەکان بۆ بەهێزیدا بە باشتر نازانرێت.

زانکۆی پۆلیتەکنیکی هەولێر
ERBIL POLYTECHNIC UNIVERSITY

کاریگەری دیزاینی پێکهاتە لەسەر هێزی پەستان و هەڵمژینی وزەی پێکهاتە جیاوازەکانی ڤۆرۆنۆی ناڕێک چاپکراوی ڕزین-D3 بە تەکنیکی SLA

نامەیەکە

پێشکەشی ئەنجومەنی کۆلێژی تەکنیکی ئەندازیاری کراوە لە زانکۆی پۆلیتەکنیکی هەولێر وەکو پەشێک لە پێداویستیەکانی بەدەست هێنانی پلەی ماستەر لە زانستی ئەندازیاری تەکنیکی میکانیک و وزە

لە لایەن

زینب زکریا علی

بەکالۆریۆس لە تەکنیکی ئەندازیاری ساردکەرەوە وهەواسازی

بەسەرپەرشتیاری

د. ژوان دلشاد ابراهیم